

ABSTRACT

Title of Document: HOMOGENEOUS AND HETEROGENEOUS
 SENSORS FOR COMBUSTION SYSTEMS

Amir Eshaghi, PhD, 2012

Directed By: Distinguished University Professor,
 Professor Ashwani K. Gupta,
 Department of Mechanical Engineering

Due to increasingly stringent emission regulations, it is important to develop clean combustors. Combustion behavior is very complex in almost all practical power plant systems. Measurement of temperature, pressure, local flow, and chemical composition inside the flame provides critical information to develop cleaner combustors. This would result in significant improvement in energy efficiency and reduce the environmental impact. A high density sensor network system would assist in understanding the various ongoing processes occurring within the combustors. This dissertation is focused on how much additional information can be gathered from multiple sensors.

Four different time delay estimation methods (using cross correlation, phase transform, generalized cross correlation with maximum-likelihood estimation, and average square difference function) were examined using two sensors. Phase

transform offered better results to calculate the time delay between a given pair of microphones. This has the potential to determine local noise generation sources from within flows and flames with the additional information on local noise generation source.

As a step towards the development of a sensor network, different sensors were examined. A micro-thermocouple, microphone and microphone probes were utilized to enhance understanding of the flame with detailed information on the various ongoing processes in a premixed swirl flame. High frequency temperature and pressure measurements were used to identify the thermal and acoustic characteristics of the flame and combustor. The local distributions of fluctuating pressure and temperature were measured in different regions, in and around the flame. Pressure fluctuation showed significant variation in different directions for the combustive case relative to non-combustive flow. Also a comparison of the pressure and temperature fluctuations revealed that maximum temperature fluctuations occur mostly near to the visible flame boundary while maximum pressure fluctuation occur further away from the flame.

Acoustic data from the premixed swirl combustor showed variation in fuel to air ratio changes the spatial distribution of noise as measured by different sensors placed around the combustor. A comparison of different sensors showed that a single sensor does not capture all the information with changes in fuel to air ratio.

HOMOGENEOUS AND HETEROGENEOUS SENSORS FOR COMBUSTION
SYSTEMS

By

Amir Eshaghi

Dissertation submitted to the Faculty of the Graduate School of the
University of Maryland, College Park, in partial fulfillment
of the requirements for the degree of
Doctor of Philosophy
2012

Advisory Committee:
Professor Ashwani K. Gupta, Chair
Professor Kenneth Yu, Dean's Representative
Professor Kenneth Kiger
Professor Miao Yu
Professor Bao Yang

© Copyright by
Amir Eshaghi
2012

Dedication

To my wife and my daughters

Acknowledgements

This dissertation would not be complete without my tremendous acknowledgement of my beloved family. I would like to especially acknowledge my wife, Niloofar Rezvani and beautiful children Anahita, and Kiana for their wonderful smile and laughter that have been an encouragement and inspiration to me.

I would also like to thank my advisor, Professor Ashwani K. Gupta for all his guidance. His highly equipped lab was instrumental in helping me improve the quality of this research.

Finally, I offer my sincere gratitude to Professor Kenneth T. Kiger for introducing me to this magnificent university. His genuine interest in helping students, both in their academic and personal lives has been an inspiration for me and a delightful experience.

Table of Contents

Dedication	ii
Acknowledgements	iii
Table of Contents	iv
List of Tables	vi
List of Figures	vii
Nomenclature	xiii
Chapter 1: Introduction	1
1.1 Background and motivations	1
1.2 Sensors for flame monitoring.....	5
1.3 The issues of sensors and flame.....	7
1.3.1 Flame diagnostic with light emission	8
1.3.2 Imaging technique (CCD camera)	9
1.3.3 Microphone and microphone probe	10
1.4. Thermocouple, microphone probes, and microphones to examine a premixed Swirl Flame.....	11
1.5 Objectives and approach	14
Chapter 2: Theory, apparatus and instrumentation	17
2.1. Experimental set-up	17
2.2. Data acquisition set-up.....	19
2.3. Thermocouple	20
2.4. Microphone probe.....	26
2.5. Microphone array.....	29
Chapter 3: Cross-correlation methods	31
3.1. Methodology	33
3.1.1. Correlation methods.....	34
3.2. Experimental setup.....	35
3.3. Results and discussion	36
3.3.1. Simulation results.....	37
3.3.2. Experimental results.....	46
3.4. Summary	50
Chapter 4: Calibration.....	51
4.1. Thermocouple	51

4.2. Microphones	51
4.3. Microphone probes	52
4.3.1. Performance characteristics via noise source	54
4.3.2. Performance characteristics via air flow	58
Chapter 5: Results and discussion.....	63
5.1. Thermal field.....	63
5.1.1. Mean temperature maps	64
5.1.2. Fluctuating temperature maps	65
5.1.3 Time constant data	66
5.2. Pressure fluctuations data	67
5.2.1. Non-reacting case.....	67
5.2.2. Combustive case	69
5.3. Shadowgraph.....	72
5.4. Power spectral density (PSD)	75
5.5. Acoustic noise spectra.....	78
Chapter 6: Multiple sensors for combustor monitoring	83
6.1. Test set-up.....	85
6.2. Data collection method	86
6.3. Results and discussions.....	87
6.4. Summary	95
Chapter 7: Conclusions	97
7.1. Correlation methods.....	97
7.2. Homogeneous, heterogeneous sensors in the flame	97
7.3. Microphone probe data	99
7.4. Microphone array placed outside the combustor	100
Chapter 8: Future work recommendations.....	101
Appendix A: Cross correlation algorithms	104
Appendix B: Numerical calculations	110
B.1. Structured meshing.....	110
B.2. Boundary conditions and solvers used	111
B.3. Acoustic modeling of the combustor	114
B.3.1. Stochastic noise generation and radiation method (SNGR).....	115
B.3.2. Segregated source propagation methods (SSPM)	115
B.4. Numerical results and discussion	115
Appendix C: List of publications	123
References.....	124

List of Tables

Table 1.1 Emission limit for gas turbines.

List of Figures

Figure 1.1. A modern gas turbine engine with its combustor.

Figure 1.2. Conventional sensor locations and its control system.

Figure 1.3. Typical sensors and diagnostic techniques for combustor.


Figure 1.4. Next generation of combustors ( Colored dots are heterogeneous sensors).

Figure 2.1. (a) Schematic diagram of the premixed swirl combustor. (b) Photograph of the test facility.

Figure 2.2. Test setup and facility in University of Maryland, Combustion Lab.

Figure 2.3. Energy balance for the thermocouple bead.

Figure 2.4. Characteristic temperature decay curve.

Figure 2.5. (a) Top: Tower for housing the microphone array around the premixed swirl combustor and Bottom: condenser microphone and its physical size as compared to one penny, (b) Angular arrangement of microphone array around the p

Figure 3.1. Time Delay Estimation for combustion noise by various algorithms when $SNR = -8.12$.

Figure 3.2. Time delay estimation accuracy for different SNR levels for white noise (a). Zoomed view of the graphs (b).

Figure 3.3. Time delay estimation accuracy for different SNR levels for real combustion noise and simulated noises (a). Zoomed view of the graphs (b).

Figure 3.4. Time delay estimation accuracy for different SNR levels for real combustion noise and noises from two uncorrelated noise microphones (a). Zoomed view of the graphs (b).

Figure 3.5. Time delay estimation accuracy for different SNR levels for real combustion noise and noise with addition of two equal background noises

Figure 3.6. Time delay estimation accuracy for different SNR levels for real combustion noise with the additional of two background noises recorded simultaneously.

Figure 3.7. (a) Cross-correlation function versus time delay for brown noise (b) zoomed view of the graph in (a).

Figure 3.8. (a) Cross-correlation function versus time delay for gray noise (b) zoomed view of the graph in (a).

Figure 3.9. (a) Cross-correlation function versus time delay for pink noise (b) zoomed view of the graph in (a)

Figure 3.10. (a) Cross-correlation function versus time delay for white noise (b) zoomed view of the graph in (a).

Figure 4.1. Calibrator toolbox was employed for calibration of microphones. (a) Calibrator view. (b) Cross-section view.

Figure 4.2. Set-up for calibration of the microphone probe. (a) Test with speaker. (b) Test with a air jet.

Figure 4.3. Output signal spectrum for white noise, $Na=250$. (a) The reference and probe microphones. (b) The probe performance spectral response plotted as ratio Probe Mic / Ref. Mic versus frequency.

Figure 4.4. Coherence function and phase angle between reference and probe microphones (for White noise) experiment ($N_a=250$ samples). (a) Coherence function spectrum. (b) Phase angle spectrum.

Figure 4.5. Cross correlation function for acoustic experiment (white noise) with resolution bandwidth of 1 Hz. (a) CC. (b) GCC-PHAT . (c) MLE ($N_a=250$).

Figure 4.6. Output signal spectrum for cold flow, $N_a=250$. (a) The reference and probe microphones. (b) The probe performance spectral response plotted as ratio Probe Mic / Ref. Mic versus frequency.

Figure 4.7. (a) Coherence function. (b) Phase angle spectrum for microphone probe and reference microphone. (c) Cross correlation with resolution bandwidth, of 1 Hz from $N_a=250$ samples using air jet.

Figure 4.8. The probe performance spectral response plotted as ratio Probe Mic / Ref. Mic versus frequency for heated probe, $N_a=250$.

Figure 4.9. (a) Coherence function and (b) phase angle for microphone probe and reference microphone using air jet with $N_a=250$ samples.

Figure 5.1. Mean temperature profile for a swirl stabilized premixed flame.

Figure 5.2 Fluctuating temperature from a swirl stabilized premixed flame.

Figure 5.3. Thermocouple time constant profiles at various radial locations for a given axial location in a premixed swirl flame.

Figure 5.4. RMS values of the amplified output signal from the microphone probe for the non-reacting case in (a) H, (b) θ , and (c) R directions, respectively, and (d) Total pressure fluctuation.

Figure 5.5. RMS value of the amplified output signal from the microphone probe for the combustive case in (a) H, (b) θ , and (c) R direction, and (d) total pressure fluctuation.

Figure 5.6. RMS values of the amplified output signal from the microphone probe with the flame overlapped to reveal the local regions of pressure fluctuations. (a) with flame, and (b) without flame (non-combustive) case.

Figure 5.7. (a) Hybrid of flame shadowgraph image, visible flame and mean temperature. (b) Illustration of vortex production and fusion in premixed flame.

Figure 5.8. Power Spectral Density (PSD) for thermocouple and microphone probe at selected discrete frequency range. The contour of the flame is shown in black dotted line. (I) PSD recorded by thermocouple (left half in each figure). (II) PSD recorded by microphone probe (right half in each figure).

Figure 5.9. A sketch illustrating the movement of flame, gas pockets and eddies in a small volume of the flame.

Figure 5.10. Sound pressure level for a premixed swirl flame.

Figure 5.11. Power spectral density of the acoustic signals.

Figure 6.1. Combustion noise spectra for microphones at varying axial distance from the burner exit (for stoichiometric condition).

Figure 6.2. Circumferential distribution of reacting and non reacting noise spectra at Z=3 inches location.

Figure 6.3. Reacting and non reacting acoustic radiation from the flame at different equivalence ratios at Z=2 inches from the burner exit (Iso shows non reacting flow).

Figure 6.4. Reacting and non reacting acoustic radiation from the flame at different equivalence ratios at Z=6 inches from the burner exit.

Figure A.1. Schematic diagram of cross correlation method.

Figure A.2. Schematic diagram generalized cross correlation method.

Figure B.1. Numerical meshing of the 2D premixed swirl combustor and its boundary conditions.

Figure B.2. Experimental velocity profiles for 30 degree swirl geometry.

Figure B.3. Experimental velocity profiles for 60 degree swirl geometry.

Figure B.4. Pressure waves propagating.

Figure B.5. Numerical velocity magnitudes. (a) For 30 degree swirl. (b) For 60 degree swirl.

Figure B.6. Numerical acoustic power level. (a) For 30 degree swirl. (b) For 60 degree swirl.

Figure B.7. Numerical power level. (a) For 30 degree swirl. (b) For 60 degree swirl.

Figure B.8. Numerical surface acoustic power level. (a) For 30 degree swirl. (b) For 60 degree swirl.

Figure B.9. Velocity magnitudes. (a) For 30 degree swirl. (b) For 60 degree swirl.

Figure B.10. Numerical Contours of acoustic power level. (a) For 30 degree swirl. (b) For 45 degree swirl.

Figure B.11. Numerical plot of power level. (a) For 30 degree swirl (b) For 60 degree swirl combustor.

Figure B.12. Numerical surface acoustic power level. (a) For 30 degree swirl. (b) For 60 degree swirl.

Nomenclature

T_g	Gas temperature within the flame
T_b	Thermocouple bead temperature
τ_T	Thermocouple time constant
τ	Time delay between the two received signals
γ	Ratio of radiative effects to convective effects
T_{surr}	Temperature of the surrounding
ε	Emissivity
σ	Stefan Boltzmann constant
m_b	Mass of the thermocouple bead
h	Convective heat transfer coefficient
A_b	Area of thermocouple junction
ρ_b	Density of the thermocouple bead
c_p	Specific heat of the thermocouple junction
r_b	Radius of the thermocouple bead
ρ	Density of fluid
$\bar{\rho}$	Time mean value of the density of gas
ρ'	Fluctuation component of the density of gas
K	Gas thermal conductivity
D	Outer diameter of the burner
P	Time mean value of dynamic pressure

\mathbf{P}_d	Pressure fluctuation
\mathbf{P}_m	Pressure measured by the microphone probe
U	Time mean value of the velocity
Na	Number of average
ϕ	Phase between the reference and probe microphones
f	Frequency
γ_{xy}^2	Coherence between signal x and y
G_{xy}	Cross spectral density between signals x and y
G_{xx}	Autospectral density of signal x
G_{yy}	Autospectral density of signal y
PSD	Power spectral densities

Chapter 1: Introduction

1.1 Background and motivations

Due to increasingly stringent emission regulations the gas turbine industry faces challenges to develop cleaner combustors. This has resulted in fundamental redesign of combustion systems used on gas turbines [1]. Table 1.1 shows some of the limits for NO_x and CO that apply worldwide for stationary gas turbines [2]. The next generation of combustors needs to be significantly more efficient with reduced pollutants emission, especially carbon emissions. A single sensor from a process or combustor provides limited information. Having the best performance of the gas turbine combustor at operating point and adjusting the equivalence ratio of fuel and gas mixture is not simple. Control system operates the combustor via partial information regarding the actual flame properties and estimated air mass flux. This method seems effective but it suffers from the potential variations of engine properties. For example natural gas companies supply fuels from different sources, so that the system has to adapt to these changes by sensing any change in combustion parameters.

In next generation of combustors, it is required to measure local flow, pressure, thermal signatures and chemical composition as well as their interactions to have optimum performance of the system. Exact knowledge of the equivalence ratio is necessary to combat undesired changes in air moisture, fuel quality, and power consumption. These changes might be responsible for change in pollutants emission.

Small changes in the operating conditions in flame must be monitored for efficient combustor operation.

Country	NO _x (at 15%O ₂)	CO (at 15% O ₂)	Rate Power
Italy	29 vppm	48 vppm	> 50 MWth
France	40 vppm	80 vppm	> 50 MWth
England	28 vppm	80 vppm	> 50 MWth
USA (California)	9 vppm	Not stated	Not stated

Table 1.1. Emission limit for gas turbines.

Sensors can be placed at a variety of locations, like sensing the flow parameters or velocity upstream, inside the combustor to see the flame, or further downstream to analyze the flue gases. Optical techniques are non-intrusive but need windows, which can be difficult to accommodate and maintain. In this regard both thermocouple and microphone probe can withstand harsh environments.

In the future, it is anticipated that using a large number of sensors (homogeneous and heterogeneous) can help provide detailed information on various ongoing processes within the system and improve the system performance. As the emissions associated with combustors become important, it is imperative that one must embark to develop functional values (output property of a unit or a plant) that may feature cleaner-burning in future smart combustors.

In the actively controlled combustors one would use sensor networks and advanced diagnostic techniques to accurately, reliably, and inexpensively detect local flow, thermal and chemical conditions within the combustor to obtain information about the integrated global performance of the combustor. Dense network of sensors around the combustor can improve the system performance. Figure 1.1 shows current gas turbine engine and its combustor.

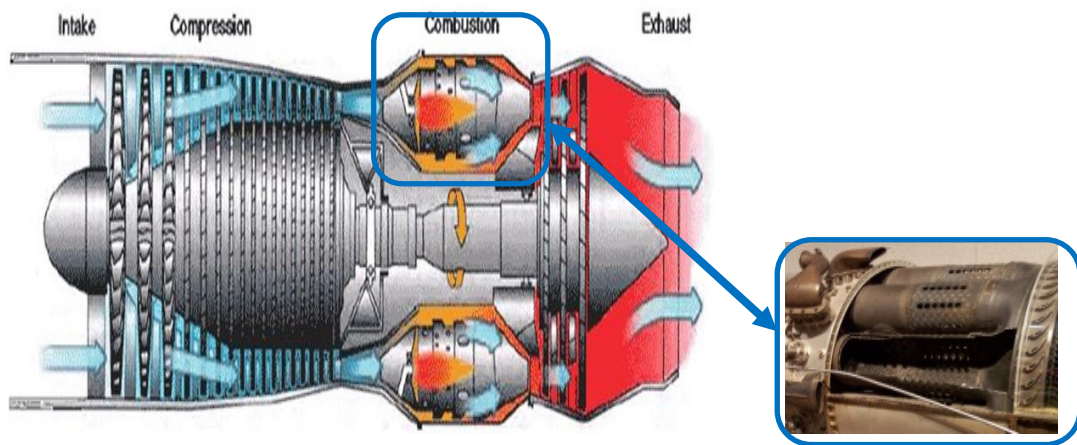


Figure 1.1. A modern gas turbine engine with its combustor.

Combustion behavior is very complex in almost all practical power plant systems; temperature and pressure information are amongst the fundamental information desired. Much reduction of NO_x emissions has been achieved by premixed fuel-lean combustion by reducing the flame temperature [2]. If we measure the temperature of the flame and provide suitable conditions at each locus, it is possible to reduce NO_x emission which depends exponentially on temperature [3]. This will significantly improve reduce the environmental impact and also enhance the energy efficiency.

The noise generated in the flame shows the coupling between pressure and temperature fluctuations in flames [4]. The noise emitted from a burner is largely

determined by the interaction between the energy conversion mechanism of the flame and the combined acoustic and aerodynamic characteristics of the system [5]. Finding the sources of noise associated with flame to control its effect on the flame characteristics and combustion phenomenon as a whole is important.

The measuring parameters of the flame are different and each diagnostic technique differs relative to time, spatial resolution, and their accuracy. One of the consequences of pressure fluctuation is a considerable increase of corrosion of the walls in combustor or boilers in power plants [6]. The understanding of concentration of pressure fluctuations near the wall can be used to estimate to wall corrosion rate.

Each individual sensor contains more information when used solely or in conjunction with other sensors; however one must seek means for additional information that can be gathered from multiple sensors. Hypothesis should be established, that signal of the sensor contains more information and one ought to correctly analyze. These can be from fast Fourier transfer and cross correlation analysis of the time series. These methods can be extending to examine power plants, and combustors using large array of homogeneous and heterogeneous sensors.

A method is successful if it provides us with meaningful parameters that help to control the flame. The results of data modeling have failed to adequately capture the underlying correlation and although usually the approach is promising; its successful application in practice requires a considerable amount of resources with respect to system setup and calibration, testing and validation [7].

The effect of different geometry of these homogeneous and heterogeneous sensors should be examined. Also the effects of increased number of sensors for more information need to be tested. Different geometry should be investigated by changing number of sensors. The effect of increase in number of sensors for extra information that can be obtained from a system should be examined. Experiments need to be carried out to support numerical simulation results. Finally, increasing the number of sensors should be tested.

1.2 Sensors for flame monitoring

A reliable monitoring or sensor tool for most industrial burner is necessary for cleaner environment. It is imperative that embark developing functional value for clean-burning smart combustors. In this regard, the optimizing of burner setting is necessary to reach this goal. Sensors are essential for control to show the state of burning process.

Conventional sensors usually measure global variables such as flue gas or the product of the combustion such as NO_x, CO or O₂, but these sensors provide limited information about inside the combustor, burner, or flame, see figure 1.2. New diagnostic techniques and sensors would be necessary to give us more information on the flame itself. This requires the collection of information directly from the flame. This can provide fast and detailed information on the various ongoing processes within the system.

This will provide optimized combustor operation, monitor the process and finally control or reduce the instabilities and its consequences on the equipment. A large

numbers of diagnostic techniques are available to characterize the flame, see figure 1.3.

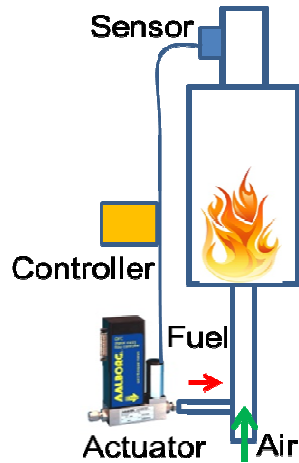


Figure 1.2. Conventional sensor locations and its control system.

These techniques should provide a good description of flame or combustor process in general and give detailed information on the various continuing processes within the flame or combustor. Figure 1.4 shows the next generation of combustors. Various physical factors within the combustor can be examined using heterogeneous sensors.

Flame diagnostic in one area can be used in other areas. The goal in this section is to study and review different current available methods for general flame diagnostics using homogeneous and heterogeneous sensors. Microphone probes, microphone arrays and thermocouples and techniques related with these sensors, which have been used in this research are considered in more details in section 2.

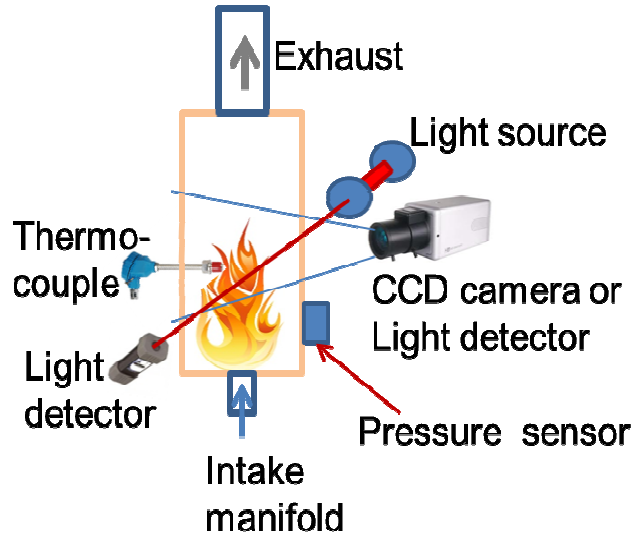


Figure 1.3. Typical sensors and diagnostic techniques for combustor.

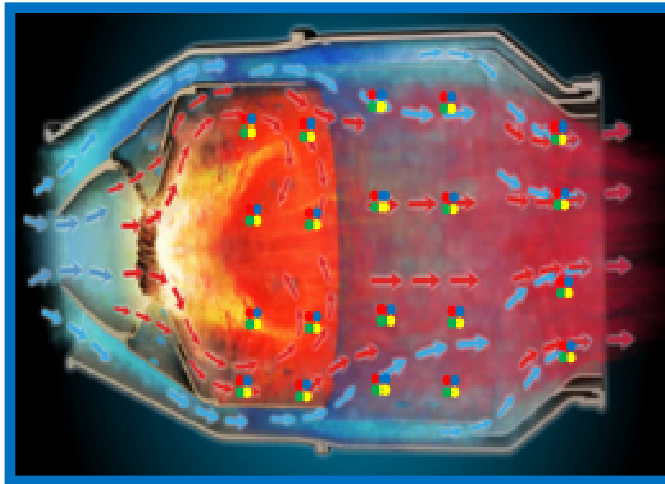



Figure 1.4. Next generation of combustors ( Colored dots are heterogeneous sensors).

1.3 The issues of sensors and flame

Velocity in the practical flames usually is high enough that the flow is turbulent at the burner outlet. Instantaneous values the velocity, temperature, pressure and composition of parameter of a turbulent flame are not constant in time and fluctuate

around the mean values. Also, the flame is not homogeneous and sensors at each point will give different values, therefore monitoring several points should be considered for correct information from a flame. Later this information can be used for more valuable process control. The information can also be used in model validation and model development.

Data modeling is required to adequately capture the underlying correlation and to find correlation between sensors. Successful function in practice needs significant amount of resources with respect to system setup and calibration, testing and validation. Using multiple sensors is new in harsh environments. Cheap energy available previously prevented precious improvement in this field. There are several issues for using multiple sensors for diagnosing flame. Some of the issues can be summarized as follows:

- Can temperature and pressure measurements in the flame identify a distinct signature of a practical flame?
- Can multiple sensors provide improved information from combustors?
- How many sensors are adequate to describe a defined combustor local and global behavior?

1.3.1 Flame diagnostic with light emission

1.3.1.1 Laser absorption emissions

Different species have different absorption spectrum, and this property is used to determine the gas composition. Absorption spectroscopy is a technique for measuring gas composition based on a decrease in intensity when a beam with a certain

wavelength passes through a gas. Based on the absorbed wavelength it is possible to specify chemical species. Tunable diode lasers are used for used for abortion measurements in high temperature gasses [8]. Some works on sensors for combustion show that diode laser sensor is suitable for flame dynamics and instability measurement in the flame [9]. Time multiplicity advantage and wavelength tuning is used to achieve simultaneous measurement of different species.

1.3.1.2 Multiple emission (sensors)

Light emission can be used as a flame signature. It works based on relation between the energy emitted at certain band and heat release rate which has a relationship with fuel air ratio in the burner. One of the challenges in this regard is selecting a correct signal / data, which is used as a reliable and meaningful signal/ data. One of the recent works had been done by installing optical fiber probes inside the burner to see different parts of the flame. This work showed the possibility of application of optical fiber monitoring system for combustion process to reduce the amount of NO_x produced and emitted [6, 10].

1.3.2 Imaging technique (CCD camera)

Flames produce visible light as well as IR and UV light. Flame by charge-couple device (CCD) camera has been used for flame diagnostics in many modern incinerators and power plants. CCD camera can be used with different narrow band filters to show different illumination from the flame. Thus by analyzing the emission spectra, it is possible to identify different species in the flame. With this diagnostic technique it is possible to specify the amount of energy emitted from the flame,

because emitted power at each wavelength has a relationship with temperature. So the temperature can be estimated from the detected radiation signals. Chemiluminescence can show heat release patterns that can be done with intensified CCD camera. High frequency Chemiluminescence imaging techniques is used to locate the sound sources from within a flame. High frequency Chemiluminescence is costly and requires rigorous data processing for the localization of acoustic sources within a flame. CCD camera integrated with band pass filters at selected wavelength can be used to estimate chemiluminescent emissions due to CH, C₂ and OH from blue, green bands and UV signals, respectively.

1.3.3 Microphone and microphone probe

Localized heat released fluctuations cause a sudden expansion of fluid which causes pressure fluctuations and sound. Turbulence causes pressure fluctuations and unsteady heat release, which can cause pressure fluctuation and noise. Therefore the noise radiated by a flame has close relationship with unsteady heat release rate. Heat release fluctuations generated by non turbulent flow instabilities, vortex shedding or PVC are reported [11]. In a combustor the noise spectrum is strongly influenced by the combustion chamber [12], so here first the flame without combustion will be considered. Pressure fluctuations can be caused by instability, so it is possible to use microphone or microphone probe as a sensor to monitor any instability in a flame [13].

Pressure and radiation sensors were used to collect direct information from the flame. Flame was used and pressure fluctuations were measured with a set of microphones. With an experimental program a relationship between output of sensors

and NO_x emissions was found. Many tests with two microphones, one inside the burner and other located at the combustor wall, were done. Artificial neural network were used to predict NO_x emissions to find out a relationship between output of sensors and NO_x emissions [13, 14].

A measurement with change in the flow characteristic, like turbulent intensity and mean flow and equivalence ratio has been done [15]. Transfer function between approach flow velocity fluctuations and heat release fluctuation and radiant acoustic pressure were presented. This study shows turbulent premixed combustion processes are unsteady and cause acoustic radiation.

1.4. Thermocouple, microphone probes, and microphones to examine a premixed Swirl Flame

In combustion systems, the minimization of the noise sources, namely noise from the turbulent flow, combustion noise and noise caused by periodic instabilities and fluctuations of the ignition zone is required. Swirl is often used in flames to provide the source of high ignition energy, wider stability and operational ranges. Frequently, the complex interplay between local flow, pressure, chemical composition, and temperature within these high performance combustors means that they must be carefully monitored in order to maintain favorable combustion condition. The complex coupling between fluctuating temperatures and pressure within the turbulent flame affects the localization of acoustic sources within the flame, which in turn affects the flame characteristics and combustion phenomenon as a whole. Understanding the coupling mechanisms between acoustic waves and flames have

become an important issue in the development of combustion systems. The use of homogeneous and heterogeneous sensors can reduce noise and avoid the structural damage that often emanates from such an interaction to produce thermo-acoustic instabilities. Currently comprehensive information is not known about the coupling between fluctuating temperatures and acoustics and its sources. The complexity of such an interaction is higher for turbulent flames than for laminar flames due to the large variety of fluid dynamic and thermo-chemical scales involved both in space and time.

Swirl is used in practically all types of combustion systems, including gas turbine combustion, furnaces and boilers. In combustion systems, the favorable effect of imparting swirl to combustion air and/or fuel has been extensively used for flame stabilization, high heat release per unit volume, and clean efficient combustion [16]. Premixed combustion is susceptible to inherently unsteady high acoustic pressure and temperature fluctuations [17]. Swirl flows and flames can generate periodic flow instabilities, which lead to an increase in noise emission and problems of flame stability [18]. Instabilities in swirl flames have been investigated by a number of investigators and reveal the importance of coherent structures in the forward flow surrounding the inner recirculation zone [18]. The existence and the influence of coherent structures on noise emission from the flame (and thus of the combustion system) requires further physical understanding to minimize combustion noise in stationary industrial gas turbine engine applications. Swirl flames can result in high noise levels, in particular under high intensity conditions.

The extent of thermal non-uniformity in premixed flames is poorly characterized but can be expected to depend upon the combustor configuration, the degree and distribution of swirl in the combustor, and other input and operational parameters of the combustor [16]. The thermal field non-uniformity can influence the combustion efficiency as well as emission levels, including NO_x [19].

Different combustion characteristics have been found by changing the radial distribution of swirl in a burner [20]. Marshall and Gupta [21] determined the thermal characteristics of different premixed flames performed through various combinations of swirl and axial inlet momentum distributions in a double concentric swirl burner. Fluctuating temperature measurements were obtained for several different flames at various spatial locations in the flames. By maintaining a constant equivalence ratio, a comparison of the dimensions and distribution of temperatures for different flames was achieved. These results provided information on the important role of radial distribution of swirl and jet axial momentum on the flame thermal characteristics.

The goal here is to implement homogeneous (same type of sensors), heterogeneous (different type of sensor) sensors system to investigate the thermal and acoustic behavior of premixed swirl flames. Such heterogeneous sensor arrays can provide detailed information on the thermal and acoustic characteristics of a premixed swirl flame. In future, smart combustors are expected to possess an array of homogeneous and heterogeneous sensors for combustion monitoring and control. However, implementation of such arrays in an optimized way is still an area of active research. Three different types of sensors have been used in the present investigation: condenser microphones, microphone probe and a micro thermocouple. Here, some

initial steps have been undertaken towards the fundamental understanding for the development of a homogeneous sensor arrays (eight microphones and three microphone probes) and heterogeneous sensor network (combination of eight microphones, three microphone probes and a thermocouple) for detailed combustion monitoring. A swirl stabilized premixed flame burner has been used in the present investigation. The effect of mean and fluctuating temperature and temperature distribution on the distribution of acoustic sources within the flame has been examined. The measurement of high frequency temperature signal allowed one to determine characteristic mean and fluctuating temperatures and thermal stratification characteristics within the flame. The measurement of microphone probes allowed determination of fluctuating components of sound pressure level at various spatial locations within the flame. Experimental data presented here provided improved insights on the thermal and acoustic behavior of a swirl stabilized premixed flame.

1.5 Objectives and approach

The main purpose of this dissertation is: examine the role of increased number of low cost sensors in combustors to provide improved understanding of the flow, reactions and flame using homogeneous and heterogeneous sensors. Each individual sensor contains more information when used solo or in combination with other sensors; how much additional information can be gathered from multiple sensors is the focus here. Hypothesis should be established, that reveals that signal from a sensor contains more information and that this should be analyzed in depth. It is expected that such understanding will help develop high performance sensor network for use in advanced power plants.

The following approach will be addressed here.

- 1- Find out which correlation methods will give better result.
- 2- Use of thermocouple, microphone probes and microphone array to examine the noise source in a flow and swirl flame.
- 3- Use microphone arrangements to examine the acoustic signatures between sensors, with change in amounts of fuel in a combustor.

In first set of experiments, different correlation methods examined. Time delay estimation may be affected by some practical difficulties, such as, background acoustic noise, reflection, and other kind of noise associated in the system. The level of signal-to-noise ratio (SNR) affects the precision of these methods. Signal-to-noise ratio is a measure used in science that compares the level of desired signal to the level of background noise. It is defined as the ratio of electrical signal power to the noise power. Some methods offer better results for the same conditions. To find out which correlation methods between sensors will give better result, four different times delay estimation methods are examined here using MATLAB. These were: cross correlation (CC), generalized cross correlation with phase transform (GCC-PHAT), generalized cross correlation with maximum-likelihood estimation (MLE) and average square difference function (ASDF).

In the second set of experiments, a micro-thermocouple, microphones and microphone probes were employed to provide detailed information on the various ongoing processes in a premixed swirl flame. High frequency pressure and temperature measurement were used in conjunction with flame imaging techniques to identify the thermal and acoustic characteristic of the flame. The local distributions of

fluctuating pressure and temperature were measured in different regions, in and around the flame. The noise generation sources were investigated using microphone probes in conjunction with an array of microphones. Temperature and pressure fluctuations were studied in detail at the boundary and immediately outside of the visible flame.

Finally, It is expected that measurements of the acoustic signatures between sensors, can be characterized the flow physics within the combustor. Tests were made at constant air and the amounts of fuel flow varied. A detailed acoustic analysis was done for a premixed swirl combustor with a microphone arrangement.

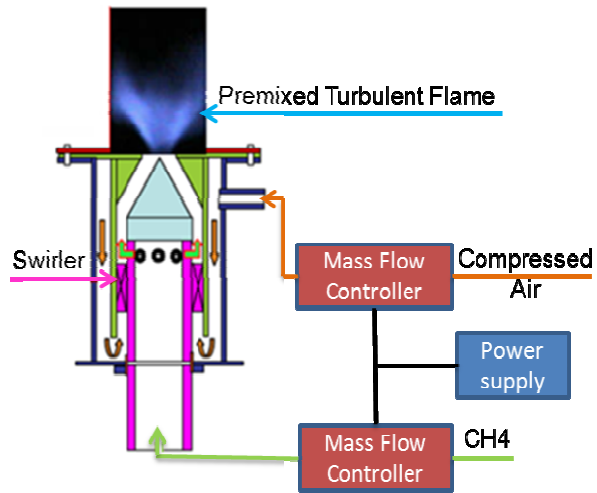
Chapter 2: Theory, apparatus and instrumentation

2.1. Experimental set-up

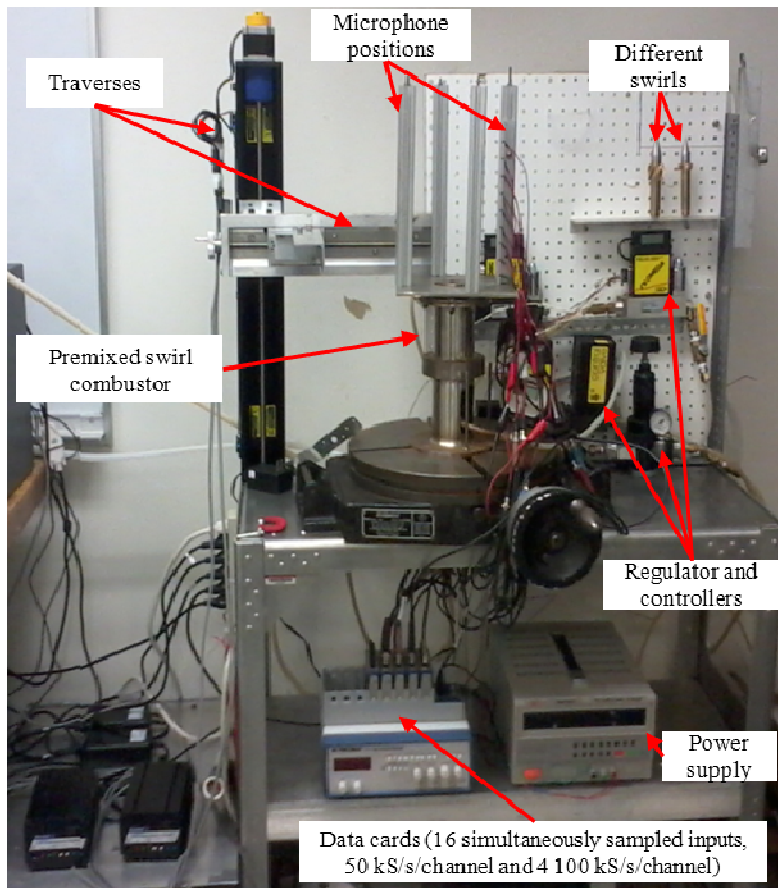
Swirl is used in almost all types of practical combustion system, including gas turbine combustion. In combustion systems, the effect of swirl to combustion air and fuel has been used for flame stabilization, high heat release and efficient combustion. Figure 2.1 shows a schematic of the 6.12 kW premixed swirl test combustor and the test facility used here. The flame is stabilized on a center body and the combustion occurs at atmospheric pressure. The fuel inlet diameter of the premixed combustor is 20mm and the combustor chamber is a 210 mm long quartz tube with a 60mm inside diameter. A laboratory-scale test combustor was used that incorporated a premixed swirl burner.

Combustion air was supplied at ambient temperature from the compressor and the flow rate monitored using a mass flow controller and regulator. High purity methane gas was metered by a mass flow meter and mixed with air at a location upstream of the combustor. The air and fuel mass flow rate were controlled by flow controllers. The regulator and controller could maintain the flow to be within +1.5/-0.5 percent of the full value.

The premixed condition was achieved by injecting fuel through five circumferentially distributed holes at 100 mm distance upstream from the combustor inlet. The flame was stabilized using 45° vane swirler in the flow path, having six swirl vanes.



(a)



(b)

Figure 2.1. (a) Schematic diagram of the premixed swirl combustor. (b) Photograph of the test facility.

2.2. Data acquisition set-up

Figure 2.2 shows the data acquisition setup. Data is logged simultaneously from all microphones and thermocouples. Hi-speed National Instrument-USB data acquisition hardware was used along with data acquisition software with the ability to record 16 simultaneous inputs (4 for thermocouple and 12 for pressure signals from microphones).

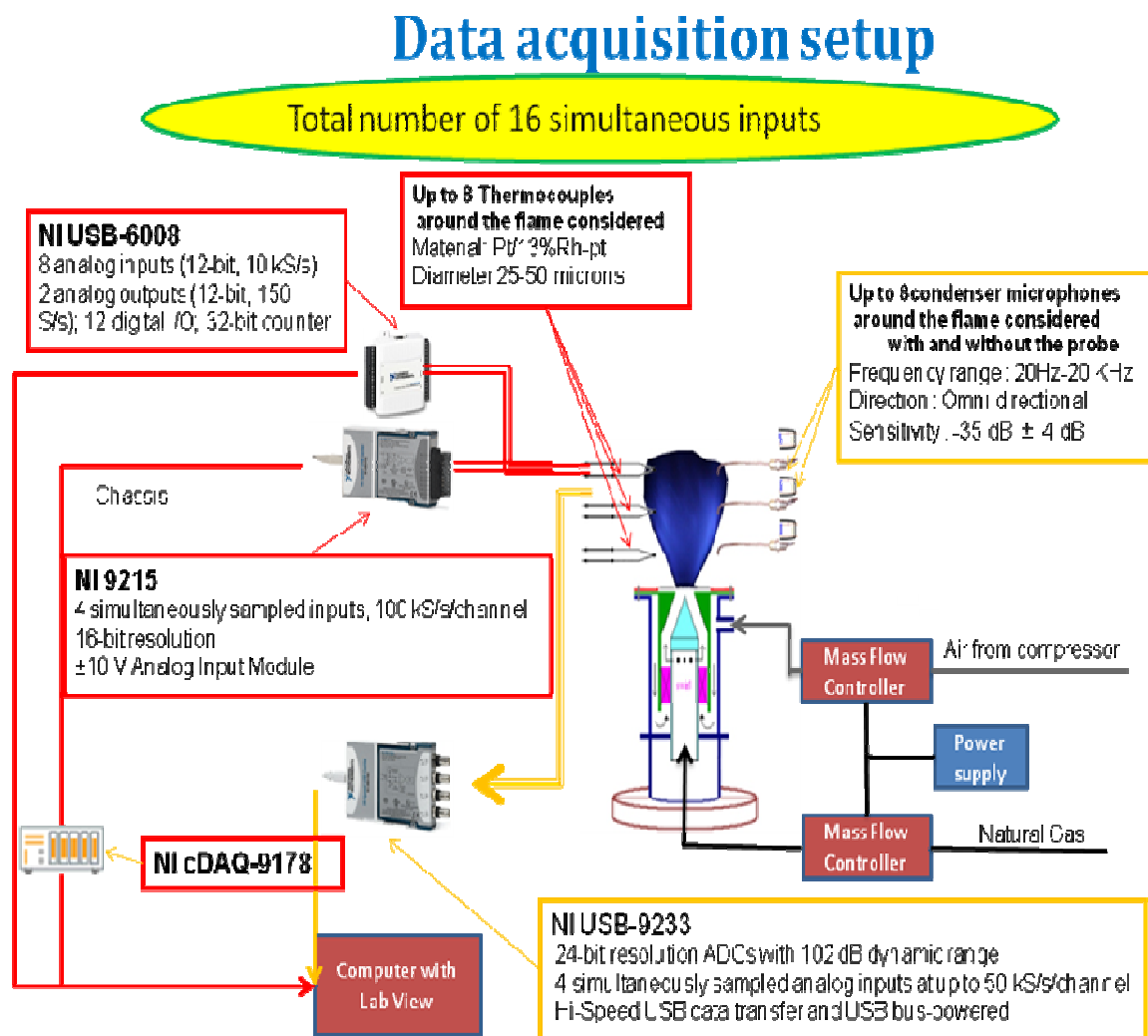


Figure 2.2. Test setup and facility in University of Maryland, Combustion Lab.

The 50k sampling frequency per second for each channel made it possible to acquire data at high frequency so that one could capture any instability in the flow and flame.

2.3. Thermocouple

High-frequency temperature measurements were obtained using 50 μ m wire diameter R-type (Pt/Pt-13 percent Rh) micro thermocouple probe. Thermocouple junction was suspended between two 1.5 mm diameter ceramic supports. The wire diameter was small enough not to cause any significant interference on the flame structure while maintaining structural rigidity of the thermocouple. The thermocouple probe was traversed at different spatial locations in the flame using a 2-D (X-Y direction) traversing mechanism.

At every probe location in the flame, the signal of the thermocouple was amplified and sampled at 10 kHz for a total of 300,000 samples (or a total sampling time of 30 s). The response time frequency for our thermocouple without compensation was about 35 Hz. Such high sampling frequency was required to be able to average over the low and high frequency turbulence and some local instability in the flame. The high frequency sampling rates ensure one to have enough resolution of the any turbulence time scales presented in the flame. According to the work of Hinze [22], turbulent flow can occur in open and closed flames at frequencies as high as 5 kHz. Therefore, with a sampling frequency of 10 kHz ($f_N = 5$ kHz), it was possible to capture and temperature variation (turbulent occurrence). It was founded that frequency greater than about 5 kHz contain noise. This can be from in the data

acquisition card and electronics used in the temperature measurement circuits. The sampling time of 30 s allowed for averaging over low to moderate temperature fluctuations measurements. It gave a good representation of the thermal field. Large temperature fluctuations were found at all locations in the flame.

The thermal inertia of the thermocouple is first order damping of the frequency response of the bead, so that compensation is required to consider for temperature. The time constant of the thermocouple should be specified. This time constant is a function of local conditions; the heat transfer coefficient, local velocity, temperature, turbulent flow, and the local Reynolds number of wire [23, 24]. Average values for the time constant at each point have been used [25, 26]. The large velocity and temporal changes of temperature show that the response of the thermocouple is non-linear. So it is required to perform compensation based on the velocity and temperature at each point in the flame [27]. Here, compensation technique in swirling flames has been used [28]. The temperature compensation technique has been used to correct for this effect in thermocouple bead size.

The condition and the response limitation of the thermocouple depend on energy balance on the bead of the thermocouple. Heat transfer takes place between the thermocouple bead and the environment. Three type of heat transfer present in this balance are radiation, conduction and convection. The heat transfer by conduction is small relative to convection and radiation [29]. Under the assumption that the heat loss of the thermocouple bead is insignificant the energy balance can be written as:

$$q_{st} = q_r - q_c \quad (2.1)$$

where, q_{st} , q_r , q_c are heat storage in the bead, radiation, and convection heat transfer respectively, see figure 2.3.

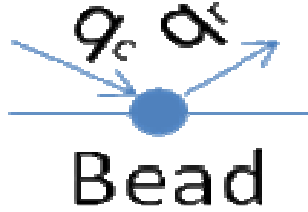


Figure 2.3. Energy balance for the thermocouple bead.

The convection heat transfer in the above equation can be written by:

$$q_c = h * A_b * (T_g - T_b) \quad (2.2)$$

where, h , is the convective heat transfer coefficient of the flow over the thermocouple junction, A_b is considered for area of thermocouple junction, T_g is the gas temperature within the flame, and T_b is considered for measured thermocouple junction or bead temperature,. The radiation heat transfer is defined as:

$$q_r = A_b * \sigma * \epsilon * (T_b^4 - T_{sur}^4) \quad (2.3)$$

where, σ is Stephan Boltzmann constant, ϵ is emissivity, and T_{sur} is the temperature of the test section. And finally the heat storage in the thermocouple bead is given by:

$$q_{st} = m_b * c_p * \frac{dT_b}{dt} \quad (2.4)$$

where, m_b is the mass of the thermocouple junction, c_p is the specific heat of the thermocouple junction, and t is the time. The response time limitations of the probe become apparent after performing an energy balance on the measuring junction or bead of the thermocouple. Convection, radiation and thermal storage are balanced in this system. As it was mentioned conduction losses of the thermocouple probe are assumed to be small. After manipulation, the energy balance can be expressed as [28]:

$$T_g = T_b + \tau_T (T_g, U) \frac{dT_b}{dt} + \gamma (T_b^4 - T_{sur}^4) \quad (2.5)$$

$$\tau_T = \frac{m_b c_p}{h A_b} \quad (2.6)$$

$$\gamma = \frac{3 \varepsilon \sigma \tau_T}{\rho_b c_p r_b} \quad (2.7)$$

where, τ_T is the characteristic response time or time constant of the probe, and γ is the ratio of radiative effects to convective effects. The response time of the probe is governed by the thermocouple probe properties and flow properties. The radiation factor, γ is also determined by the thermocouple junction properties and the flow properties where ε is the emissivity, and σ is the Stefan-Boltzmann constant. It is apparent from Equation (2.5) that the gas temperature in the flame differs from the measured thermocouple bead temperature by the ‘thermal inertia’ and radiative loss offsets.

These offsets are increased by slow response time and high bead temperatures. From the measured values of τ_T , the gas temperature (compensated) is calculated from the uncompensated temperature data from Equation (2.5) above. A circuit was designed to switch between heating and cooling cycles for characterization of the probe's response to temperature changes at any given location in the flame [30]. The DC heating current was applied to thermocouple for heating the thermocouple. The voltage was about 10 V. When the heating current was turned off (the thermocouple started to cool off) the input from the thermocouple and data acquisition was activated to collect the data from the thermocouple output that indicated the temperature decay at the local prevailing conditions. The circuit's short switching time assists in improving the accuracy of this method. The digital compensated thermocouple measurement technique described above is a feasible method for extracting detailed turbulent information from swirl flames. Before compensation, a limit on the maximum frequency was applied to the raw temperature data [30]. The cutoff frequency of the probe was selected as 1400 Hz. While, the response frequency for the thermocouple without compensation was about 34 Hz, the compensation extended the effective response time of the thermocouple probe to increase by a factor of more than 40. The response time of the thermocouple increased with compensation (up to 1.4 kHz after compensating for the probe thermal inertia) to allow improved resolution of the turbulent mixing process which governs these flames. Earlier studies have also shown the presence of temperature fluctuations in swirling flames [20, 21]. Even with the small size thermocouples used it is required

to resolve the flame thermal behavior at high frequencies by corrections made to thermal inertia of the thermocouple.

To extend the frequency response of thermocouples to high frequencies, compensation to the thermocouple output must be carried out. In this regard it was required to specify the time constant that depends on temperature and velocity for a given thermocouple. The time constant is a function of local temperature and velocity in the flame, so that it varies at various spatial locations in the flame. The time constant was measured at different spatial locations in the flame by electrically heating the wire to some higher temperature and recording the temperature decay as a function of time in the computer program. This process was repeated up to 30 times at each position of the flame. Then the resulting temperature decay curves were averaged to obtain a smooth decay curve. This curve could be categorized as:

$$T(t) = T_o + \Delta T * e^{-\frac{t}{\tau}} \quad (2.8)$$

where, $\Delta T = T_{final} - T_o$, and T_o is measured initial temperature and T_{final} is measured final temperature. A time constant τ_T was defined as the value at which the overheat temperature ΔT has decreased by a factor $1/e$, figure 2.4. This time constant was used to compensate the thermocouple output for determining the true high frequency fluctuations. The effect of the radiation was also considered in the compensation, equation 2.5.

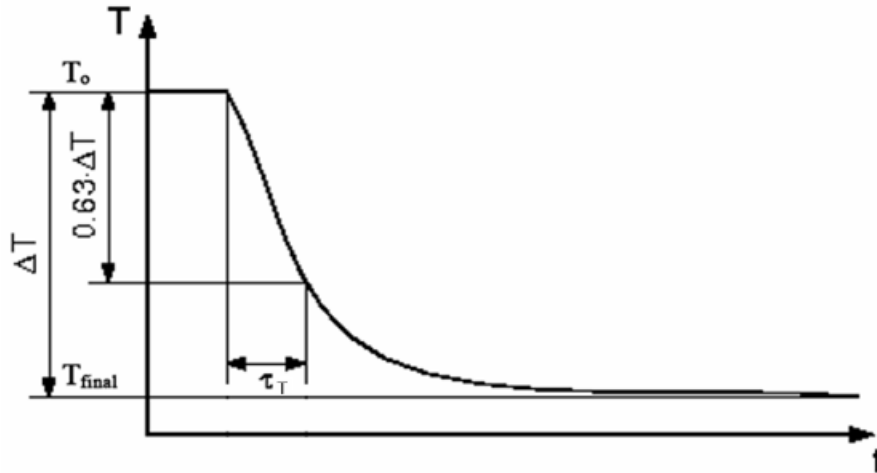


Figure 2.4. Characteristic temperature decay curve.

In our case, effective response time of the thermocouple probe was improved by a factor of 40 via the digital compensation technique. Temperature measurements were taken only on one half plane and the results were mirrored for the other half assuming flame symmetry. In order to obtain detailed information, temperature measurements were taken for a grid size of 10×30 (300 data points) with 10 radial locations and 30 vertical locations at 2.54 mm (0.1 inch) intervals. The value of time constants was measured at 60 locations in the flame. The time constant was then obtained at every measurement location (at every other measurement location) within the flame by interpolating the data. The hardware used for the mean and fluctuating temperature measurements is discussed elsewhere in sufficient detail [28].

2.4. Microphone probe

Several probe microphones were assembled and used to evaluate the pressure signals in a still and air jet environments. Probe diagnostics showing good promise to

seek additional information were then selected for initial calibration and subsequent additional insights on the sound pressure level fluctuations from within the flame. Three microphone probes that had same size and the same performance were used to measure pressure fluctuation levels at each special location from within the flame. The inside diameter of the water cooled probe used was 2 mm and the tip hole diameter was 1 mm in order to damp resonance and improve the frequency response from this probe. The microphone was placed at a distance of 120 mm from the entrance of the probe. The excited fluctuating pressure propagated down the probe and the signal measured at the microphone. Note that the pressure wave should not reflect and that the reflected wave should be weak and negligible. The results showed that the small condenser microphone used here had negligible pressure wave reflection effects using water cooled probe.

In turbulent flow region the instantaneous velocity include a mean value and fluctuating component of the velocity. Microphones are used to capture the fluctuating component of the dynamic pressure or dynamic pressure fluctuation. A condenser microphone is chosen as the transducer to detect fluctuating pressure. It is possible to measure the pressure fluctuations with the microphone probe. There is a relationship between the steady and fluctuating components of the pressure, velocity and density. Dynamic pressure is the difference between stagnation pressure and static pressure, and since it has a relation with kinetic energy of a fluid particle through the density, it can be written as:

$$P + P_d - 0.5 \times (\bar{\rho} + \rho') \times (U + u)^2 = 0 \quad (2.10)$$

where, P is mean of dynamic pressure, P_d is dynamic pressure fluctuation, $\bar{\rho}$ mean density of the gas, ρ density fluctuation, U mean velocity, and u velocity fluctuation. Considering a low turbulent intensity, and an isodensity turbulent flow, the dynamic pressure fluctuation can be given [31]:

$$\left(\overline{P_d^2}\right)^{0.5} = P \frac{2\sqrt{\overline{u^2}}}{U} \quad (2.11)$$

For flows where the turbulence intensity is too high an empirical fit can be used to correct Eq. 2.11. [32] This equation shows that the root-mean-square of the fluctuating pressure is proportional to the root-mean-square of the velocity fluctuation. Equation 2.11 shows that pressure fluctuation is proportional to velocity fluctuation. Hence the measured pressure fluctuations have directionality with respect to the reference frame of the burner. Equation 2.11 has been derived for isodensity turbulent flow which is not for the flame zone where the velocity and density fluctuations can occur at the same time. However, microphone probes are still expected to give good information on velocity fluctuation or density fluctuations in flame zone.

Microphone probes have been used to measure the local distribution of turbulent intensity in the flame [32, 33]. Measurements of the distribution of the pressure fluctuations were made here and turbulent intensity was not considered. The pressure fluctuation data provided information on the spatial distribution of noise sources in the flames. Dynamic pressure fluctuations have been done in three different directions

(homogeneous sensors) and pressure and temperature fluctuation have been performed simultaneously (heterogeneous sensor) to obtain a better understanding of application of these kind of sensors and sound generation in the flame.

In order for a microphone probe to be effective, the resonant qualities of the probe must be characterized. The probes used in the experiments with a condenser microphone were characterized and the performance characteristics examined. The calibration consisted of a measurement of the attenuation of pressure wave between the open end of the probe and the microphone (see chapter 4).

2.5. Microphone array

The sound pressure levels were measured using an array of condenser microphones at various axial positions above the exit plane of the burner. The microphones were housed in an array tower. The microphones were placed around the burner at a radial distance of 3.5 inches from the burner central axis. The microphone was 6mm in diameter and 3.4mm long having a nominal sensitivity of -35 dB +/- 4dB. The sound pressure levels (as amplitude-frequency spectra) were measured up to 25,000 Hz. Signal was measured and recorded using high-speed data acquisition cards. The data were acquired simultaneously using eight microphones. The samples were acquired at a sampling rate of 50 KHz for total time duration of 300 seconds. Data acquisition and analysis were carried out using Lab View software.

Figure 2.5.a shows the UMD swirl combustor in operation and condenser microphones used for acoustic data. Angular arrangement of the microphones around the premixed swirl combustor is shown in Figure 2.5.b. It shows the tower

constructed for housing the microphone array around the premixed swirl combustor. Microphones were attached to the towers at various heights of the combustor at 1 inch intervals starting from the combustor exit to a downstream position of eight inches downstream from the combustor exit. Spacing at smaller intervals did not yield statistically significant variations.

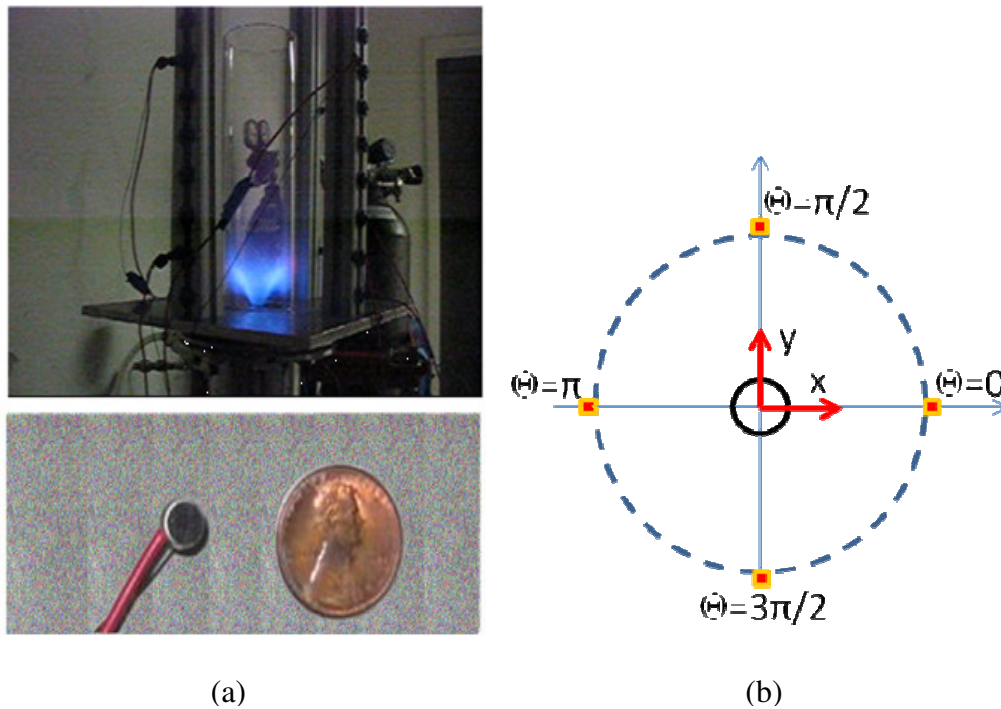


Figure 2.5. (a) Top: Tower for housing the microphone array around the premixed swirl combustor and Bottom: condenser microphone and its physical size as compared to one penny, (b) Angular arrangement of microphone array around the premixed swirl flame.

Chapter 3: Cross-correlation methods

To examine the correlations between sensors, the time delay of arrival of the signal was obtained from the measured time delays between two microphones. Most practical acoustic signal processing schemes are based on time difference of arrival estimation (TDOA). The time delay estimation techniques present various good improvements for acoustic source localization too [33]. Time delay estimation (TDE) between signals received at two microphones depends on type of the signal and especially gets degraded by the signal-to-noise ratio which is one of the main parameter for signal processing.

Time delay estimation may be affected by background acoustic noise, reflection, and other kind of noise associated in the system. Even different microphones from the same company could give different output signals for the same input signal. The time delay can be estimated under various SNR levels. The level of signal-to-noise ratio (SNR) is a logarithmic function as a ratio of power signals, affects the precision of these different methods.

Several methods were tested with different main and noise sources. It is found out that some of correlation methods offer better results for the same signal to noise ratio conditions while other methods do not. To find out which method will give better correlation result for our condition (combustion noise), four different time delay estimation methods are examined here using MATLAB program. These estimation methods were: cross correlation (CC), generalized cross correlation with phase transform (GCC-PHAT) [33, 34], generalized cross correlation with maximum-

likelihood estimation (MLE) and average square difference function (ASDF) [35, 36, 52].

In acoustic source location by means of microphone array requires accurate time delay estimation to achieve a desired degree of precision. It is connected to the high speed of sound pressure transmission when considered in connection with the distance between microphones placed in a given space. Weighting functions have been used to improve the performance of TDOA. The cross correlation (CC) algorithm with selecting the correlated expectation function correlates the recorded signals and considers the time delay value that maximizes the value of the correlation function.

Techniques such as CC, GCC-PHAT, MLE and ASDF methods were used for TDOA estimation. A Comparison of location estimations with different methods is presented [38]. These methods can give excellent results if the source is selected as a white noise (with a flat power spectral density). The shape of the correlation function, the source signal and type of noises modifies the shape of the cross correlation function. Average square difference function (ASDF) is just subtract the values based on the minimum difference between signals from the microphones and the time delay estimation.

The GCC-PHAT and MLE methods are based on maximizing certain expected function. ASDF algorithms have been used to compare the cross correlation of microphone signals with the signal from reference microphone. The numerical simulations were carried out in Matlab program and favorable algorithms identified. The numerical simulation results obtained from them are compared in terms of

precision. The experiments were carried out in a large open room to reduce the reverberation effects. Two microphones, separated by a fixed distance (d), were employed to estimate the time delay between the two signals. In each case a single sound source was employed to generate the sound and different algorithm was employed to estimate the time delay between a pair of microphones to examine the precision of each method.

3.1. Methodology

To find out which correlation method will give better results acoustic source localization technique has been used to determine the positional location of an acoustic source relative to some defined reference frame. Acoustic source present in the near field to a combustor can be localized with data on the time difference of arrivals measured using a pair of microphones and known speed of sound in the medium containing the acoustic source.

Most practical acoustic noise source localization schemes are based on time difference of arrival estimation due to their conceptual simplicity, reasonably effective in moderately background noise and reverberant environments. Time delay estimation is used to localize the targets depending on the sound [33].

The signal received at 2 microphones separated by a specified distance can be modeled by:

$$\begin{aligned} r_1(t) &= s(t) + n_1(t), \\ r_2(t) &= a_2 s(t - \tau) + n_2(t), \end{aligned} \quad 0 \leq t \leq T \quad (3.1)$$

where, $r_1(t)$ and $r_2(t)$ are the outputs signals of two separated microphones, $s(t)$ is the source signal, $n_1(t)$ is the additive noise to the first microphone and $n_2(t)$ is the additive noises to the second microphone, a_2 represents the relative signal attenuation, T denotes the observation interval, and τ yields the time delay between the two received signals.

3.1.1. Correlation methods

Time difference of arrivals was measured with a pair of microphones. Selected algorithms were considered that were used to estimate the time delay. These methods estimate the time delay between two signals that varies in their precision and complexity. Four methods used here were cross correlation (CC) method, generalized cross correlation with phase transform (GCC-PHAT) method, generalized cross correlation with maximum-likelihood estimation (MLE) method, and average square difference function (ASDF) method. In the following a brief consideration about these methods is presented.

3.1.1.1. CC method

Cross correlation method determines the degree to which the signals are correlated with other signal. Maximum value of evaluated function provides the time delay value of the cross correlation function. This method especially is considered efficient in a case where there is low reverberation or reflection with high signal-to-noise ratio.

3.1.1.2. GCC-PHAT method

Generalized cross correlation with phase transform method normalizes the cross power spectrum of the signals to some constant value. This method especially is

efficient in a case where there is low reverberation or reflection with high signal-to-noise ratio. This method usually can provide very sharp correlation peak. This method works in frequency domain.

3.1.1.3. MLE method

Generalized cross correlation with maximum-likelihood estimation method (based on expectation function) the time difference of arrival is the value that maximizes the likelihood function of the observed data. This method works in frequency domain which is associated with the generalized cross correlation family with different expectation function.

3.1.1.4. ASDF method

Average square difference function method just subtracts two different signals. So it can be derived from finding the position of square of the minimum error received from two signals. Similar other methods, it gives very good estimation in the absence of noise. ASDF method requires no multiplication, which probably is the most considerable advantage of this method over the other methods, but it took considerable time for calculation.

3.2. Experimental setup

These investigations were carried out using both numerical simulation and experimental methods. A pair of spatially separated microphones and a single sound source which was capable of generating diverse types of sound was used. The signals received at the two microphones were processed using cross correlation method to estimate the time delay between them. The distance between the noise source and first

microphone was 152 mm in a normal lab environment. The microphones were located in a straight line away from the sound source and were at a distance of 610 mm apart.

Broadband sound signals were used for the sound source. Data acquisition card (equipped with anti-aliasing filters) was used. The samples were obtained at a sampling rate of 50 KHz that allowed for simultaneous acquisition of data from the 4 channels, using Lab View software. The signals from the two microphones were then processed in Matlab and time delay between the signals estimated using various above defined algorithms.

3.3. Results and discussion

Acoustic noise source carry ambiguity in the TDOA estimation. Beside noise, in reverberation media multipath effects may arise as property of reflection on surrounding walls. This may cause reflected sound waves to reach the microphones after the main direct signal. These reflections cause dissimilarity between recorded signals by microphones that increases with increase in distance. The dissimilarity between signals causes TDOA estimation to become unreliable and imprecise [36, 39].

The distance between each pair of microphones cannot be made large without reducing the coherence between the signals that their delay must be estimated. In our case, performance of various TDE algorithms were compared for different cases at various levels of SNR and best method identified. The numerical simulation and experimental results are presented below. In this regard SNR mechanism is

considered the undesirable noise in the form of reverberation, background, mechanical, and any kind of the noise at the microphone output.

3.3.1. Simulation results

The four algorithms for time delay estimation have been simulated using Matlab program. Firstly, the source signal is taken to be white noise which is a random signal with a flat power spectral density. In other words, the white signal contains equal power within a fixed bandwidth at any center frequency. White noise was recorded with microphone from another white noise signal. The numerical simulation carried out by adding two simulated noise signals $n_1(t)$ and $n_2(t)$.

Secondly, the source signal taken from the combustion noise was recorded from the premixed flame. The numerical simulation were carried out using the simulated noisy signal, wherein the additive random signal noises were $n_1(t)$ and $n_2(t)$. Thirdly, the combustion noise was used with two different noises $n_1(t)$ and $n_2(t)$. These noises were recorded with one microphone at two different times from the background noise in the lab environment. Fourthly, the combustion noise was superimposed on the previously recorded $n_1(t)$ noise with one microphone (the background noise in the lab). Finally, the combustion noise was used with different noises $n_1(t)$ and $n_2(t)$. These noises were recorded with two microphones simultaneously from the background noise in the lab.

The numerical simulations were carried out with 25000 data points in all cases. The signal was then delayed by a time period of 0.8 ms to estimate the performance

of all methods. The time delay estimation between the two signals was carried out by the four methods described above.

3.3.1.1 TDE using various algorithms

Four methods have been simulated in Matlab. They include cross correlation, generalized cross correlation with phase transform, generalized cross correlation with maximum-likelihood estimation (MLE) and average square difference function methods. In order to simulate different signals with the noise signal, white and combustor sound recorded. These signals are used in Matlab and have been used as sound source signals. Two uncorrelated signal sound noise was used to evaluate the performance of each method. One of the two signals was delayed to show the time that the signal needs to reach to the other microphone. The second signal delayed by 0.8 ms. The time delay estimated between the two signals by the four methods.

Figure 3.1 shows the cross correlation results for various TDE algorithms namely CC, GCC-PHAT, MLE and ASDF methods. The x coordinate denotes the time delay while y coordinate denotes the resultant cross correlations. The y coordinate for ASDF shows the error square of the two difference signals. For evaluation, this test was carried out using a combustor sound and time delay was 0.8 ms. In order to simulate the real situation, combustion sound from our turbulent premixed flame was recorded by microphone and chosen as a sound source signal.

All the four TDE methods gave the correct estimated time delay of 0.8 milliseconds for high SNR levels. Figure 3.1 shows the performance of the different algorithms when noise was increased in the given signal to noise ratio equal to -8.12.

CC, GCC-PHAT and ASDF methods gave the correct time delay while the MLE method completely breaks down and were not able to predict the time delay at all.

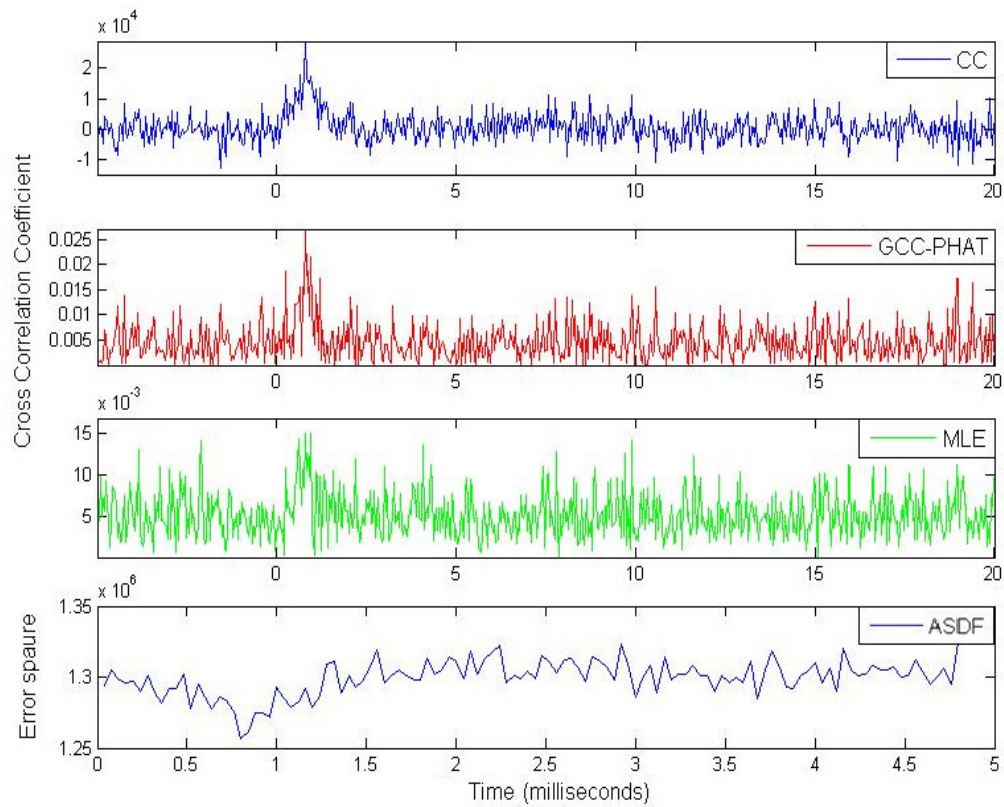


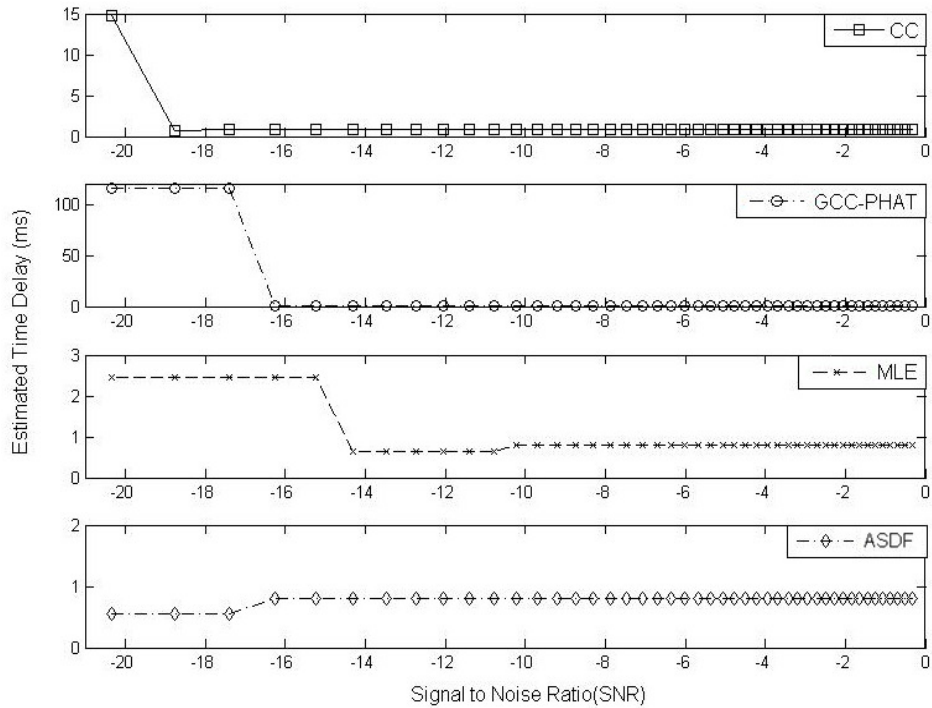
Figure 3.1. Time delay estimation for combustion noise by various algorithms (SNR = -8.12)

The results show that the CC and GCC-PHAT and ASDF methods have a better performance than MLE. CC, GCC-PHAT and ASDF worked very well in recorded combustion noise.

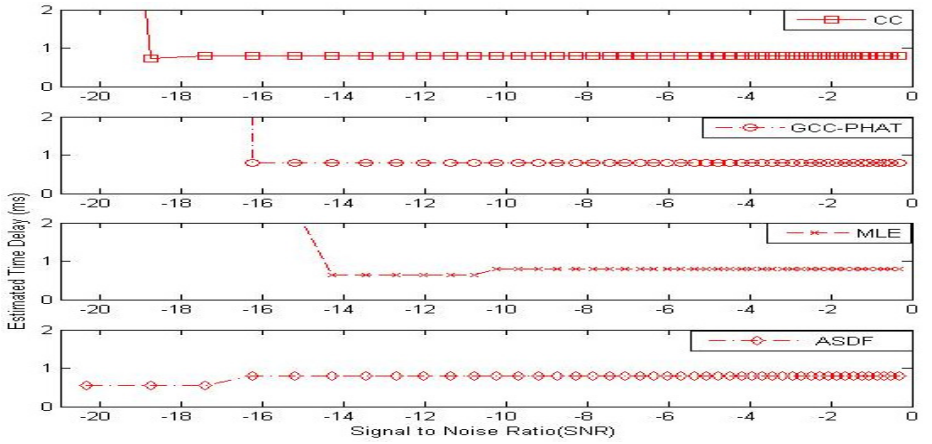
3.3.1.2 Signal-to-noise ratio (SNR)

Figure 3.2 shows time delay estimation (TDE) for different SNR levels under simulated white noise condition. The time delay was estimated under various SNR levels. Figures 3.3 and 3.4 show the results for real combustion noise case for

different kind of noises. These figures show that each method gives correct answer until some minimum value of SNR. When the time delay showed 0.8 ms for the time delay the method work good. While, any number below or above this correct time delay show that the method failed.

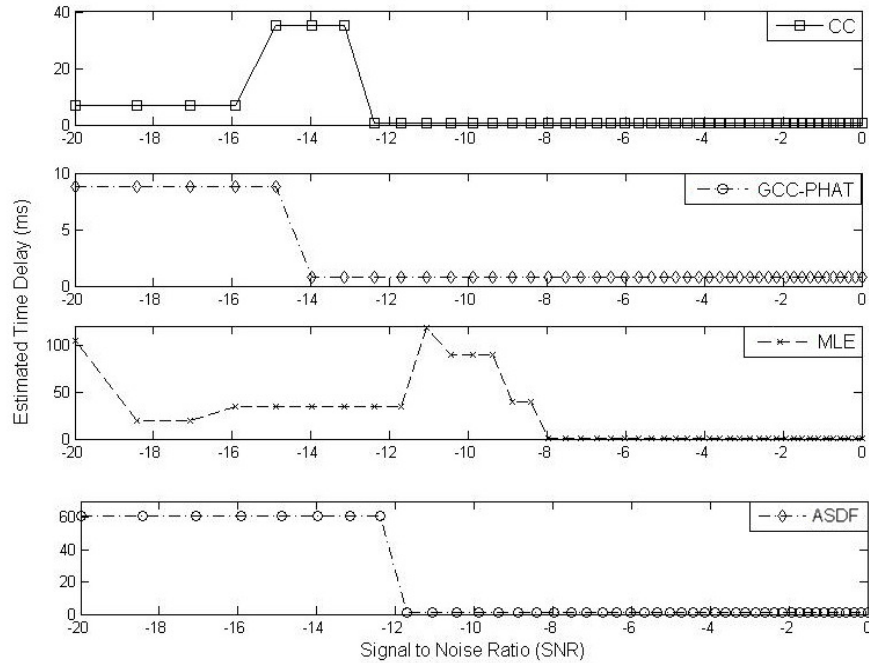


(a)

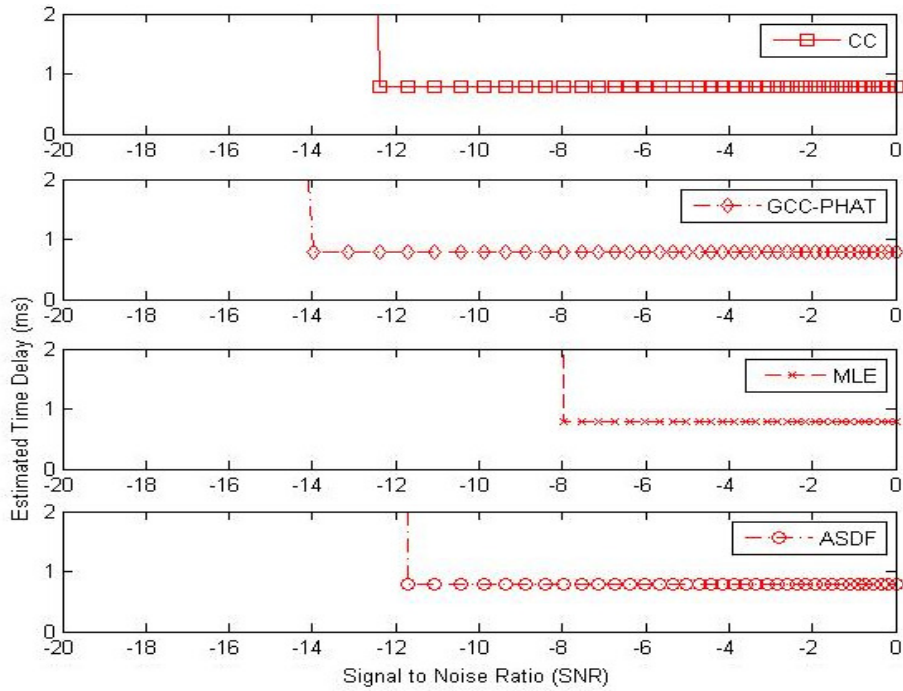


(b)

Figure 3.2. Time delay estimation accuracy for different SNR levels for white noise (a). Zoomed view of the graphs (b).

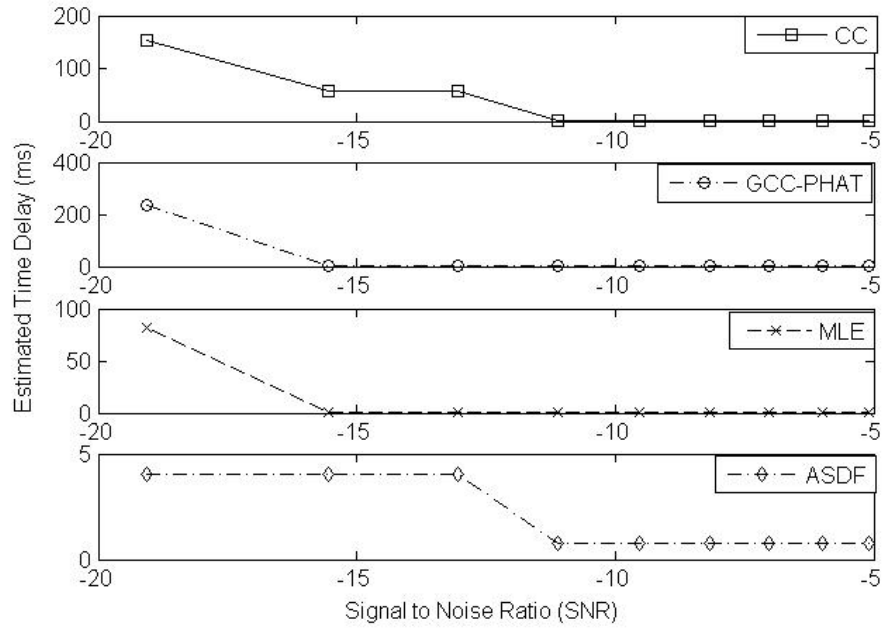


(a)



(b)

Figure 3.3. Time delay estimation accuracy for different SNR levels for real combustion noise and simulates noises (a). Zoomed view of the graphs (b).



(a)

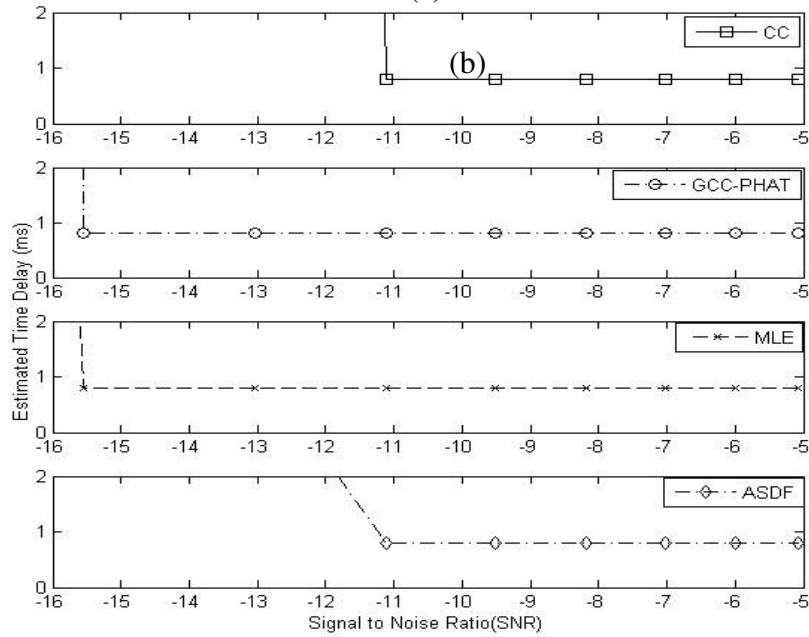


Figure 3.4. Time delay estimation accuracy for different SNR levels for real combustion noise and noises from two uncorrelated noise microphones (a). Zoomed view of the graphs (b).

CC method has the smallest SNR for the white noise case, while GCC-PHAT has the smallest SNR in combustion noise case and two added simulated noise signal. But, GCC-PATH has the smallest SNR in combustion noise condition and two added signals recorded with two microphones. The phase information was used in GCC-PHAT method. The results show that CC method provides better performance for white noise, while the GCC-PHAT method provides better performance for real combustion noise.

Also figures 3.4 and 3.5 show the results of real combustion noise for the case of different kinds of noise signals. These figures have been shown to demonstrate the effect of noise signals on the SNR values. Each method has its own SNR value limit. Above this value, the estimated time delay becomes accurate and it fails below the SNR value limit. A comparison of the SNR values from figure 3.2 to 3.4 with those of figures 3.5 and 3.6 depicts higher SNR values in the later figures (see figures 3.5 and 3.6). This observation is due to the signal correlation between the noise signals which add up to the main signal source.

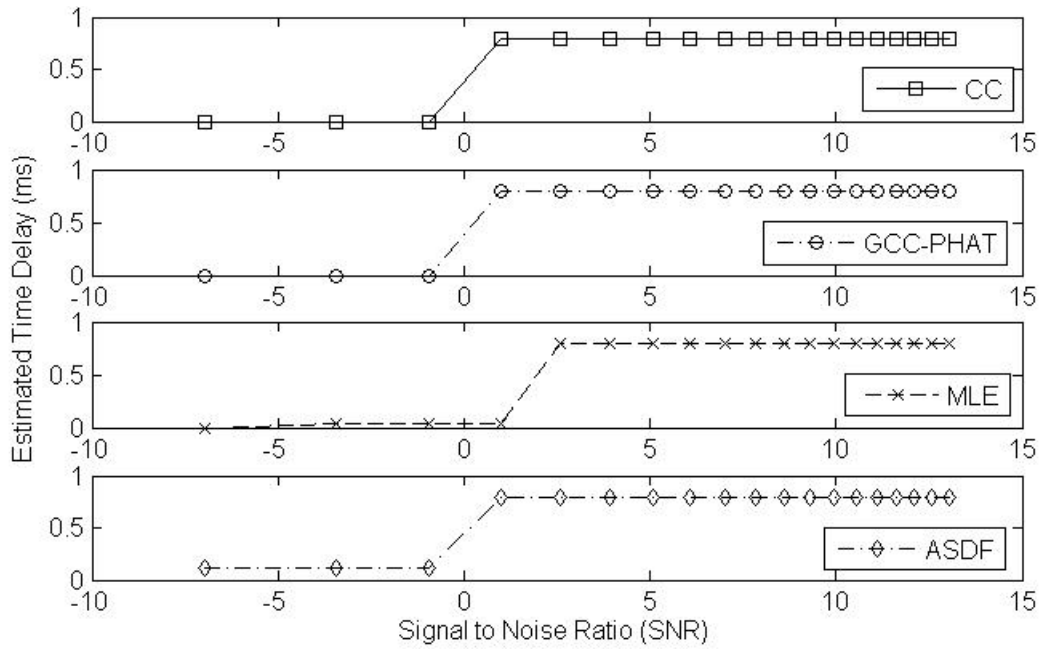


Figure 3.5. Time delay estimation accuracy for different SNR levels for real combustion noise and noise with addition of two equal background noises

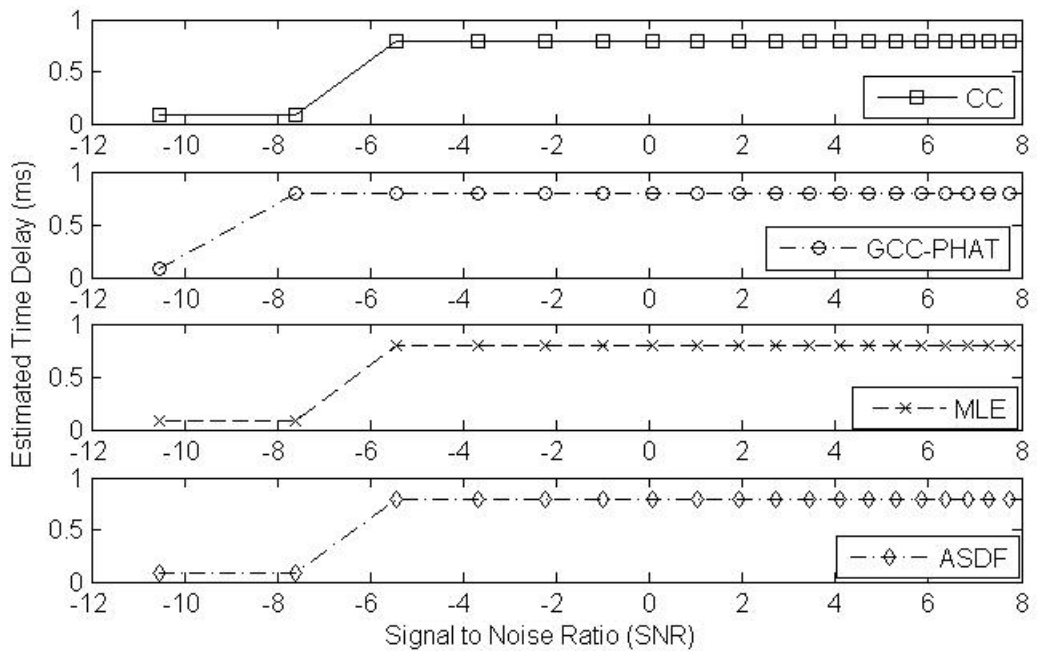


Figure 3.6. Time delay estimation accuracy for different SNR levels for real combustion noise with the additional of two background noises recorded simultaneously.

Figures 3.5 and 3.6 show that GCC-PHAT has the smallest SNR in combustion noise condition. This reveals that GCC-PHAT method provides better performance for real combustion noise.

Figures 3.2, 3.3 and 3.4 show that the values of SNR were smaller than that observed in practical values. The correlation between two signals is:

$$R_{1,2} = R_{s1,s2} + R_{s1,n1} + R_{s1,n2} + R_{s2,n1} + R_{s2,n2} + R_{n1,n2} \quad (3.2)$$

where, $R_{s1,s2}$ is the correlation between signal sources s1 and s2. $R_{s1,n1}$ is a correlation between signal source s1 and noise n1. $R_{s1,n2}$ is a correlation between signal source s1 and noise n2. $R_{s2,n1}$ is a correlation between signal source s2 and noise n1. $R_{s2,n2}$ is a correlation between signal source s2 and noise n2. $R_{n1,n2}$ is a correlation between noise n1 and noise n2.

Case 1: White source and two uncorrelated noise sources, figure 3.2:

$$R_{s1,n1} \approx R_{s1,n2} \approx R_{s2,n1} \approx R_{s2,n2} \approx R_{n1,n2} \approx 0$$

So, only one term is not zero. Therefore the correlation between signals is:

$$R_{1,2} \approx R_{s1,s2}$$

Case 2: Combustion noise and two uncorrelated noise sources, figure 3.3:

$$R_{s1,n1} \approx R_{s1,n2} \approx R_{s2,n1} \approx R_{s2,n2} \approx R_{n1,n2} \approx 0$$

So, only one term is not zero. Therefore the correlation between signals is:

$$R_{1,2} \approx R_{s1,s2}$$

Case 3: Combustion noise and two semi-correlated noise sources (two noises recorded at different time form background noise), figure 3.4:

$R_{s1,n1} \approx R_{s1,n2} \approx R_{s2,n1} \approx R_{s2,n2} \approx 0$ and $R_{n1,n2} \neq 0$ (but its value is close to zero).

so, only two terms is not zero. Therefore the correlation between signals is:

$$R_{1,2} \approx R_{s1,s2} + R_{n1,n2}$$

It is interesting that in this case the difference in SNR between CC and PHAT method is more than other cases.

Case 4: Combustion noise and two same noise sources, figure 3.5:

$$R_{s1,n1} \approx R_{s1,n2} \approx R_{s2,n1} \approx R_{s2,n2} \approx 0$$

so, only two terms is not zero. Therefore the correlation between signals is:

$$R_{1,2} \approx R_{s1,s2} + R_{n1,n2}$$

Case 5: Combustion noise and two correlated noises recorded background noise with two microphones simultaneously, figure 3.6:

$$R_{s1,n1} \approx R_{s1,n2} \approx R_{s2,n1} \approx R_{s2,n2} \approx 0$$

so, only two terms are not zero. Therefore the correlation between signals is:

$$R_{1,2} \approx R_{s1,s2} + R_{n1,n2}$$

The difference between case 4 and 5 is that in case 5 $R_{n1,n2}$ has less correlation than case 4.

3.3.2. Experimental results

The experiments were carried out in an open room environment. A single sound source was used to generate different kinds of noise. The different kinds of noise used in a given experiments included white noise, brown noise, grey noise, pink noise and purple noise [53]. A single sound source speaker was used as the sound source for

generating different kinds of noises. The microphones were separated by a known distance of 610 mm.

A single sound source speaker was used to generate two kinds of noise sources and the signals were recorded by the microphones placed at a given distances from the source (speaker). The microphones were placed 610 mm apart. The sound source was excited using a broadband signal and the signal was captured by each of the microphones. The time difference of arrival was estimated from the captured audio signals. The TDOA for a pair of microphones and the source is defined as the time difference between the signals received by the two microphones.

The time delay between the two microphones for brown noise and gray noise was calculated using CC algorithm owing to its simplicity and effectiveness at low SNR. Figures 3.7 and 3.8 show the cross correlation coefficient plot for the received signals by two microphones for brown and gray noise sources, respectively.

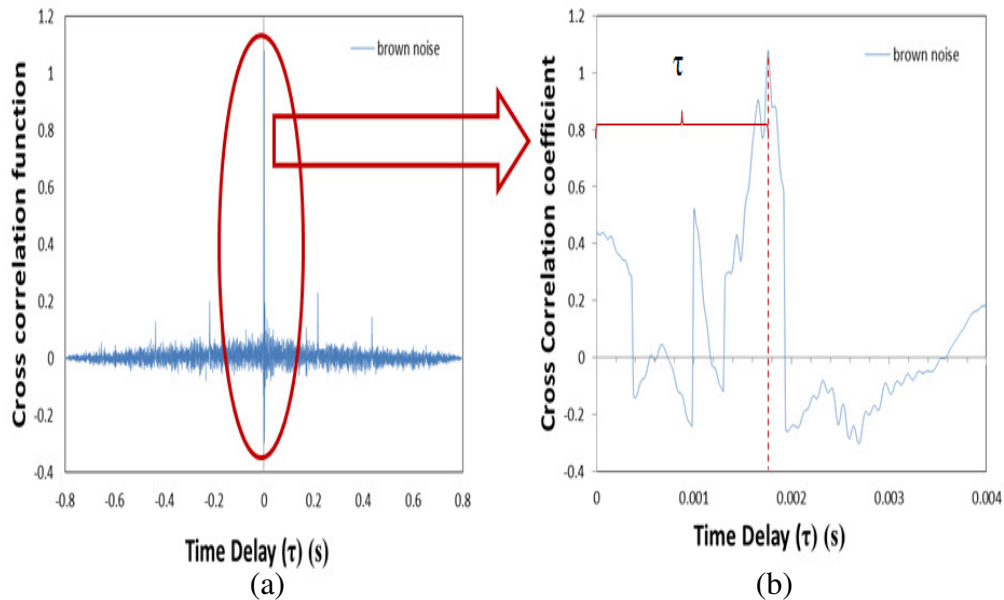


Figure 3.7. (a) Cross-correlation function versus time delay for brown noise (b) zoomed view of the graph in (a).

The value of τ that maximizes this cross correlation function gives the estimated time delay. Experimentally the time delay was calculated to be 1.74 milliseconds. The theoretical time delay between the 2 microphones was calculated to be 1.76 milliseconds. The CC algorithm works efficiently in estimating the time delay between the 2 microphones in real practical environments. The error associated with the CC technique in estimating time delay was found to be 1.1 %, which is due to the room reverberation and additive noise effects.

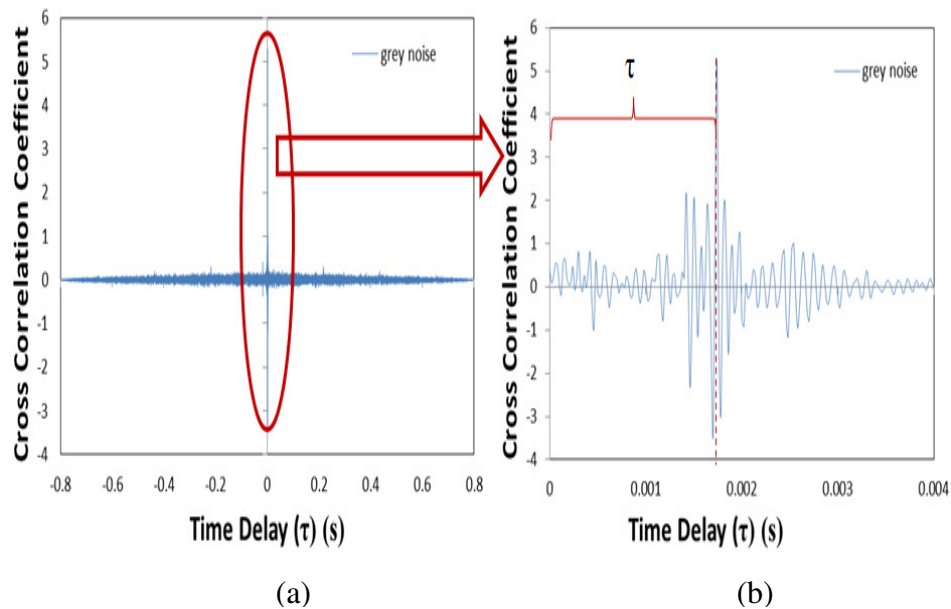


Figure 3.8. (a) Cross-correlation function versus time delay for gray noise (b) zoomed view of the graph in (a).

The time delay between the two microphones for pink noise and white noise was calculated using CC algorithm owing to its simplicity and effectiveness at low SNR. Figures 3.9 and 3.10 show the cross correlation coefficient plot for pink and white noise sources, respectively.

The value of τ that maximizes this cross correlation function gives the estimated time delay. Experimentally the time delay was calculated to be 1.74 milliseconds. The theoretical time delay between the 2 microphones was calculated to be 1.76 milliseconds.

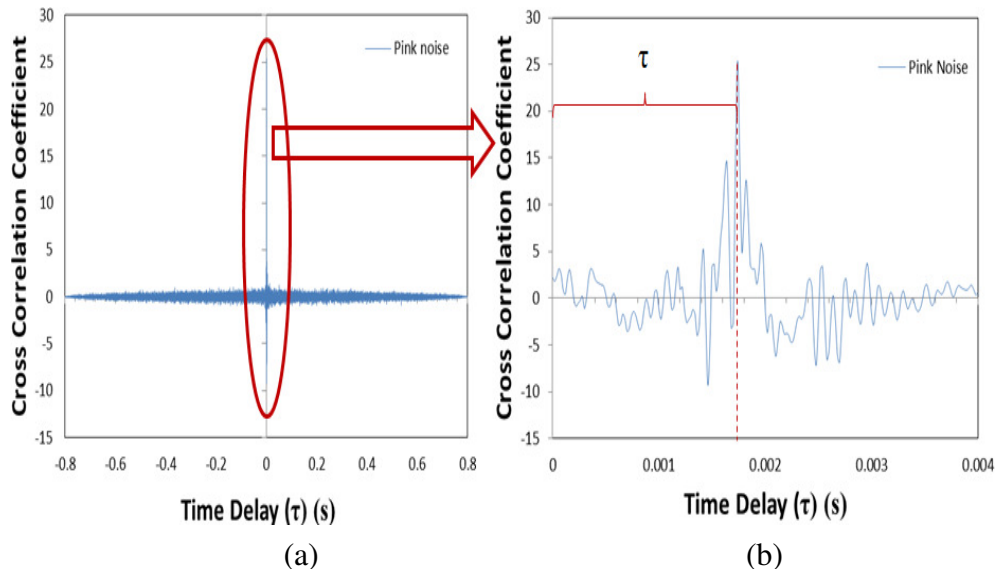


Figure 3.9. (a) Cross-correlation function versus time delay for pink noise (b)

zoomed view of the graph in (a)

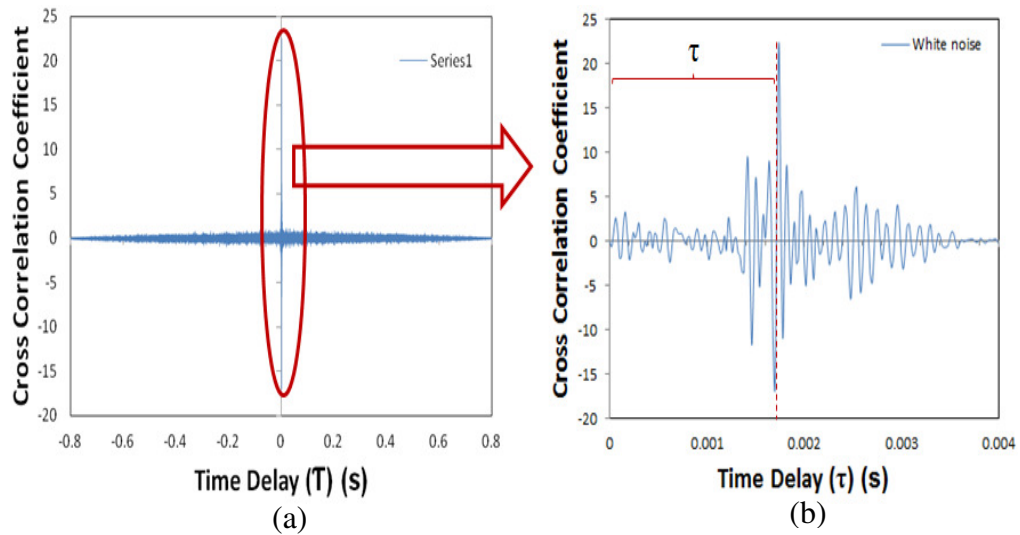


Figure 3.10. (a) Cross-correlation function versus time delay for white noise (b)

zoomed view of the graph in (a).

3.4. Summary

In the simulation for white noise, CC and GCC-PHAT approved because of their better results. In the different combustion noise cases, GCC-PHAT seems to be more favorable. The accuracy of all methods decreases in estimating the time delay under different combustion sound. When the signal to noise ratio was below specified value, the estimated time delay by all methods were degraded. Experiments were carried out in the real combustion and different cases using CC algorithm to estimate the time delay. The results with different sound were found to be in good agreement with the theoretical calculations. However, minimum error of 1.1 % was found to estimate the time delay using the CC algorithm which could be due to reflection and additive noise effects. The results show that the time delay method can be used to locate a noise source in a combustor or gasifier in addition to the overall sound pressure levels from the noise source. Thus the incorporation of multi-sensors in a test unit can help assist in gaining more information in reactors and gasifiers.

Chapter 4: Calibration

4.1. Thermocouple

Calibration of the thermocouple is necessary for reliable experimental results. To minimize the effect of radiation and the effect of oxidation on thermocouple performance, new shiny thermocouples were used here. The R-type thermocouple can be used up to temperature of around 1800 °C. The DC offset adjustment of the thermocouple signal was performed for calibration purposes. Two thermocouple with the ends one centimeter apart were positioned together to assure that they measure the same temperature. The Lab view program acquires the analog outputs of the thermocouple and transforms the voltage into temperatures using the given calibration function in the program. Any time the temperatures are equal one achieves the DC offset. Therefore, it is possible to determine if recalibration is necessary or not (based on the size of offset). When the offset reaches the value with small divergence, it is defined as a variable in the program.

4.2. Microphones

Panasonic WB-61A condenser microphones with diameter of 6mm and 3.4mm long having a nominal sensitivity of -35dB +/- 4dB were used for noise and pressure fluctuations measurements. Microphone sensors have linear high sensitivity and they can be used in large range from 20 Hz to 25,000 Hz. The sensitivity of each microphone was established before experiment with calibrator- Bruel & Kjaer 4321 – for calibration at 94 and 114dB SPL. The calibration pressure of 94 ± 0.2 dB re 20 μ Pa

is equal to 1 Pa (1 N/m²). The +20 dB level step gives 114 dB SPL which is convenient for calibration in noisy cases. The sensitivity of each microphone was established before experiment at 94 dB re 20 μ Pa (1 Pa at 1 kHz) and 114dB (10 Pa at 1 kHz). Signal was measured and recorded using high-speed data acquisition cards. The samples were acquired at a sampling rate of 50 KHz for a total duration of 300 seconds. The calibrator gives a constant sound pressure level during the tests. Data acquisition and analysis was carried out using LabView software. The sensitivity of the each microphone can then be adjusted in the written software in LabView until it indicates the correct sound pressure level.

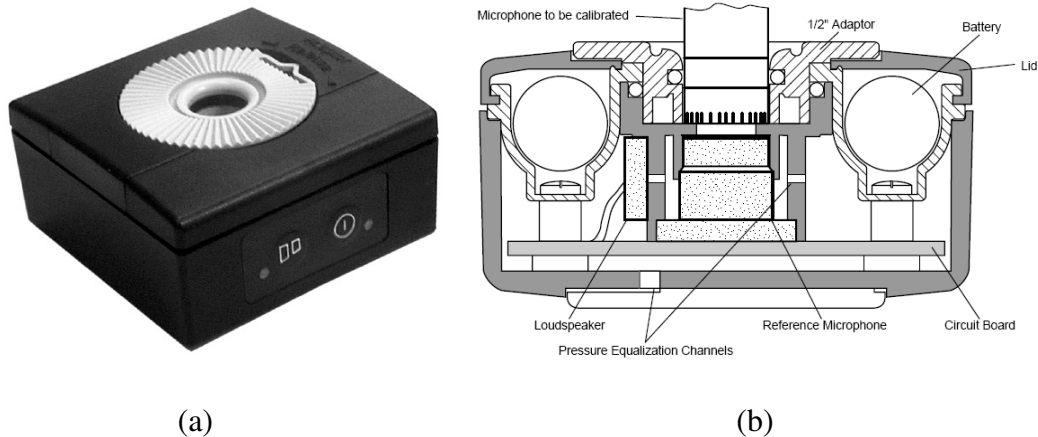


Figure 4.1. Calibrator toolbox was employed for calibration of microphones. (a) Calibrator view. (b) Cross-section view.

4.3. Microphone probes

Measurement of fluctuating pressure is a common requirement in combustion diagnostic. This measurement is required to know the structure of the flame accurately [40]. This measurement is appropriate to study the flame dynamics of the

flame. For a microphone probe to be effective the resonant qualities of the microphone probe must be characterized [40- 43]. The calibrations done consisted of measurement of the attenuation of pressure wave between the open end of the probe and the microphone.

Figure 4.2 shows a sketch of the microphone probe test procedure used with speaker and air jet. For the air jet test two condition were considered; with and without temperature gradient in the probe. The pressure fluctuation to be measured, P_d , excites a dynamic pressure fluctuation at the microphone probe, P_m . The microphone probe was calibrated for frequency response characteristics; frequencies spectrum, and pressure ratio.

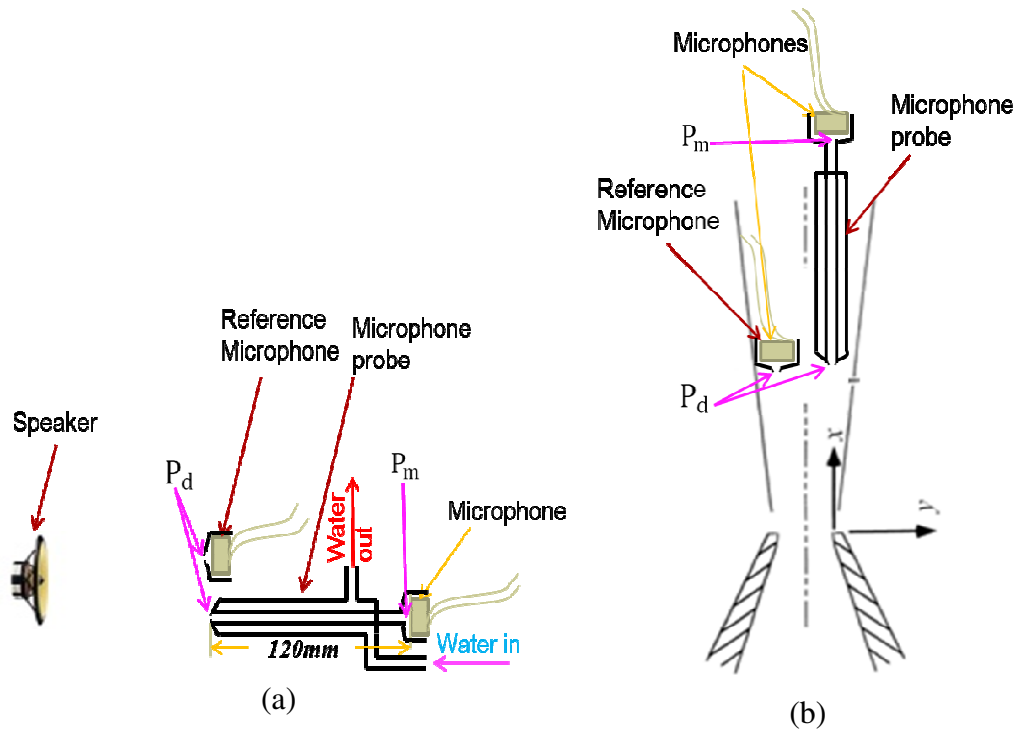


Figure 4.2. Set-up for calibration of the microphone probe. (a) Test with speaker.
(b) Test with an air jet.

The data was recorded and analyzed. The analysis was performed with a resolution bandwidth of 1 Hz, and averaged over $N_a=250$ samples. The random error apparent in the spectral estimation has been estimated to be about 10 % of the measured value.

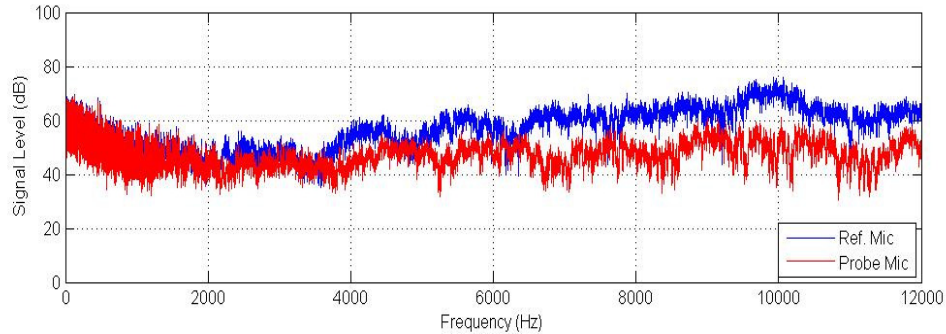
4.3.1. Performance characteristics via noise source

Several tests were carried out for the specific conditions encountered in our experiment and measurement system. First, the frequency of the microphone probe was compared with another microphone, figure 4.3. White and combustion noises were used in these acoustic experiments with a resolution bandwidth of 1 Hz. Secondly, signal coherence between the signals acquired through condensed microphone and the microphone probe was studied and investigated. The spectral coherence is a statistic that can be used to examine the relationship between two signals or data sets. It is commonly used to estimate the power transfer between input and output of a linear system. The coherence function between two signals $x(t)$ and $y(t)$ is a real valued function that is defined as [43],

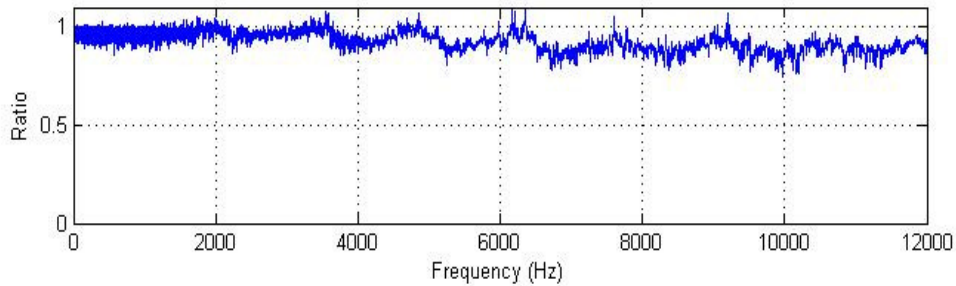
$$\gamma_{xy}^2(f) = \frac{|G_{xy}(f)|^2}{G_{xx}(f)G_{yy}(f)} \quad (4.1)$$

where, G_{xy} is the cross spectral density between x and y , and G_{xx} and G_{yy} the auto spectral density of x and y respectively. Figure 4.3.a shows the response of microphone and microphone probe. The difference is from the effects of the probe

that was 120 mm long. This figure shows that the signal from the microphone probe closely resembles the microphone. The probe performance is plotted as ratio Ref. Mic/ Probe Mic (P_m/P_d) versus frequency so as to compare the spectral response from the two microphones, figure 4.3.



(a)



(b)

Figure 4.3. Output signal spectrum for white noise, $Na=250$. (a) The reference and probe microphones. (b) The probe performance spectral response plotted as ratio Probe Mic / Ref. Mic versus frequency.

It was found that amplitude ratio between the two microphones is almost unity in the combustion noise frequency spectrum ($f < 1500$ Hz). However, above 2 KHz, the pressure amplitude ratio between the 2 microphones falls below unity. Hence,

microphone probe data must be compensated in various frequency bands, by utilizing the information of average pressure amplitude ratio in respective bands. In the measurements with microphone probe, great care was taken to compensate the data in various frequency bands.

The signal spectrum from the two microphones was examined from the similarity between the two signals from the ratio of P_m/P_d (input/output) using the coherence function. Assuming linear propagation and no external noise, the signal from the second microphone should be coherent with the first microphone, independent of propagation path or reverberation between the two microphones. Figure 4.4 shows the spectral measurements with the two microphones. This result shows the calculated coherence and phase ϕ between the reference and probe microphones.

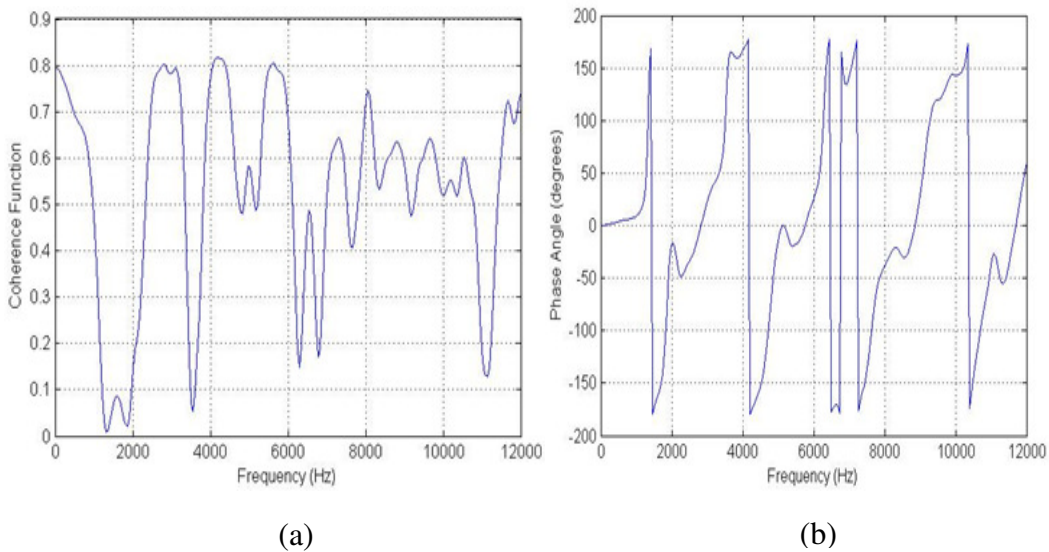


Figure 4.4. Coherence function and phase angle between reference and probe microphones (for White noise) experiment ($N_a=250$ samples). (a) Coherence function spectrum. (b) Phase angle spectrum.

The coherence function is near 0.8 at some frequencies, except for some frequencies. The destructive interference sometimes drop the spectrum into in coherence function at certain frequencies and are due to the interference pattern and background noise, causing a loss of coherence. This type of (notching) of coherence function is commonly observed and is not so important [43]. However, the phase data are relatively clean, with a ramp function closely corresponding to $\phi = .35 \times 10^{-3} (2\pi) f$ with a single propagation time delay of 0.35 msec, which almost corresponds to the time required for sound to propagate a distance between two microphones (120 mm).

Correlation was carried out in order to compare the performance. Figure 4.5 shows the three different time delay estimation methods examined here. Three different time delay estimation methods examined here include; cross-correlation (CC), generalized cross correlation with phase transform (GCC-PHAT), generalized cross correlation with maximum-likelihood estimation (MLE). The correlation peak occurs at time delay of 0.35 ms and this supports general agreement of the actual probe geometry. These methods are considered in more details in next sections.

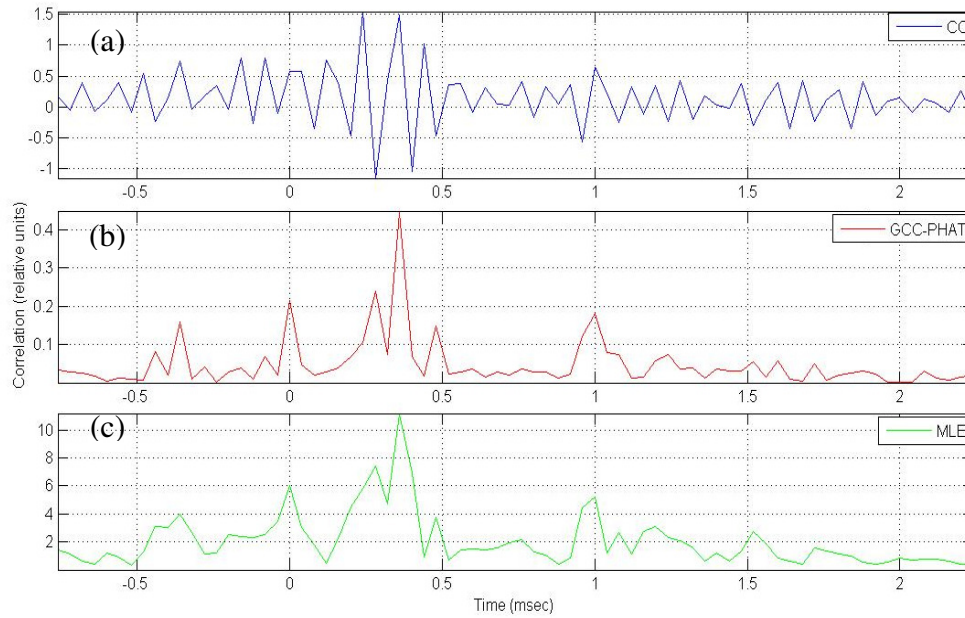


Figure 4.5. Cross correlation function for acoustic experiment (white noise) with resolution bandwidth of 1 Hz. (a) CC. (b) GCC-PHAT. (c) MLE (Na=250).

4.3.2. Performance characteristics via air flow

The reference (without a probe) and probe microphones were examined with uniform air stream flowing directly into the microphone probe in an isothermal setting, figure 4.6.a. Pressure fluctuations were measured from the two microphone arrangements. Figure 4.6.b shows the ratio of P_m/P_d versus frequency for the two microphone arrangements. The results show that this ratio is around 0.9. The microphone probe data was then compensated against the actual data by using the amplitude ratio behavior determined earlier between the probe microphone and direct microphone. It should be noted that average value of amplitude ratio in various frequency bands was chosen to compensate for the microphone probe measurements.

The microphone probe data was compensated in various frequency bands to give actual realistic data.

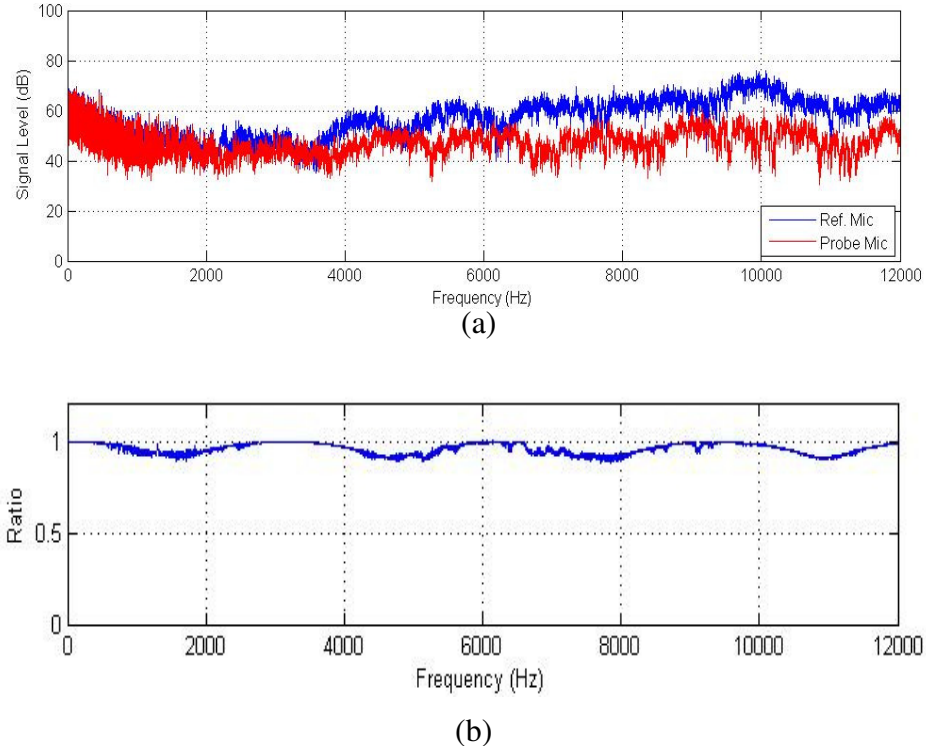


Figure 4.6. Output signal spectrum for cold flow, $Na=250$. (a) The reference and probe microphones. (b) The probe performance spectral response plotted as ratio Probe Mic / Ref. Mic versus frequency.

The correlation between microphone probe and reference microphone was determined, (see figure 4.7). The resulting coherence and phase measurements were calculated with a resolution of 1 Hz over the frequency range from zero to 12000 Hz. Figure 4.7 (c) shows time delay estimation method. The correlation peak occurs at time delay of 0.35 ms and this supports general agreement of the actual probe geometry. Other methods failed to give the correct time delay.

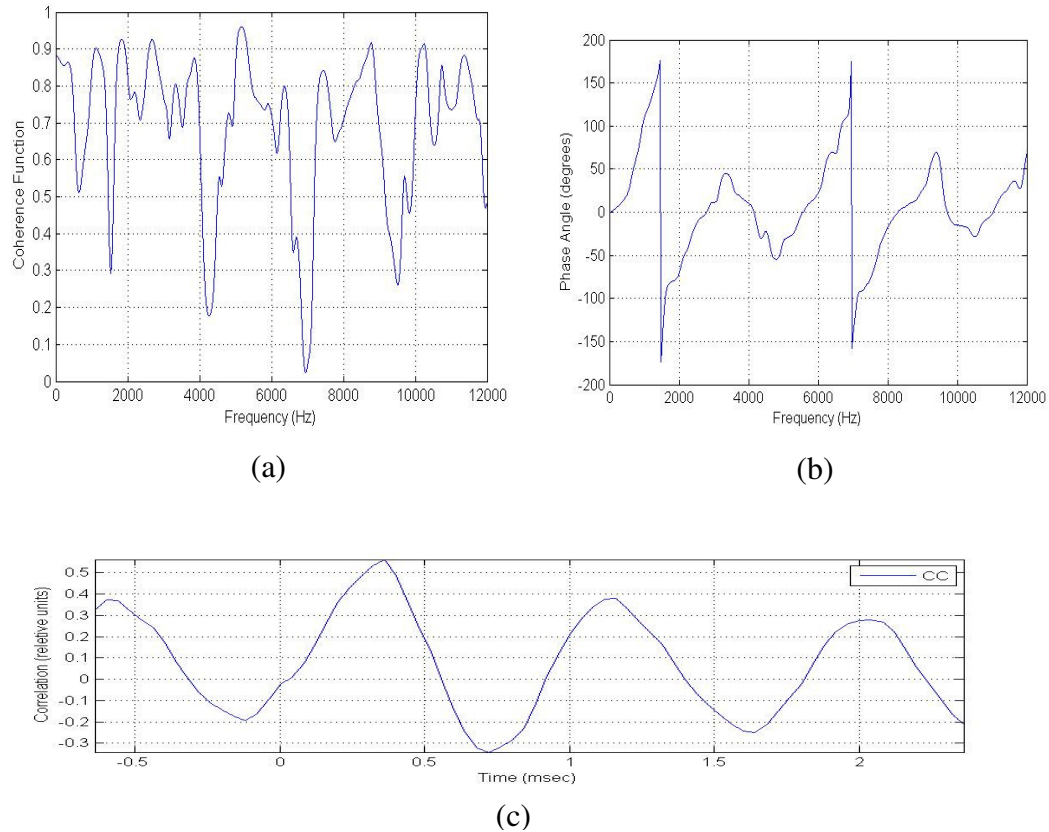


Figure 4.7. (a) Coherence function. (b) Phase angle spectrum for microphone probe and reference microphone. (c) Cross correlation with resolution bandwidth, of 1 Hz from $N_a=250$ samples using air jet.

The tip of the probe was heated and the performance characteristics evaluated with the temperature gradients presence in the probe. The effect of 240°C temperature gradient over first 6 mm length of the microphone probe was examined. Figure 4.8 shows the probe performance spectral response plotted as ratio for the microphone probe and reference condenser microphone.

Figure 4.9 shows the correlation function and phase angle results for the microphone probe and reference condenser microphone. The coherence is almost the

same with no major effect of temperature gradient at most frequencies. The dip in coherence function at certain frequencies is due to interference pattern in the probe. The phases were more complicated ramp function. It shows that the temperature gradient to the very front of the microphone probe does not change the signal significantly. Comparing figures 4.7.b and 4.9.b show that phase angle curves below 3500 Hz were almost the same and corresponded to $\frac{\phi}{f} = \frac{2\pi}{3000}$ and above 3500 Hz they did not.

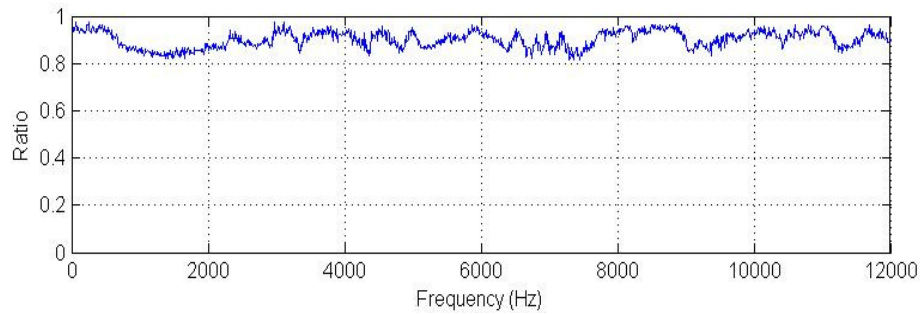
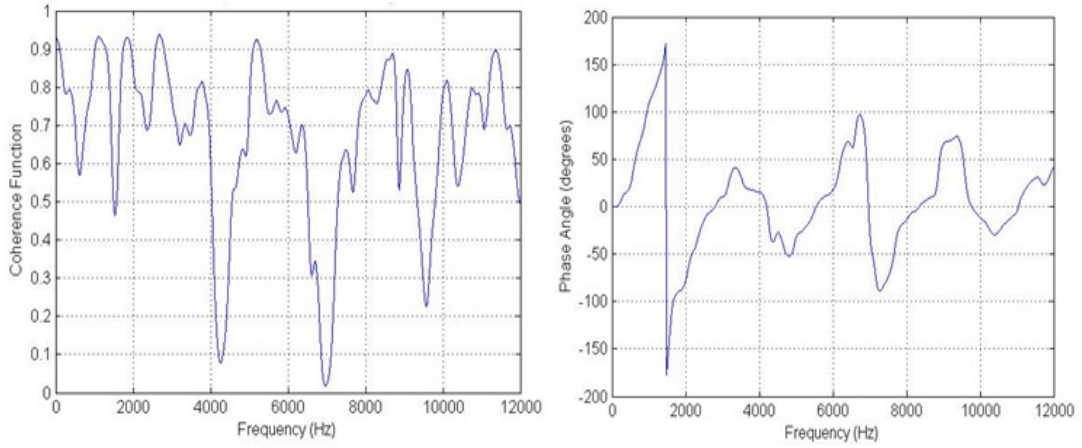


Figure 4.8. The probe performance spectral response plotted as ratio Probe Mic / Ref. Mic versus frequency for heated probe, $Na=250$.



(a)

(b)

Figure 4.9. (a) Coherence function and (b) phase angle for microphone probe and reference microphone using air jet with $N_a=250$ samples.

Chapter 5: Results and discussion

The use of a combination of sensors gives more adequate information on what exactly is going on in the process. With microphone probe it is possible to measure pressure fluctuations, which enables us to have a map of pressure fluctuations. This shows the regions where pressure fluctuation is high. However, when we use thermocouple, it is possible to measure mean and temperature fluctuations which reveal that temperature fluctuations happened in the regions of high temperature gradient. Now when we use these sensors together what additional details information can be obtained by using more sensors. Also, flame shadowgraphy imaging technique was used here to visualize the non-uniform characteristics in and around the flame.

5.1. Thermal field

Thermal field maps are presented to provide an understanding of the global thermal behavior and local structure of the swirling flames. The raw temperature data from thermocouple was compensated for thermal inertia effects of the bead as well as radiation losses of the thermocouple bead. The radiation losses can be significant, in particular at high temperatures. Similarly, the level of temperature fluctuations obtained within a swirl stabilized premixed flame can be significant. An evaluation of the uncompensated and compensated thermocouple output reported previously [44] reveals that fluctuating temperatures were high (as much as 350°C) at some locations in the flame without compensation. The mean temperatures (without radiation effect) can therefore be affected without any compensation. The temperature corrections were significant for the 45 degree swirl premixed flames. An evaluation between the

uncompensated and compensated data of temperature measurements showed that the calculated temperature difference (standard deviation) can be up to 350°C at some location in the flame. Thus, the compensation technique should be considered when examining the acoustics source localization within a flame with the help of mean and fluctuating temperature maps.

5.1.1. Mean temperature maps

The mean temperature at various locations in the flame for stoichiometric burning is shown in the Figure 5.1. The high temperature regions in the flame are due to mixing and intense combustion of the fuel/air mixture thus defining the flame surface.

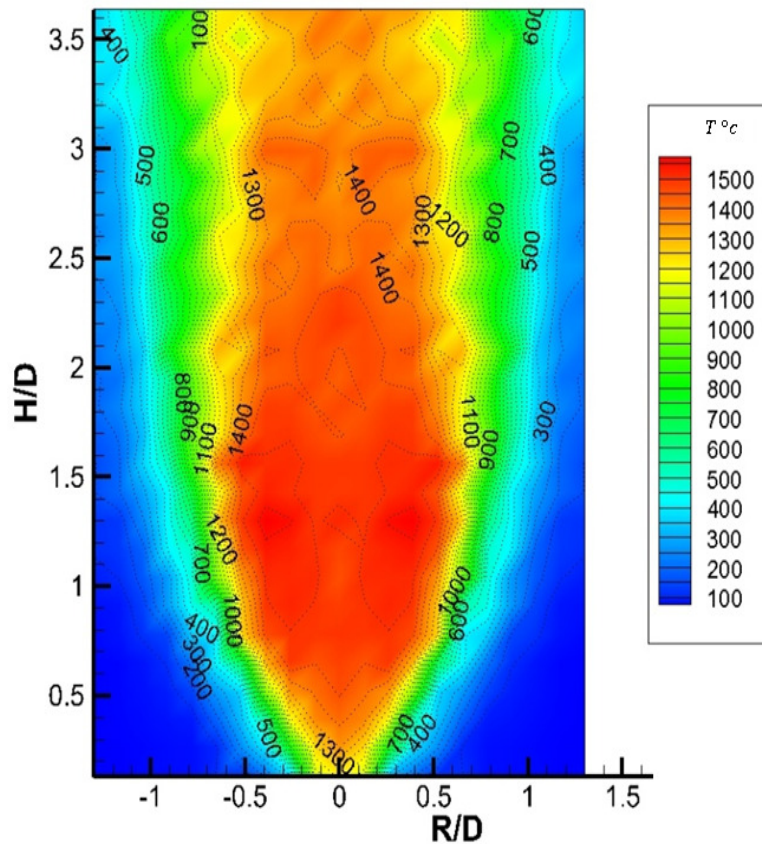


Figure 5.1. Mean temperature profile for a swirl stabilized premixed flame.

The large temperature magnitude and narrower distribution suggests that this region mainly consists of well mixed hot combustion products. The close proximity of the mean temperature contours at the outer periphery of the flame with the surrounding ambient cold region results in large temperature gradients. The regions of high temperature gradients give rise to large temperature fluctuations.

5.1.2. Fluctuating temperature maps

The fluctuating temperature map is shown in the Figures 5.2. Comparing figures 5.1 and 5.2 shows that maximum temperature fluctuations occur just outside and at the boundary of the region of maximum mean temperatures.

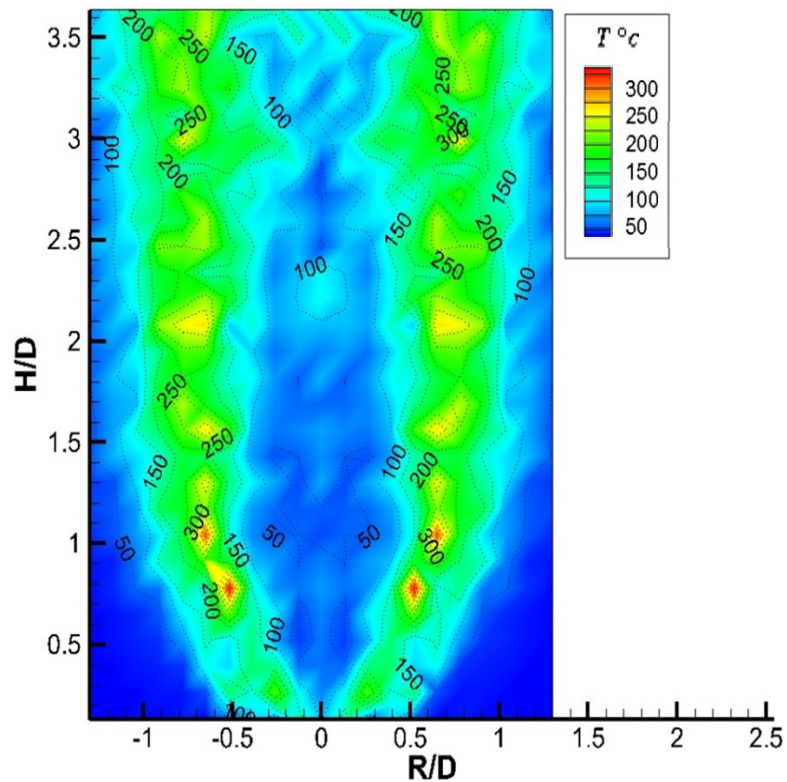


Figure 5.2. Fluctuating temperature from a swirl stabilized premixed flame.

Large temperature fluctuations can be seen in the vicinity of the shear layer while fluctuations are moderate (but still quite high, as much as 50°C) in central region of the flame. The large temperature fluctuations in the reacting flow field in the central region are due to thermal stratification and intense turbulence.

The results show that the regions of high temperatures are not necessarily the regions of high temperature fluctuations. Large fluctuations in temperature within a premixed flame can be due to increased levels of turbulence or due to local fluctuations in equivalence ratio. These regions of high temperature fluctuations can cause local changes in pressure to give rise to acoustic sources within the flame.

5.1.3 Time constant data

Time constant of a thermocouple decreases with increase in flow velocity and temperature. In order to obtain a correct temperature profile within the flame, it is essential to compensate for thermal inertia effects of the bead as well as radiation losses of the thermocouple bead for the temperature measurements obtained from a thermocouple. Figure 5.3 shows the thermocouple bead time constant obtained at various radial locations at a given axial location in the flame.

The time constant of the thermocouple varies with the properties of the surrounding flame gases and the forced convection that heated or cools down the thermocouple bead. Accordingly the time constant of the thermocouple for a particular thermocouple bead varies at different spatial locations within the flame

[45]. This figure shows that the measured time constant decreases with increase in temperature and this is found to be consistent with the previous studies [45].

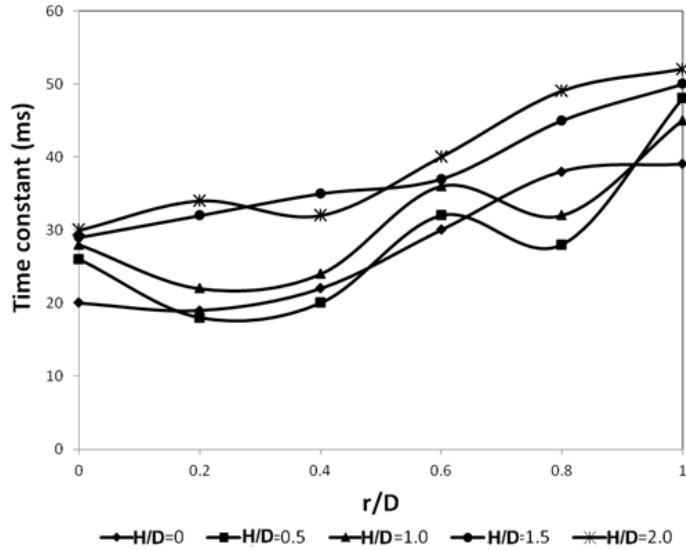


Figure 5.3. Thermocouple time constant profiles at various radial locations for a given axial location in a premixed swirl flame.

5.2. Pressure fluctuations data

5.2.1. Non-reacting case

The compensated root-mean square (RMS) values of the output signal amplitude from the microphone probe in the non-combustive case in H, θ , and R direction are shown in figure 5.4. The results show that the maximum pressure fluctuations occur at exit of the burner due to high turbulence levels in this region. Different values of pressure fluctuations in different direction reveal that for measuring the total pressure fluctuations three microphone probe are required (because of the directionality of the sound or pressure fluctuations).

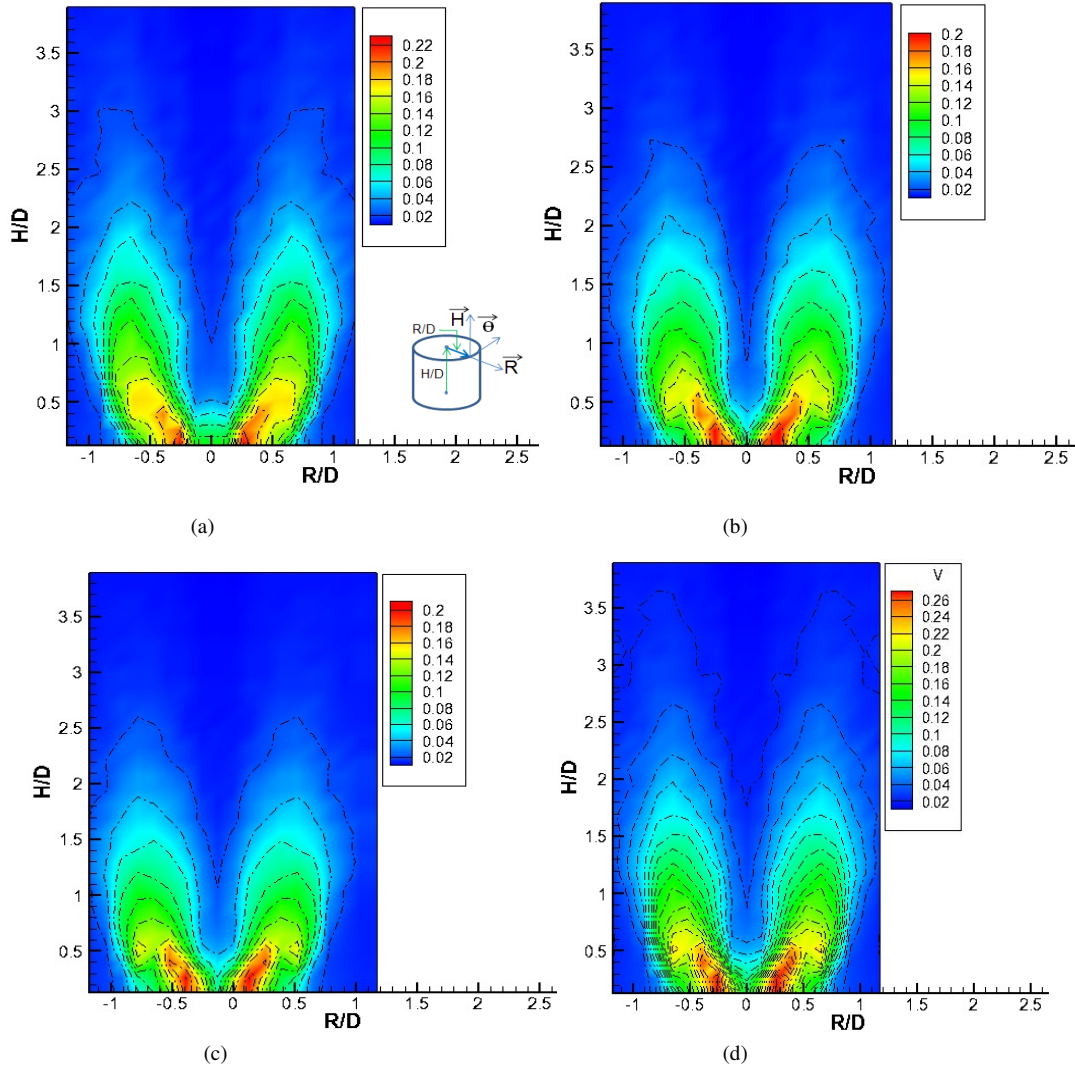


Figure 5.4. RMS values of the amplified output signal from the microphone probe for the non-reacting case in (a) H, (b) θ , and (c) R directions, respectively, and (d) Total pressure fluctuation.

The sources of the pressure fluctuation (sound field and waves) that vary with all three space coordinates are the usual response to sources that are smaller than the characteristic dimension of the space in which they are confined [46]. The RMS value of the total pressure fluctuation was calculated by considering the three pressure fluctuation simultaneously.

5.2.2. Combustive case

The RMS values of output signal amplitude from the microphone probe for the combustive case in H, θ , and R directions are shown in figure 5.5. Different values of pressure fluctuations in different direction reveal that for measuring the total pressure fluctuations three microphone probe are required (because of the directionality of the sound or pressure fluctuations). The sources of the pressure fluctuation (sound field and waves) that vary with all three space coordinates are the usual response to sources that are smaller than the characteristic dimension of the space in which they are confined. The results show that the pressure fluctuations start at the combustor exit and extend downstream as radially outwards away from the exit of the burner with the maximum being around $H/D=0.75$.

The results also show that the magnitude of pressure fluctuations in H direction is more than the other two directions. This may be attributed to initial momentum and the buoyancy of the fluid in H direction. Figure 5.5.d shows the calculated aggregate value of the total RMS value of pressure fluctuation that stem from the three pressure fluctuation. Comparing the differences between fluctuation in H, θ , and R directions for non-reaction case and combustive case shows that for combustive case differences between pressure fluctuation in H, θ , and R directions were higher. It shows the directivity of pressure fluctuation. It also shows that combustion noise is not a monopole source of sound. The total pressure fluctuation can be established by simultaneous pressure fluctuation measurements.

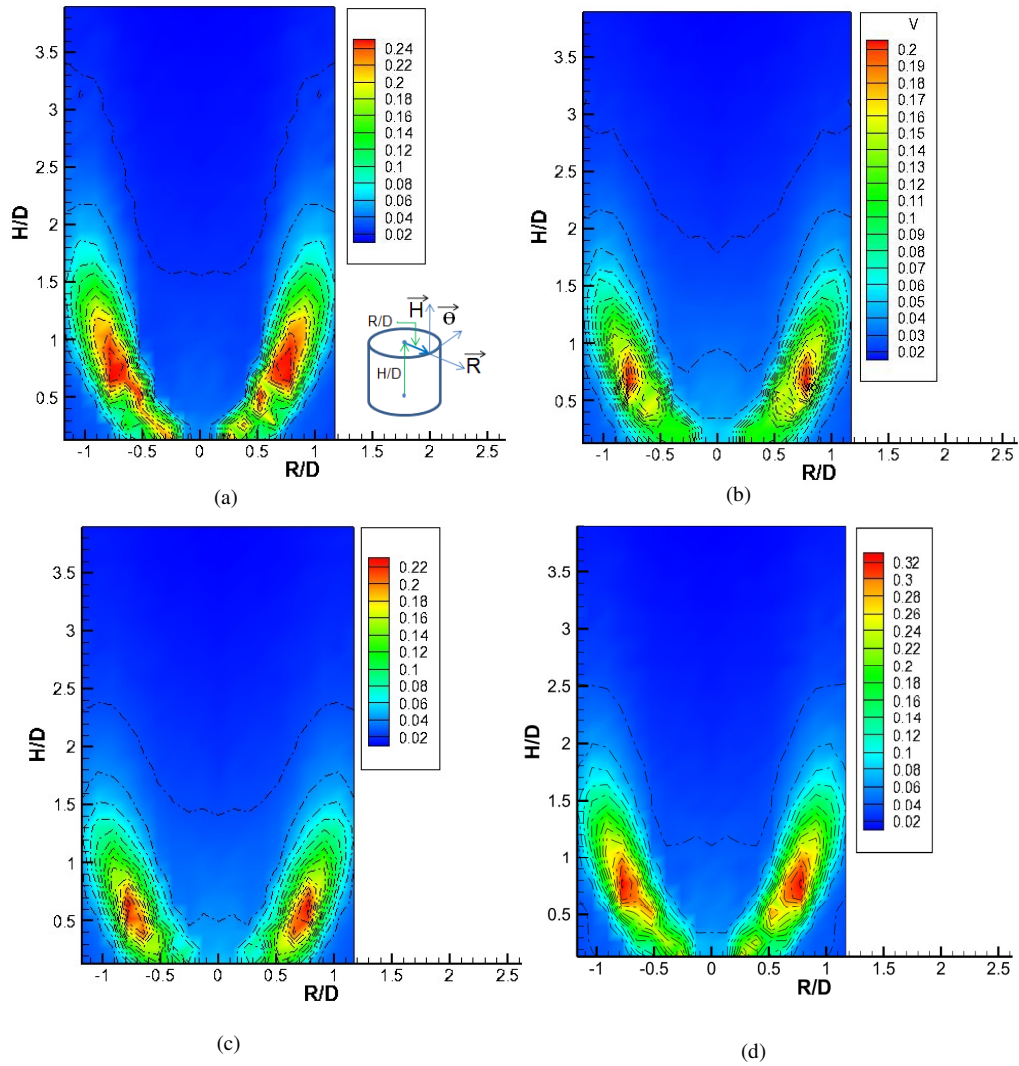


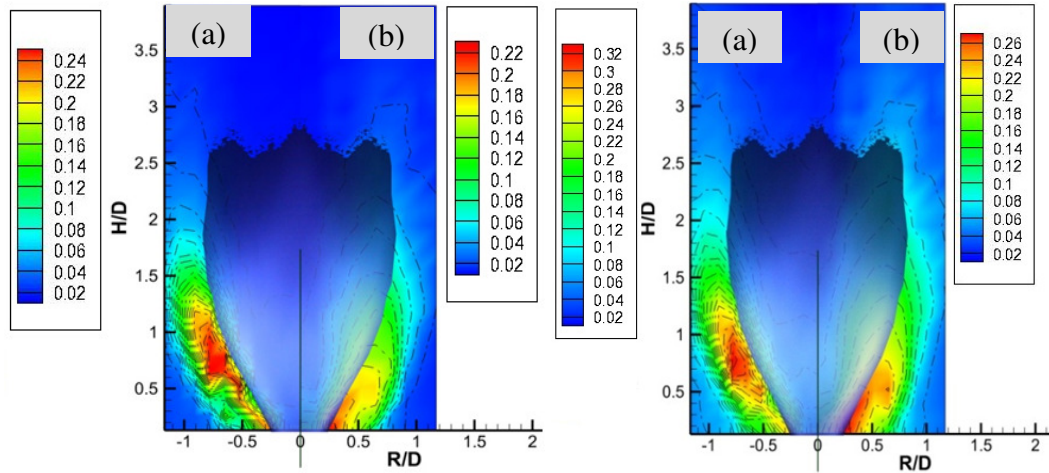
Figure 5.5. RMS value of the amplified output signal from the microphone probe for the combustive case in (a) H, (b) θ , and (c) R direction, and (d) total pressure fluctuation.

Figure 5.6 shows total pressure fluctuation as well as the pressure fluctuation measured in H direction with the microphone probe, for the combustive and non-combustive cases. Visible flame is shown in this figure to help identify regions of fluctuations relative to the flame. A comparison between the two cases reveals not only the magnitude but also the area over which the pressure fluctuations occur. The

maximum pressure fluctuations occur outside and around the flame front. The flame acts as a barrier against the outside fluctuations, flows and eddies diffusing inwards. For the reacting case, increased fluctuations were observed as compared to the non-reacting case. This is attributed to the fact that the sources of acoustic energy emanate from gas pockets and small eddies.

A comparison of the pressure and temperature fluctuations reveals that maximum temperature fluctuations occur mostly near to the boundary of the flame while maximum pressure fluctuation occurs further away from the flame. This may be due to small size and low concentration of gas pockets relative to the size of thermocouple bead. Also the maximum pressure fluctuation decreases beyond $H/D=1.5$ while temperature fluctuation do not increase any further beyond this distance. There was no visible flame beyond $H/D=2$ and beyond this point only cold air mixed with the burned gas to cause temperature fluctuations in the gas flow. Only a slight increase in pressure fluctuation was observed in the flame zone. This increase in pressure fluctuations is due to the density fluctuations.

Based on temperature and pressure fluctuation, the flow field of a turbulent premixed flame can be divided into three regions. Inside of the flame the effect of pressure and temperature fluctuations are of small. Maximum pressure fluctuation occurs outside of the flame. In between these two regions maximum temperature fluctuation and fluctuation of density coexist.



Pressure fluctuations In H direction

Total pressure fluctuations

Figure 5.6. RMS values of the amplified output signal from the microphone probe with the flame overlapped to reveal the local regions of pressure fluctuations. (a) With flame, and (b) without flame (non-combustive) case.

The acoustic sources in the vicinity of shear layer showed that their localization depends upon regions of high temperature fluctuations and velocity gradients. The temperature fluctuations were large in the vicinity of shear layer. These large temperature fluctuations in the regions of high turbulence could rise to temporal fluctuations of pressure which in turn determine the noise emission spectra of the turbulent flame.

5.3. Shadowgraph

Self-sustained flame propagation of a localized reaction zone occurs only in a small portion of the combustible mixture, with the evolution of a non-uniform temperature profile. The flame shape is related to the velocity distribution of the

approach gas mixture amongst other parameters, such as, pressure, temperature, and fuel type, all of which affect the flame velocity. Also, turbulent flows cause pressure fluctuations to cause noise. The agents of entrainment are turbulent eddies that form a mixing layer between the turbulent jet and the surrounding fluid. Flame shadowgraphy imaging technique is used here to visualize and unravel the non-uniform characteristics in the transparent media.

Shadowgraphy was used to examine the flow behavior around the flame, see figure 5.7. Visible flame and mean temperature distribution are superimposed to help identify different regions of the flame. In the first region, starting from close to the nozzle exit to about one nozzle diameter downstream (to $H/D=1$) the flow can be referred to as development region. The second region starts at about $H/D=1$ in which the turbulent regime penetrate to the axis of the flame and is termed as a fully developed region. This figure shows that a cold flow around the flame moves with the flame propagation and that the initial growth of turbulent jets is a direct consequence of large-scale motions generated near to the boundaries of the flame.

Pressure fluctuations measured with microphone probes showed that the fluctuations at the beginning of the second region to be very high. These fluctuations reveal that the shear layer is unstable and grows very rapidly to form ring vortices that carry turbulent pocket of unburned gas jet fluid into the irrotational ambient fluid, and irrotational ambient fluid back into the jet. Mixture of unburned gas vortices engulf ambient fluid about themselves to finally mix the flame jet and ambient fluids. This unburned gas propagates downstream and as it moves downstream its

temperature increases to bring the mixture conditions for their burning from the direct interaction between the fluid flow and vortices. Thus unburned gas pockets start to burn which subsequently causes more pressure fluctuation.

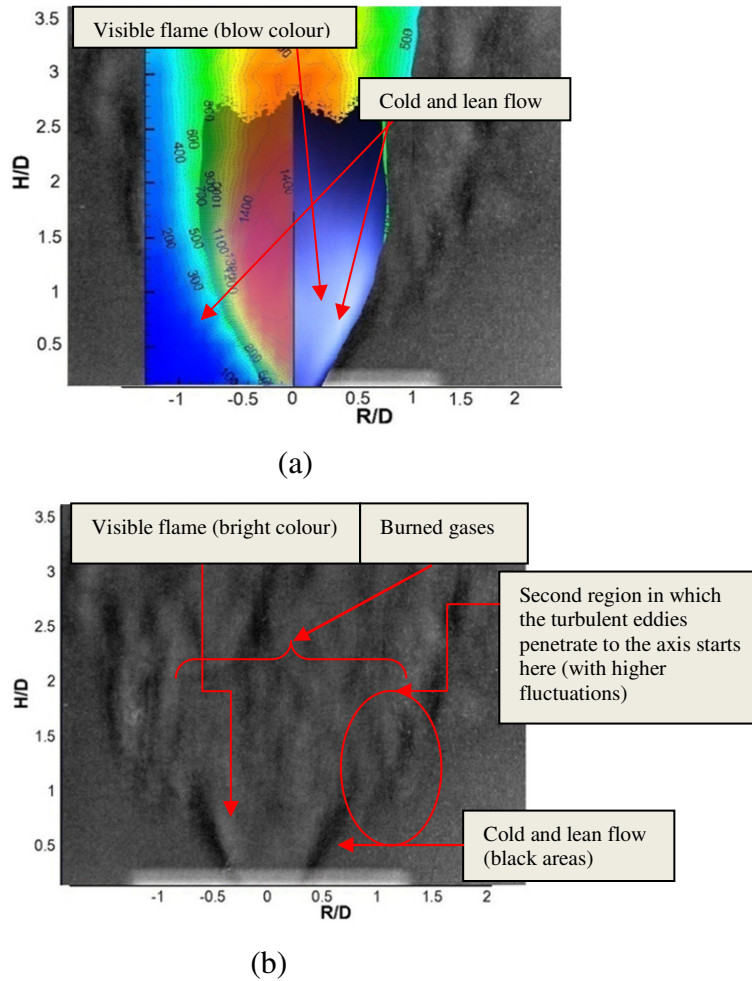


Figure 5.7. (a) Hybrid of flame shadowgraph image, visible flame and mean temperature. (b) Illustration of vortex production and fusion in premixed flame.

In Large temperature gradients were found in close proximity to the mean temperature contours in the vicinity of the shear layer. Very high temperature fluctuations outside the combustion zone are caused from mixing between the hot combustion products and the surrounding air with the resulting fluctuating

temperatures responsible for high pressure fluctuations. Pressure and temperature fluctuation cause other unburned pockets of fuel and air located near to these areas that upon combustion results in more pressure fluctuation to cause noise. The localization of high acoustic sources occurs in regions of high pressure and temperature fluctuations. Acoustic sources occur in these regions of the flame to significantly affect the noise spectra. Regions of combustion noise (combustion roar) generation in a flame can thus be located by identifying the regions of high pressure and temperature fluctuations.

5.4. Power spectral density (PSD)

Figure 5.8 shows power spectral density (PSD) recorded by thermocouple and microphone probe. Flame boundary is shown in black dotted line to visualize the flame front. Power spectral density was measured at each spatial location within the flame. PSD plots at a particular frequency were then mapped on to the regions surrounding the flame. Visualization of PSD plots at a particular frequency show the formation of coherent structures in and around the flame. The results show that in swirling flames low frequencies pressure and temperature occur almost in the same vicinity that lies mostly in the outer boundary of the flame. Figures 5.8.a and 5.8.b show power spectral map for temperature and pressure at low frequencies of 50 and 100 Hz respectively. Regions of high pressure fluctuation which are characterized by formation of coherent structures in those regions, serve as the sources of noise generation within the flame. The pressure in the radiated sound wave is proportional to the rate of change of volume increase of the gases during combustion. In turbulent premixed flames the noise may be taken to arise from the sudden expansions due to

the chemical reactions at the boundaries of the flame. In an unsteady flame the fluctuating density acts as a volume source of sound (the volume of the flame fluctuates with the reciprocal of the density). The main cause for the fluctuating density is unsteady heat release. Presumably, a significant if not predominant reason for the generation of pressure waves by unsteady combustion would be the unsteady heat release produced by unsteady combustion. This phenomenon is primarily responsible for the combustion generated noise in turbulent flames.

Figures 5.8.c and 5.8.d show the power spectral density maps for thermal and acoustic field at frequencies of 500 Hz and 1000 Hz respectively. Coherent structures for thermal field seem to appear everywhere in and around the flame. Also, coherent structures for thermal field were seen above the flame tip. Coherent structures for the acoustic field were seen near the burner exit near the vicinity of flame front. The figures show that thermal field and acoustic field affect each other and determine the formation of coherent structures within a turbulent flame. However, coherent structures formed by the thermal and acoustic field do not occur at the same places. It seems the pressure fluctuations embark from the boundary of the flame and propagate outward to generate pressure waves from the unsteady combustion, figures 5.8 c and d. The higher frequency pressure fluctuations cause higher frequency of sound waves that are observed outside the boundary of the visible flame.

The pressure fluctuations showed that combustion noise is not a monopole source of sound. The pressure in the radiated sound wave is proportional to the rate of change of volume increase of the gases during combustion. In turbulent premixed

flames the noise may be taken to arise from the sudden expansions due to the exothermic reactions at the boundaries of fuel rich and lean turbulent eddies, see figure 5.9. In an unsteady flame the fluctuating density acts as a volume source of sound (the volume of the flame fluctuates with the reciprocal of the density).

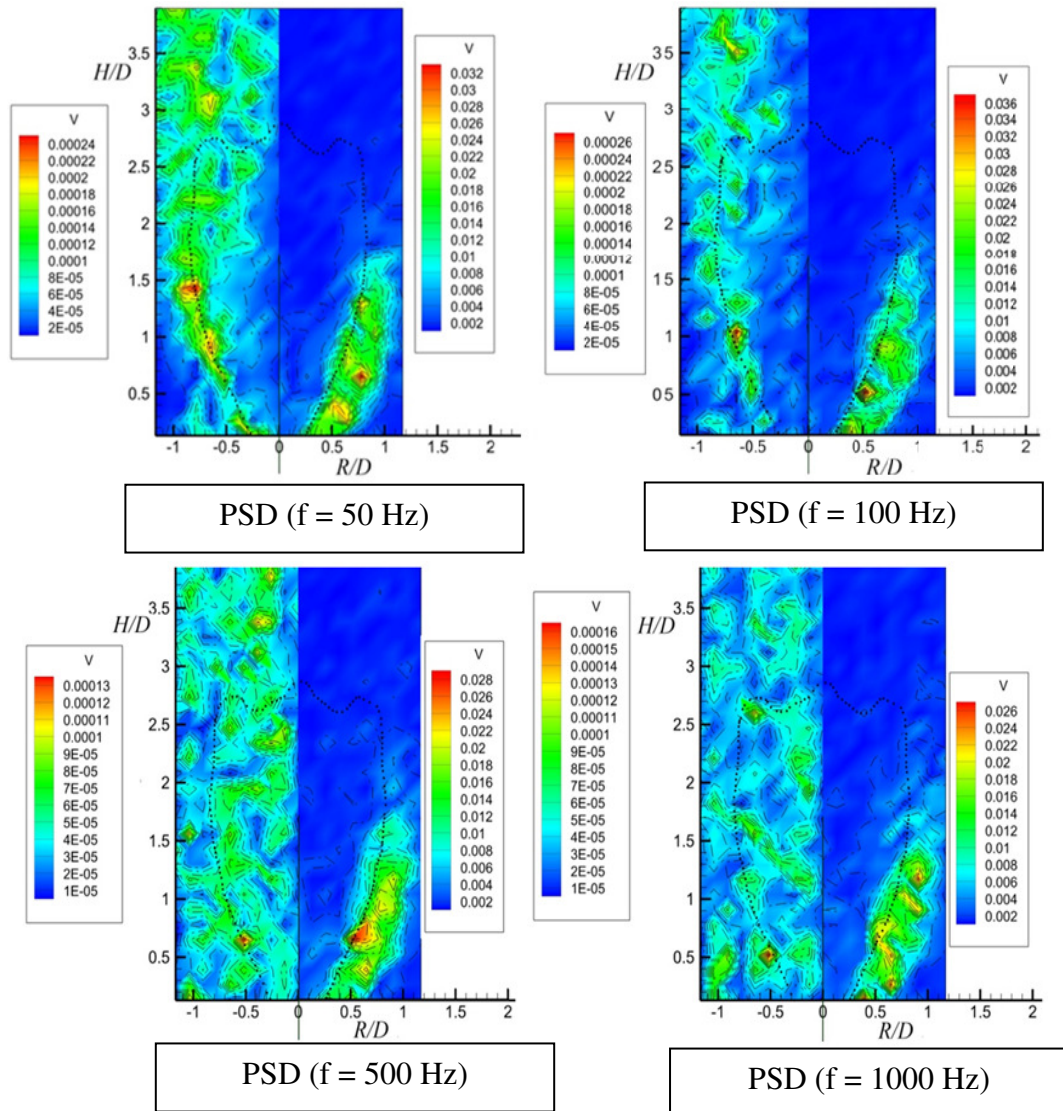


Figure 5.8. Power Spectral Density (PSD) for thermocouple and microphone probe at selected discrete frequency range. The contour of the flame is shown in black dotted line. (I) PSD recorded by thermocouple (left half in each figure). (II) PSD recorded by microphone probe (right half in each figure).

The main cause for the fluctuating density is fluctuations in the heat release. Presumably, a significant if not predominant reason for the generation of pressure waves by unsteady combustion would be the unsteady heat release produced by unsteady combustion. This unsteady heat release gives rise to large temperature fluctuations in the turbulent flame.

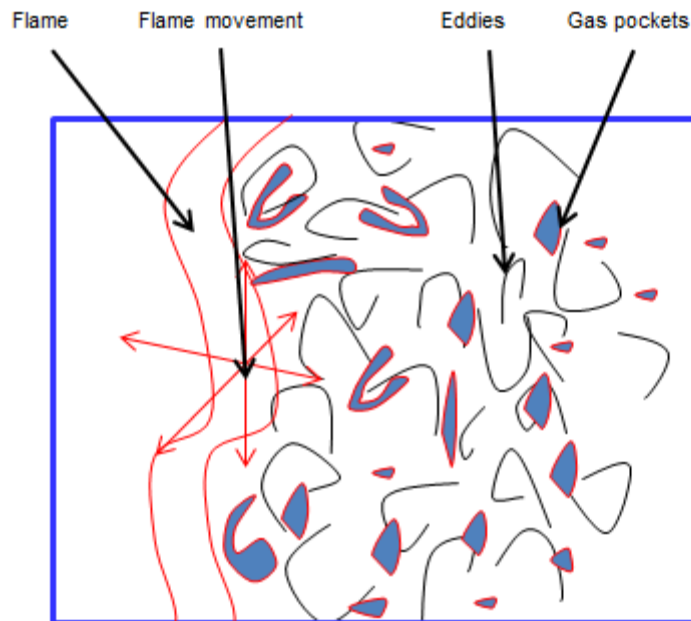


Figure 5.9. A sketch illustrating the movement of flame, gas pockets and eddies in a small volume of the flame.

5.5. Acoustic noise spectra

Acoustics signatures were examined using condenser microphones which were placed at various axial locations above the burner exit plane to provide information on the noise spectra associated with premixed turbulent flame. The spectral analysis of the sound pressure level was carried out at various axial locations. Figure 5.10 shows the overall sound pressure level in decibels obtained from multiple

microphones placed at varying axial distance from the burner exit. Figure 5.11 shows power spectral density of the acoustic signals obtained from multiple microphones placed at varying axial distance from the burner exit. The acoustic radiation measurements were carried out simultaneously. Combustion noise contains lower portion of the audible frequency spectrum ($f < \sim 1500$ Hz) and has a characteristic frequency of maximum sound output and depends both the flow velocity and reaction chemistry [47]. The acoustic radiation (SPL) from different microphones at different axial positions show that in its appropriate frequency range combustion noise has more PSD than jet noise. The acoustic spectrum (SPL) that fills the audible frequency range from 100-1500 Hz is called as combustion noise in frequency domain. As it was mentioned this portion of the frequency spectrum called combustion noise. The figure shows that the spectrum peaks at 340 Hz. The temporal response from different microphones located at varying axial locations around the turbulent flame suggest that at locations further downstream of the burner exit there is a subsequent decrease in the overall sound pressure level. The overall sound power registered from microphones located at $H/D=0$ to $H/D=2.5$ with the maximum at $H/D=1.25$ was found to be more as compared to the microphones located further downstream. This proposes the location of the acoustic sources started at the burner exit where unsteady heat release due to chemical reaction. Also, it shows that overall sound power of PSD for the microphones closer to the burner exit is higher as compared to the microphones located further downstream. The flame jet (mixed fuel and air) coming out of the burner exit expands and therefore its velocity decreases as it moves further

downstream of the burner exit, so the combustion noise associated with the jet velocity, decreases.

Figure 5.10 shows that combustion noise was broadband (up to 20 kHz). It shows that the spectra of combustion noise emissions were exceed background noise levels for frequencies from 20 Hz to over 20 kHz. It shows that broadband spectrum of combustion noise increases with increase in frequency, arrives at a maximum at $f = f_{peak}$, and then decreases towards to almost jet noise and background noise level. Experiment results revealed that f_{peak} occurred in the frequency range of 200-1000 Hz at 232 Hz.

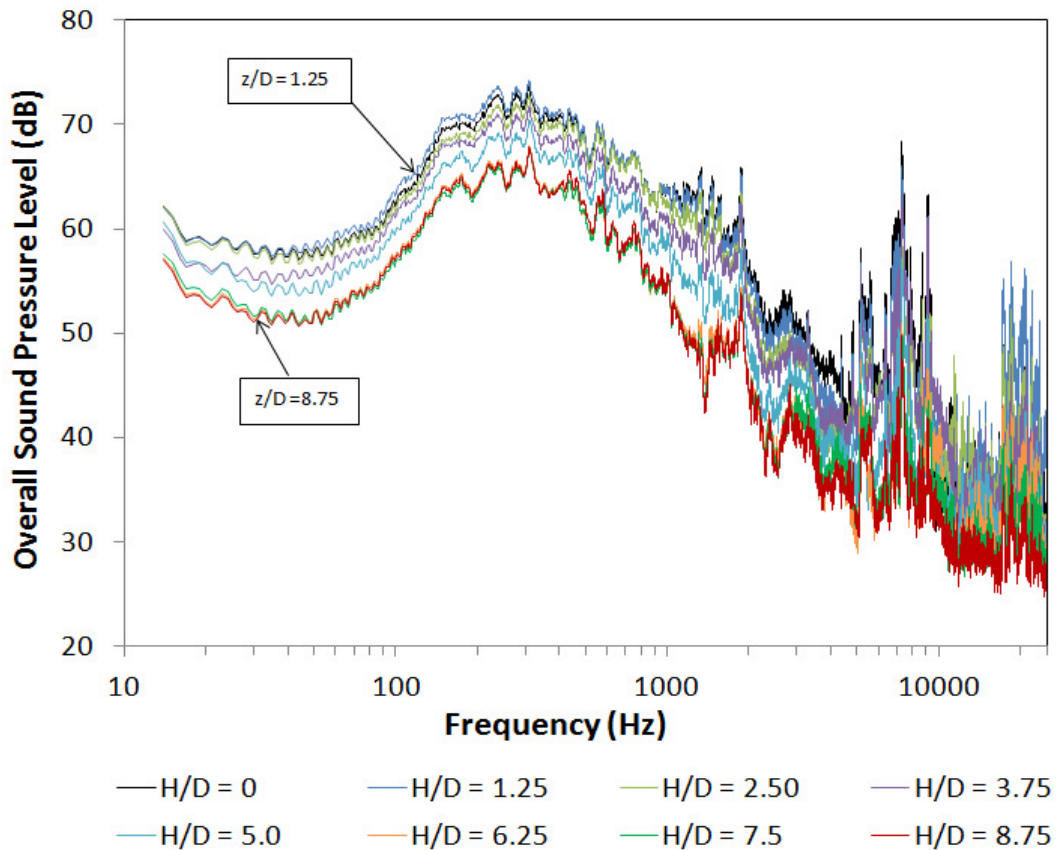


Figure 5.10. Sound pressure level for a premixed swirl flame.

The peak frequency for the stoichiometric fuel-air ratio was observed at 232 Hz. Combustion noise is shown with different color. Figure 5.11 implies that as one moves further downstream of the burner exit there is a subsequent decrease in the overall sound pressure level (SPL).

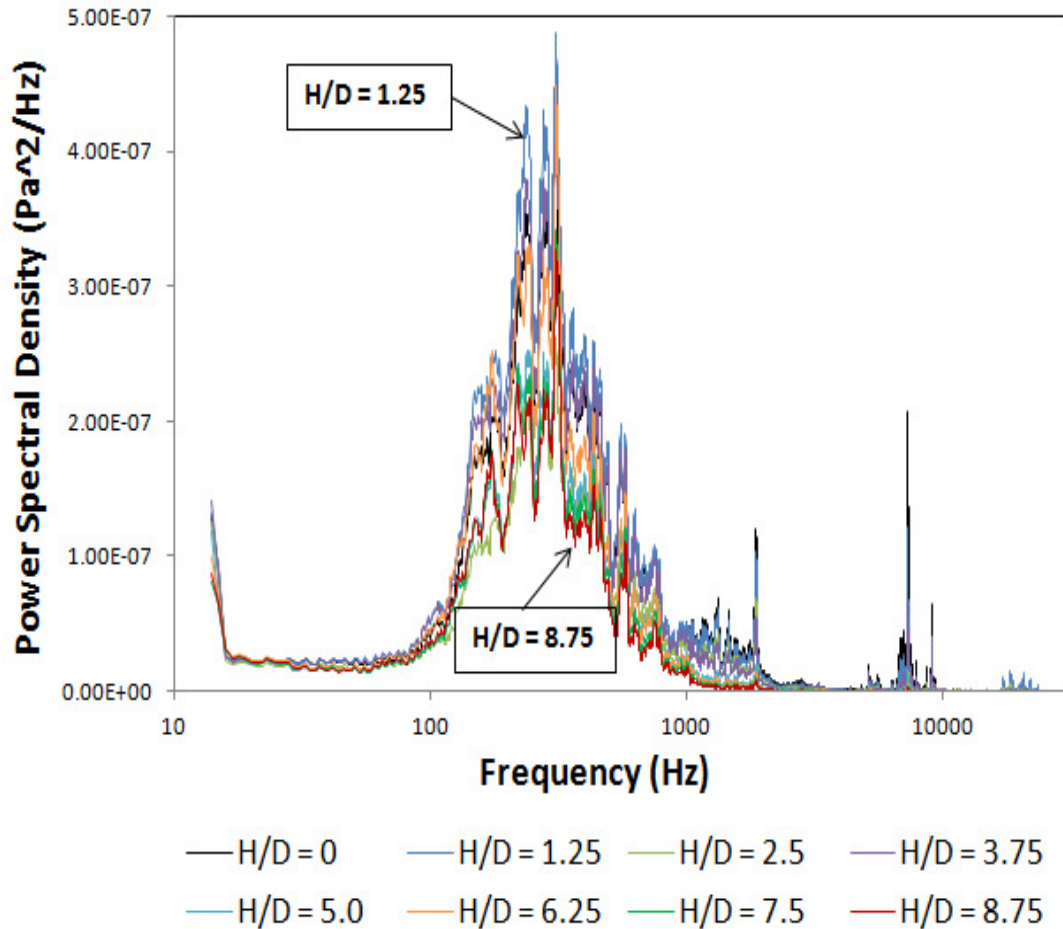


Figure 5.11. Power spectral density of the acoustic signals.

It was concluded that regions of maximum temperature fluctuations do not coincide with the regions of maximum pressure fluctuations which act as the noise sources in a premixed turbulent flame. The overall sound power registered from microphones located at H/D=0 to H/D=1.25 was found to be more as compared to the

microphones located further downstream. This supports the location of the acoustic sources within axial regime of $H/D=0$ to $H/D=2.5$, downstream of the burner exit. Results with the microphone probe support similar trends.

Chapter 6: Multiple sensors for combustor monitoring

The current practice of using a single sensor to measure certain parameters at a single location cannot provide enough spatial resolution to properly convey the overall performance of the combustor. With extensive knowledge of the local conditions within the flow field, it is expected that a high density sensor network and incorporating advanced combustion diagnostic techniques would provide better information to the combustor controller that can improve the overall system performance. Such sensor networks and advanced diagnostics will have a wide spectrum of applications including industrial furnaces and incinerators, chemical reactors and distillation towers, high temperature fuel cells, and gas turbine and piston engine monitoring and preventative maintenance.

Currently little research has been conducted on the location and number of sensors that are needed within and/or around the combustor in order to create a full and complete picture of the phenomena occurring inside. Premixed combustion, although expected to be steady, is susceptible to inherently unsteady high acoustic pressures. In this chapter, acoustic pressure has been chosen as one of the initial representative signature parameter. Our initial efforts have been focused on the acoustic signals emitted from a 6.12 KW premixed swirl combustor, which are obtained by a multiple channel acoustic sensor array arranged around the combustor. Each channel is sampled simultaneously, allowing for the comparison of both magnitude and phase differences between channels. The non-symmetry of the 3D turbulence wake will produce local variation in both circumferential and axial directions along the

combustor. A numerical calculation by considering symmetry condition has been done that is presented on appendices C.

Swirl flows and flames tend to produce periodic flow instabilities, which lead to increased noise emission and flame stability. Instabilities in combustion have been examined severely in the recent years [47]. Instabilities in combustor and flame have been examined and reveal the importance of coherent structures in the forward flow surrounding the central recirculation zone [48].

The presence and the impact of coherent structures on the noise emission from the flame or combustion system need more physical information to decrease flame and combustion noise in all industrial uses is already reflected during the design. A disadvantage of swirl flames is high noise levels caused by high reaction qualities or conditions of being dense and amplified by the use of premixed flames in industrial combustors.

Our first goal should be to choose zones most sensitive to change of input parameters (fuel to air ratio). Tests were made at constant air and the amounts of fuel flow varied. At any given operation point (stoichiometric) of the swirl combustor changes to fuel flow rate were made while maintaining the other parameters constant, i.e. input air. These situations are usually named, fuel-lean mixture (Equivalent ratio less than one), stoichiometric or normal operation (Equivalent ratio equal to one), or fuel-rich mixture ((Equivalent ratio more than one).

6.1. Test set-up

A microphone array that was able to accommodate up to 32 microphones for sound acoustic measurements at varying locations around the combustor was built, figure 2.5.a. This system allowed us to measure both spatial and temporal variation of the local sound pressure level signal. The top view of the premixed swirl combustor is shown in Figure 2.5.b. The array was comprised of four towers, each 90 degrees apart on the circumference of a 6 inch diameter circle. A photograph of the array is shown in figure 2.1.b. Microphones were attached to the towers with setscrews above the combustor base plate. The array was free to be rotated around the central axis of the combustor, thus allowing for change in angular orientation with regards to the air inlet and swirl.

The microphones were 6mm in diameter and 3.4mm in height, figure 2.5.a. They had a nominal sensitivity of -35 dB +/- 4dB (where 0dB is 1 V/Pa). The sensitivity for every microphone used was established before experimentation and periodically rechecked. To pick up the signal from the microphones, a data acquisition setup was used, figure 2.2. Signals were measured and logged by two National Instruments 9233 4-channel high-speed sampling cards and stored in the computer.

The UMD Combustion Laboratory's 6.12 kW premixed swirl test combustor was used for the experimental study, figure 2.5.a. It is chosen because of its similarity with the practical combustors. The combustion occurs at atmospheric pressure under semi-confined condition. The flame is stabilized on a center body with six swirl vanes that can set the swirl angle to be 30, 45, or 60-deg to the flow, figure 2.2.a. The

experiments were done by fixing the swirl geometry to 45 degree swirl. Methane was used as the fuel for the given experiments.

The air and fuel mass flow rate were controlled by flow controllers. The controller had a time constant of 1.8 seconds. The controller could maintain the flow to be within +1.5/-0.5 percent of the full value.

The microphones were calibrated using a computer generated tone of 1000 Hz and calibrator (chapter 2). The amplitude of the produced tone was quantified using a second calibrated microphone placed closely to the WB-61A microphones. Two frequency responses were obtained: one from the output voltage of the WB-61A microphones and the other from the calibrated microphone output. The magnitude associated with 1000 Hz was compared for both frequency response and sensitivity for each WB-61A. The process was repeated 5 times for 1000 Hz and to obtain the averaged sensitivity.

6.2. Data collection method

The air flow was set to 108 L/min, and the fuel Methane was adjusted to give stoichiometric combustion. After every time the mixture was ignited in the combustor, the entire setup was allowed to warm up for two minutes.

In each test, one of the microphones was employed as a reference microphone. Data was logged simultaneously from all microphones for about 150 seconds. For circumferential measurements four of the microphones are positioned at the same axial plane. For axial measurements the microphones are all positioned onto the same

tower. Measurement was repeated until all axial locations in a single tower have been covered.

The recorded signal was sampled at 25 kHz and then passed through a high order filter that removed signals below 100 Hz and above 6 kHz. The frequency responses were averaged over 10 seconds.

Particular attention was paid to the frequencies between 100 Hz and 1000 Hz; these frequencies were widely thought of as the regions of combustion roar. Above 1000 Hz, significant jet noise appears. As a result of the highly transient nature of turbulent jet noise, frequencies above 1000 Hz have greatly increased uncertainty and large oscillations in the phase angle.

In the experiments, to examine magnitude variation due to differences in axial location and circumferential location, the data was obtained with both circumferential and inline measurements. Figure 2.5 shows each circumferential location. The circumferential data was measured with the microphones all in the same axial plane. The only difference between the microphones was circumferential location around the combustor. The inline measurements have the microphones all at the same circumferential location and varying axial location.

6.3. Results and discussions

Measurements of sound pressure level (SPL) magnitude can help to give an indication if the pressure fluctuations within the combustor are of dangerous levels (combustor resonance and noise pollution monitoring). It is expected that

measurements of the acoustic signatures between sensors outside of the combustor, which is due to acoustic propagation, can help to describe the flow physics within the combustor. Particular attention was paid to frequencies between 100 Hz and 1000 Hz as these frequencies are widely thought of as the regions of combustion roar. In the experiments, to examine the magnitude variation due to differences in axial location and circumferential location, the data was obtained on both circumferential and inline acoustic measurements.

Figure 6.1 shows the variation of sound pressure level (SPL) with frequency for different axial locations of the microphones around the combustor. The axial location was varied in the positive Z direction and was measured from the fuel inlet plane of the swirl combustor. The peak frequency at which the sound pressure level was the maximum was found to be at 170 Hz. The plots were plotted for $Z=2, 3, 4$ and 5 inches in the axial direction above the fuel inlet plane of the swirl combustor. It was observed that SPL increases as we go near the exhaust. While it shows that at $Z=2$ inches, where the flame tip is located, the SPL is less decreases as compared to that at $Z=3$ inches. The flame tip area was characterized by recirculation zones and reaction zones within the flame which serve as the acoustic noise sources from within the combustor. The noise here was characterized by both the turbulent jet noise as well as the combustion noise.

The peak frequency at which the sound pressure level becomes maximum was the combustion roar frequency for the given premixed swirl combustor (at 170 Hz). If one had a flame without combustor, the sound pressure levels were maximum at an

axial location of $Z=2$ inches and decreased further downstream of the flame. But because of the combustor wall, the flame pressure fluctuation completely did not transfer through the wall to the microphone. It seems sound pressures that reached microphone at $Z=2$ inches were a combination of transferred pressure fluctuation through the wall and pressure fluctuation from other places, especially exhaust. The SPL increased near to the exhaust.

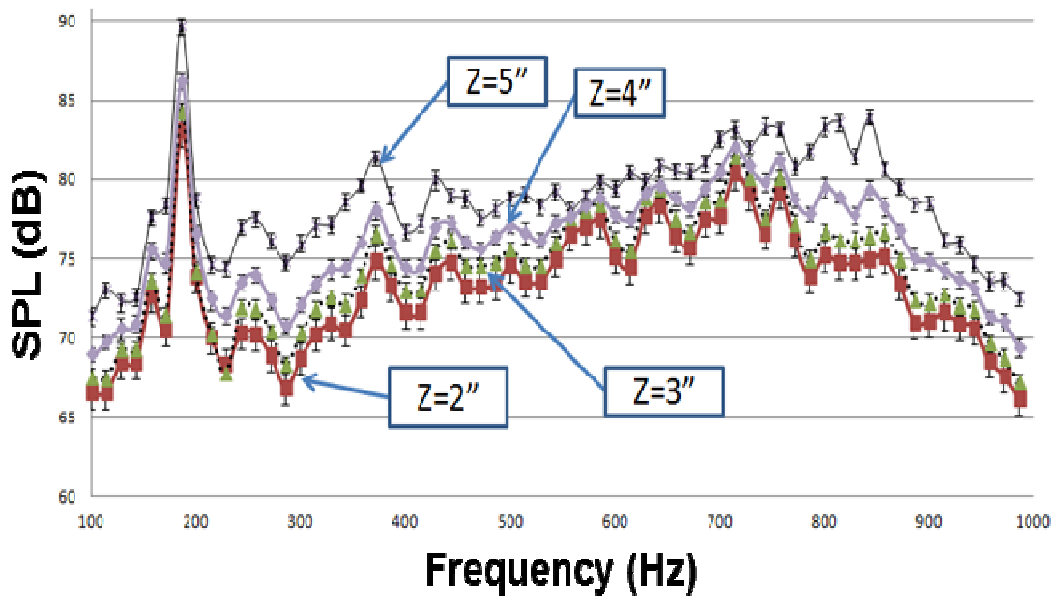


Figure 6.1. Combustion noise spectra for microphones at varying axial distance from the burner exit (for stoichiometric condition).

Figure 6.2 shows the circumferential distribution of SPL at a given axial location above the fuel inlet plane. The microphones were placed around the combustor in the same axial plane. The microphones were placed at angles of 0, 90, 180 and 270 degrees around the combustor for an axial plane location of $Z=3$ inches above the fuel inlet plane. It was seen that acoustic signatures differ very little circumferentially.

The change is much higher for difference in the axial positions of the microphones, figure 6.1. The flame from the swirl burner was almost symmetric around the burner axis and therefore the circumferential variation in the sound pressure level was found to be less.

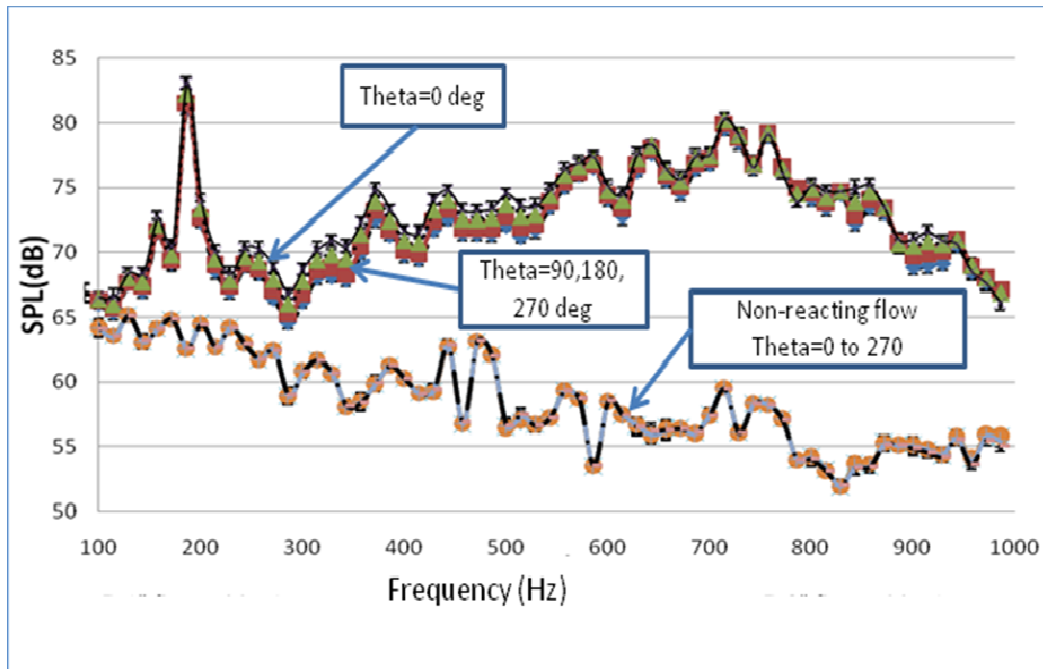


Figure 6.2. Circumferential distribution of reacting and non reacting noise spectra at Z=3 inches location.

To comprehend combustion roar, the mixing procedure happening between the fuel and the oxidant on a very minute scale must be considered. If the mixture is within the flammability limits for a fuel well mixed with air, the mixture of fuel and air will burn rapidly. Alternatively, fuel that mixes on turbulence and momentum in the ambient and create a flammable mixture, has a slower combustion time. In both

cases, when the well mixed mixture of fuel and air meets a source of ignition, combustion will occur.

Noise generated from region of rapidly combusting mixture creates combustion roar. Consequently, combustion roar is a function of how rapidly the fuel is being burned. The closer a mixture of fuel is to stoichiometry condition the more rapid will be the combustion process so that more energy is released into roar noise. In combustion equipment, such as burners and flares, the large fuel release causes more turbulence in the combustion process. Since turbulence directly manipulates the mixing rate of the mixture, turbulence flows produce more combustion noise.

Figure 6.2 also shows the effect of reacting and non-reacting flow on SPL at a given axial location of $Z=3$ inches above the fuel inlet plane. The Acoustic signatures for reacting and non reacting case were compared for the stoichiometric mixture of fuel-oxidizer. The results show that SPL for the non-reacting case is much less as compared to the reacting case. Direct noise usually associated with the generation of pressure waves by unsteady combustion is primarily responsible for the difference in the SPL distribution of reacting and non-reacting case. Presumably, a significant if not predominant reason for the generation of pressure waves by unsteady combustion would be the unsteady heat release produced by unsteady combustion [49].

Figures 6.3 and 6.4 show the effect of equivalence ratio on SPL level for different axial locations of the microphones. From $\Phi=0.6$ to $\Phi=1$ it is clearly seen that as the equivalence ratio for the fuel/oxidizer mixture increases it was accompanied by a substantial increase in the SPL level. Since the air flow rate was kept constant and

only the fuel flow rate was changed, the increase in the local velocity field resulted in increase in the turbulent jet noise considerably. The noise coming from each small region of rapidly combusting mixture added up to create combustion noise. As the fuel flow rate was increased the local flow velocity fluctuations increases which in turn increases the turbulence intensity of the flow. Therefore, larger the fuel release, the more the turbulence in the combustion process [49]. Because turbulence directly influences the mixing rate, high turbulence processes also produce more combustion roar. Also comparing these figures show that for microphone at $Z=2$ inches, and between 300 Hz to 1000 Hz changes in equivalence ratios caused completely different noise spectra. Therefore microphone at $Z=2$ inches was more sensitive to the equivalence ratio at this fuel/oxidizer mixture.

Figure 6.3 shows that SPL distribution for the stoichiometric mixture was lower than $\Phi=1.2$. This could be attributed to the fact that increasing burning process within the combustor was due to higher fuel flow rate. As the fuel flow rate was increased the local flow velocity fluctuations increased which in turn increased the turbulence intensity of the flow. Here as the equivalence ratio for the fuel/oxidizer mixture was increased, at $Z=2$ inches, where the flame tip was located, the SPL was increased. Therefore, larger the fuel release, the more the turbulence in the flame tip. Because turbulence directly influences the mixing rate, high turbulence processes also produce more combustion roar.

For $\Phi=1$ to $\Phi=1.3$ it can be seen that as the equivalence ratio for the fuel/oxidizer mixture was increased for microphone at $Z=2$ inches, the SPL first increased for

$\Phi=1.2$ and then decreased somewhat SPL. While for $Z=6$ inches it was accompanied by little decrease in the SPL. It shows that microphone installed at $Z=2$ inches zone was more sensitive to the equivalence ratio for the fuel/oxidizer mixture.

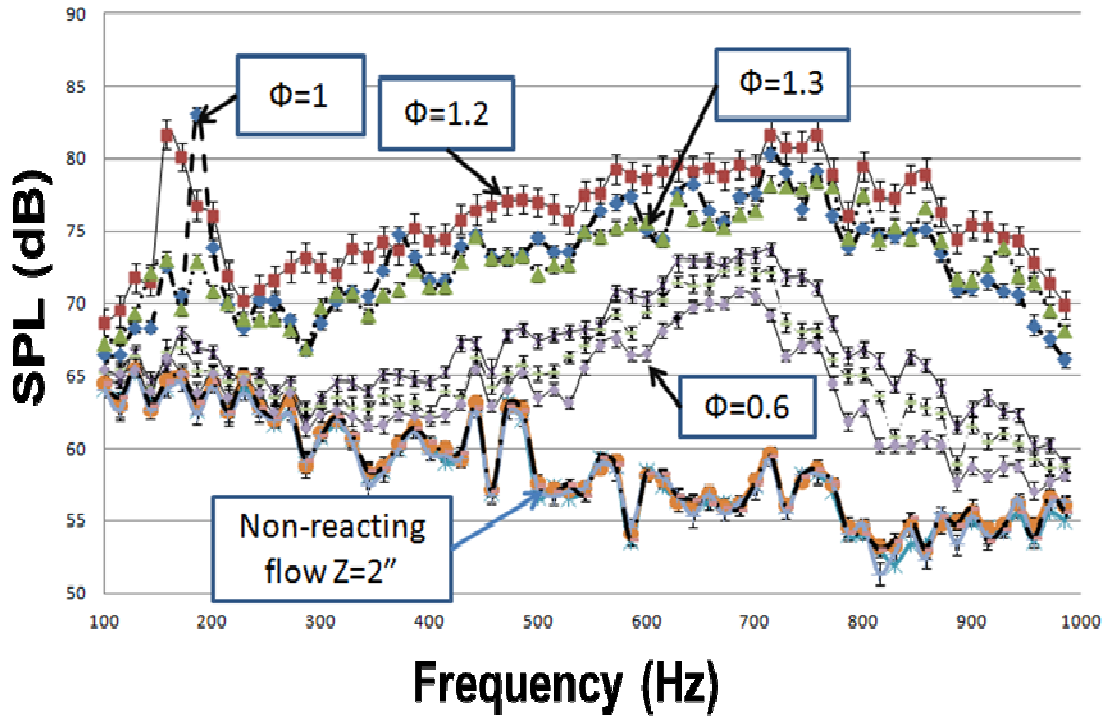


Figure 6.3. Reacting and non reacting acoustic radiation from the flame at different equivalence ratios at $Z=2$ inches from the burner exit.

The spectral distribution of the sound pressure shows that as equivalence ratio for the fuel/oxidizer mixture was increased from $\Phi=1$ to $\Phi=1.3$, it accompanied a change in dominating peaks at frequencies between $f = 170$ Hz to $f=200$ Hz, figures 6.3 and 6.4. As the fuel flow rate was increased from the $\Phi=1$ local flow pressure fluctuations distributed in the combustor changed which in turn showed a decrease with multiple peaks instead of one peak, figures 6.3 and 6.4. Therefore, in general larger the fuel

release from the $\Phi=1$, the more damped the peak frequencies (frequencies between 170 Hz to 200 Hz).

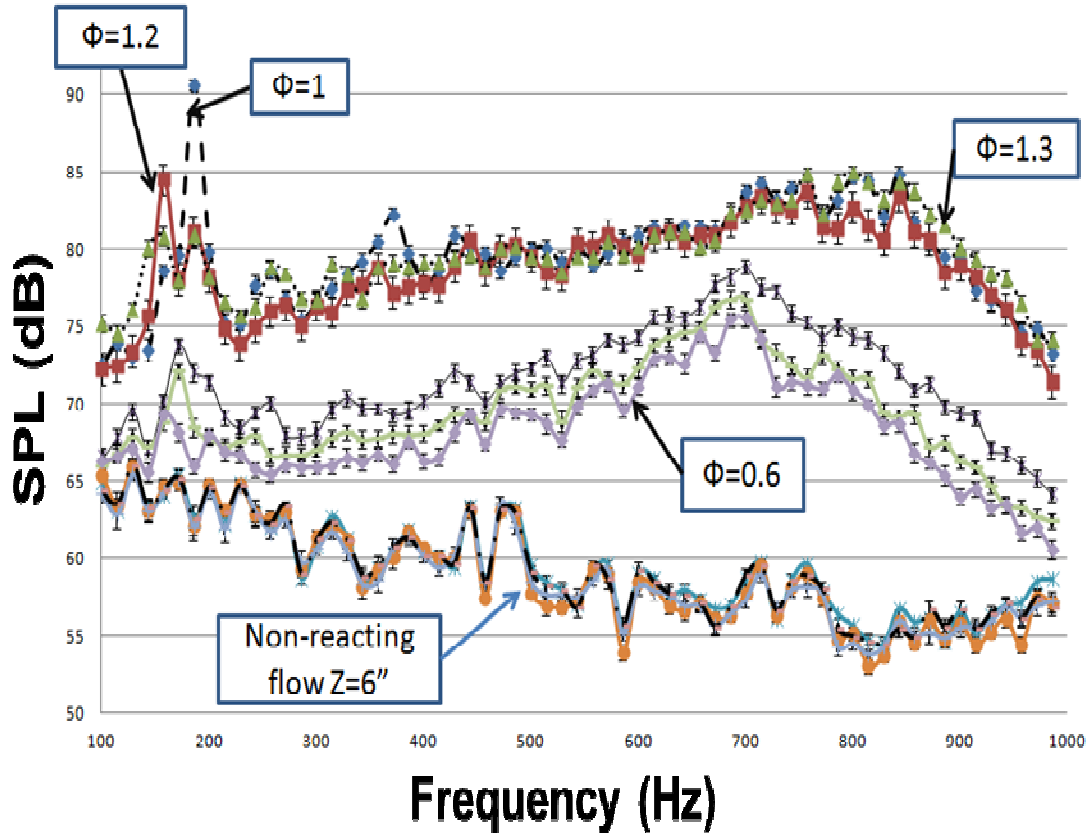


Figure 6.4. Reacting and non reacting acoustic radiation from the flame at different equivalence ratios at $Z=6$ inches from the burner exit.

Comparing these figures shows that microphone installed at $Z=2$ inches zone is most sensible to the equivalence ratio for the fuel/oxidizer mixture, while signal from microphone at $Z=6$ inches can be used as information about stability of the process.

6.4. Summary

The combustion performance is dictated by various parameters that include fuel concentration, fuel to air ratio, temperature, pressure, flow dynamics and residual gas concentration. Each signal contained more information that should be appropriately analyzed. This contributes to achieve results from Fourier transform analysis. A detailed acoustic analysis was done for a premixed swirl combustor. The results have proven that a significant spatial variation in the combustors.

The results showed that using a single sensor to measure fuel to air ratio at a single location ($Z=2$ inches alone or signal at 6 inches alone), one cannot provide enough spatial resolution to properly convey the overall noise emission from the combustor. Therefore a single sensor is inadequate to provide detailed information from the combustor.

The microphone installed at $Z=2$ inches zone was most sensitive to the equivalence ratio for the fuel/oxidizer mixture examined. While, signal from microphone at $Z=6$ inches can be used as information on stability of the process and prevent from any ambiguity response that can be caused by signal from microphone at $Z=2$ inches zone. Multi-sensor network placed around the combustor and employing advanced diagnostics for seeking detailed information can allow one to seek better control to achieve higher efficiency and performance.

Multiple sensors are required to measure certain parameters or to find any changes in the combustor. More sensors are better to provide enough spatial resolution to properly convey the overall performance or changes of the combustor. An example of

the application would be detection of hot spots (that causes increase in pressure fluctuation near the wall similar to what was provided on higher SPL near the flame tip) in a gas turbine combustion that can cause damage to the combustor.

Chapter 7: Conclusions

This dissertation has investigated the role of increased number of sensors in the flame or a combustor to provide detailed information using homogeneous and heterogeneous sensors. The focus here is on how much additional information can be gathered from multiple sensors.

7.1. Correlation methods

Different cross correlation methods were used to determine their suitability in flows and flames using two sensors placed around the source. The results showed that phase transfer method (PHAT) offer better performance as compared to the other methods examined here. This has the potential to determine local noise generation sources from within flows and flames with the additional information on local noise generation source (in addition to the overall sound pressure levels).

7.2. Homogeneous, heterogeneous sensors in the flame

It has been demonstrated that the use of a single sensor, can be used to provide valuable information in a flame. Here the main interest was to find what additional information can be obtained by employing homogeneous and heterogeneous sensors; thermocouple, microphones probes, and array of microphones. Experimental investigations have been carried out on turbulent premixed swirling flames to determine the flame characteristics such as distribution of mean and fluctuating temperature, and pressure fluctuation in and around the flames with defined sensors. The interdependence of fluctuating temperature regime and acoustic source

localization within the swirl stabilized turbulent premixed flame was investigated experimentally.

Thermocouple and microphone probes

Pressure fluctuations (non combustive flow)

- The simultaneous pressure fluctuation in different directions showed variation in different directions.
- Maximum total pressure fluctuations were found to occur at the burner exit. This is attributed to high turbulence levels in this region.

Pressure and temperature fluctuations (combustive flow)

- The minimum pressure fluctuation was observed inside the flame (in regions with almost uniform temperature distribution).
- Pressure fluctuation observed at the boundary of the visible flame showed also high temperature fluctuation.
- The magnitude of pressure fluctuations along longitudinal direction of the flame were more than the other two directions. This may be attributed to initial momentum and the buoyancy of the fluid in that direction.
- Pressure fluctuation in different directions showed significant variation in different directions for the combustive case as compared to the non-combustive flow. This is attributed to dynamic expansion of the gases as a direct result of combustion.

- A comparison of the pressure and temperature fluctuations at the same location revealed that maximum temperature fluctuations occur near to the boundary of the flame while maximum pressure fluctuation occurs further away from the flame (at about $L/D=0.15$).
- Pressure fluctuation data showed flame to act as a barrier against outside perturbations (negligible effect of out fluctuation, flow and eddies that may diffuse inwards).

Microphone array

Acoustics noise localization was examined using condenser microphones which were placed at various axial locations above the burner exit plane. Location of the acoustic sources were found to be near the burner exit in a well defined axial regime varying from $H/D = 0$ to $H/D = 2.5$ with the maximum being at $H/D=1.25$. A correlation between the locations of fluctuating temperatures and pressures, indicate that major part of the noise generation occurs in regions of maximum pressure and temperature fluctuations.

7.3. Microphone probe data

Microphone probe data, using sound source and jet air as pressure fluctuation source, showed different pressure signals at the probe tip as compared to end of the probe due to the direct effect of probe. Different methods (cross correlation, output signal spectrum, amplitude ratio verses frequency, coherence function and phase spectrum) have been used to find out the correlation between the output signal from reference microphone and probe microphone.

7.4. Microphone array placed outside the combustor

Measurements of acoustic signatures between sensors placed outside of the combustor, can help assist in understanding the local acoustic sources from within the combustor. With change in the fuel to air ratio and array of microphones, investigation was carried out to identify which microphone (zone) is more sensible to changes in fuel to air ratio relative to others. Data has been obtained from a premixed swirl combustor with the change in fuel to air ratio. The data showed that the distribution of sound around the combustor, as measured by different microphones, changed with variation in fuel to air ratio so that the microphone array showed uneven sound distribution. Also, microphone at $z=2$ inches placed near to the tip of the flame showed higher sound levels with change in equivalence ratio from 1 to 1.2. These show that a single sensor cannot provide enough spatial resolution to show the direct effect of change in equivalence ratio.

Chapter 8: Future work recommendations

As it was mentioned before, combustion systems have to meet more air pollution standard requirements, and it is necessary that the design of combustors becomes more complex. Monitoring of the any change from operating point of the combustion has to be achieved with grate precision. There are several diagnostic techniques that are trying to diagnose and characterize the flame. These diagnostic techniques should provide a good explanation of flame characteristic and combustion process in general. A high density sensor network system would enhance in providing detailed information on the various continuing processes happening within the combustors. In spite of the great efforts developed, the techniques for using multiple sensors are still at the beginning.

This research has consider different sensors calibration, and considered how correlate different parameters. Experimental investigations have been carried out on turbulent premixed swirling flames to determine the influence of mean, fluctuating temperature and pressure fluctuation distribution on the flame characteristics with defined heterogeneous sensors. Also this research has considered different approach in terms of information contain in different sensors and showed the requirement of multiple sensor for better monitoring that contribute significantly to the understanding of the problem. Nevertheless, more details still require further substantiation and are thus recommended for future work, as summarized below.

Use different fuel

The present study has established a link between the input parameters (fuel to air ratio) and sound pressure measured by different microphones. Fourier transform was used for signal analysis. This work can be done by choosing another parameters for example change in fuel property. At any given operation point of the swirl combustor changes to fuel property can be made while maintaining the other parameters constant, i.e. input air. In the second step the observed function should be represented by a mathematical fitting or calibration curves.

Noise localization in the flame

Acoustic source localization in flames have gained much interest in the past few decades as the acoustics of the flame is responsible for flame dynamics in a given combustion system. Conventional methods that are being used to locate the sound sources within a flame employ high frequency Chemiluminescence imaging, IR imaging and planar laser induced Fluorescence (PLIF).

High frequency Chemiluminescence imaging techniques require hardware that is costly and requires rigorous data processing for the localization of acoustic sources within a flame. The need to locate the acoustic sources within such systems inexpensively has thus pushed the efforts for localizing acoustic sources within flames and combustors by employing microphone arrays in and around the system of choice.

Position location is a complex process that comprises a hybrid of mathematical methods for its implementation. Each of these methods must be considered carefully to ensure that the chosen method does not degrade the overall performance of a locator. Methods based on time delay of arrival are completed in two steps. The first step involves the time difference of arrival (TDOA) estimation of the signal for sets of pairs of receivers. The second step involves employing algorithms to create an unambiguous solution to a set of non-linear equations.

Microphone arrays can be used to locate the acoustic sources from within flames and combustors both efficiently and inexpensively. Various approaches have been considered in the past for position location of sound source with the help of microphone arrays. The approaches of source location problem are classified into three classes: steered beam former based locators, high-resolution spectral estimation locators, and TDOA based locators. It is based on estimating the time delay of arrival of the sound wave between a microphone pair.

Appendix A: Cross correlation algorithms

Most practical acoustic source localization schemes are based on time difference of arrival estimation due to their conceptual simplicity, reasonably effective in moderately reverberant environments, and low computational complexity. Time delay estimation is used to localize the targets depending on the sound and can be used in active and passive sound localization systems [33].

The signal received at 2 microphones separated by a specified distance can be modeled by:

$$\begin{aligned} r_1(t) &= s(t) + n_1(t), \\ r_2(t) &= a_2 s(t - \tau) + n_2(t), \end{aligned} \quad 0 \leq t \leq T \quad (A.1)$$

where, $r_1(t)$ and $r_2(t)$ are the outputs signals of two separated microphones, $s(t)$ is the source signal, $n_1(t)$ is the additive noise to the first microphone and $n_2(t)$ is the additive noises to the second microphone, a_2 represents the relative signal attenuation, T denotes the observation interval, and τ yields the time delay between the two received signals. The signal and noises are assumed to be uncorrelated having zero mean and Gaussian distribution.

A.1. Cross Correlation Algorithm

This algorithm tries to resolve the degree to which the signals are correlated using cross correlation function. Upper limit provides the time delay of the cross correlation function. Assuming a microphone array of i microphone m_1, m_2, \dots, m_i , the signals picked up by them will be [50]:

$$r_i(t) = a_i s(t - \tau_i) + n_i(t) \quad (A.2)$$

where $s(t)$ is the sound signal, $n_i(t)$ is the stationary additive noise, τ_i is the propagation time delay difference between two microphones and a_i is the signal attenuation. The Fourier transform for the previous equation gives:

$$R_i(f) = a_i S_i(f) \exp(-j2\pi f \tau_i) + N_i(f) \quad (A.3)$$

$$R_{r_1 r_2}(\tau) = E[r_1(t)r_2(t - \tau)] \quad (A.4)$$

where, $E[.]$ is the expected value, the value of τ which maximizes this function is the time delay estimation. Figure A.1 shows a schematic diagram for this method.

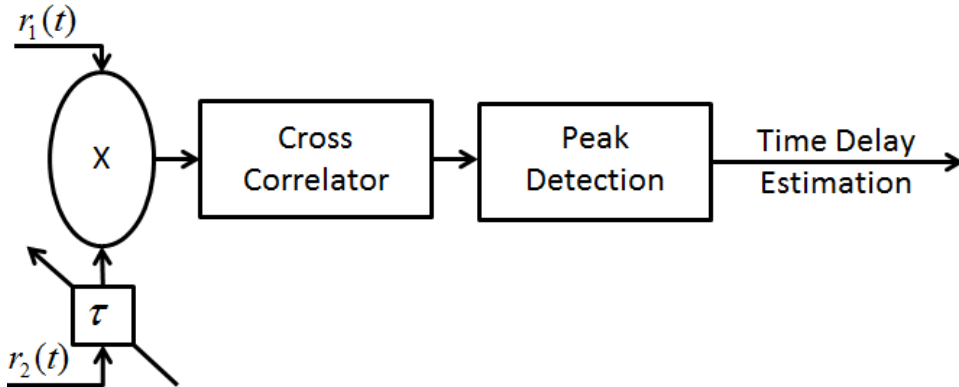


Figure A.1. Schematic diagram of cross correlation method.

A.2. Generalized cross correlation with phase transform

This algorithm is another version of cross correlation algorithm with main gains of accuracy and low computational cost [34]. Figure A.2 shows a schematic diagram for this method. Two filters H_1, H_2 are added to ensure large sharp peak in the obtained cross correlation, which improves the accuracy of time delay estimation and

improves the SNR. After filtering the signals $r_1(t), r_2(t)$, the consequential signals are delayed, multiplied, and the consequential signals are then integrated for a range of delays until peak output is obtained.

The signals estimated by two microphones are presented in equation (A.1). It is assumed sound signal $s_1(t)$ and the noises $n_1(t), n_2(t)$ are mutually independent zero mean Gaussian processes. The cross spectrum between the signals $r_1(t), r_2(t)$ is given by [38]:

$$S_{r_1 r_2} = E\{R_1(f)R_2^*(f)\} \quad (A.5)$$

where $E\{.\}$ denotes the algebraic probability, $(.)^*$ denotes the complex conjugate operator, $R_1(f)$ and $R_2(f)$ represent the Fourier transform of $r_1(t)$ and $r_2(t)$, respectively.

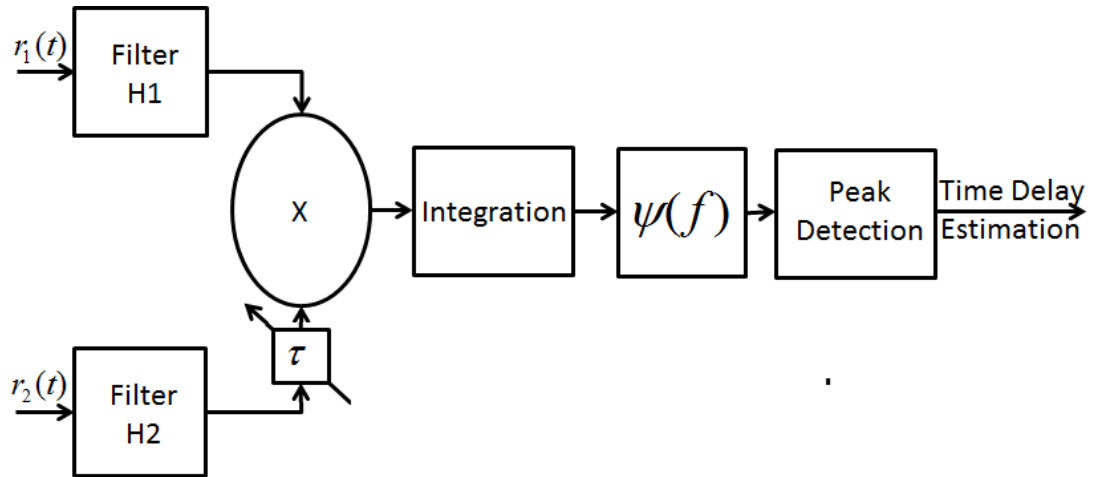


Figure A.2. Schematic diagram generalized cross correlation method.

The time delay is obtained as [34, 38].

$$\tau_\phi = \arg \max \psi_{r_1 r_2}(\tau), \quad (\text{A.6})$$

where, $\psi_{r_1 r_2}(\tau)$ is the generalized cross correlation function, and is equal to [34]

$$\psi_{r_1 r_2}(\tau) = \int_{-\infty}^{\infty} \phi(f) S_{r_1 r_2}(f) \exp(j2\pi f\tau) df = \int_{-\infty}^{\infty} \psi_{r_1 r_2}(f) \exp(j2\pi f\tau) df, \quad (\text{A.7})$$

where, $\phi(f)$ is the weighting function (sometimes also called the pre filter function) is given by [34]

$$\phi(f) = H_1(f) H_2^*(f) \quad (\text{A.8})$$

The role of the weighting function is making sharper peak in the cross correlation between the signals obtained from the microphones. One can get the cross correlation method by choosing the weighting filter equal to one. Other methods are derived from generalized cross correlation method by choosing different weighting filters or expectation functions, for instance the generalized cross correlation with phase transform (GCC-PHAT) and the generalized cross correlation with maximum-likelihood estimation (MLE).

A.3. Generalized cross correlation with maximum-likelihood estimation

Generalized cross correlation with maximum-likelihood estimation method is another the same as generalized cross correlation with different expectation function. The weighting function in generalized cross correlation method is equal to [34, 36, and 38]

$$\psi_{ML}(f) = \frac{1}{|NG_{r_1 r_2}(f)|} \frac{|\gamma_{r_1 r_2}(f)|^2}{|1 - \gamma_{r_1 r_2}(f)|^2} \quad (A.12)$$

where,

$$R_{ML}(\tau) = \int_{-\infty}^{\infty} \psi_{ML}(f) R_1(f) R_2^*(f) \exp(j2\pi f\tau) df = \int_{-\infty}^{\infty} \psi_{ML}(f) G_{r_1 r_2}(f) \exp(j2\pi f\tau) df, \quad (A.13)$$

where, $R_i(f)$ is the Fourier transform of $r_i(t)$, $\psi_{ML}(f)$ is the MLE weighting function, $G_{r_1 r_2}(f)$ is the cross spectrum of the received signal, where the magnitude coherency squared is [34]

$$|\gamma_{r_1 r_2}(f)|^2 = \frac{|G_{r_1 r_2}(f)|^2}{G_{r_1 r_1}(f) G_{r_2 r_2}(f)}, \quad (A.14)$$

Then we get the value of the time difference of arrival as the value that maximizes the likelihood function of the observed data [51]

$$\hat{\tau}_{ML} = \arg \max_{\tau \in D} R_{ML}(\tau) \quad (A.15)$$

A.4. Average square difference function (ASDF) method

The ASDF method is based on difference between signals. It is a function of time delay and with changing the time delay; it is minimize the error square between the two microphone signals. The equation for this method is defined by [52].

$$R[\tau] = \frac{1}{N} \sum_{n=0}^{N-1} [(r_1(n) - \bar{r}_1) - (r_2(n - \tau) - \bar{r}_2)]^2 \quad (A.16)$$

And since the minimum error square will consider this attenuation function in the signals, it is will be:

$$R [\tau] = \frac{1}{N} \sum_{n=0}^{N-1} [(r_1(n)) - (r_2(n - \tau))]^2 \quad (A.17)$$

$$D = \arg \min[R(\tau)] \quad (A.17)$$

This method gives very good estimation in the absence of noise. It requires no multiplication, which is the most significant practical advantage of this method over the other methods. It was found that this method was very time consuming method.

Appendix B: Numerical calculations

The CFD numerical calculations were done for the premixed swirl combustor to compare the CFD results against the experimental results. These results were different in detail from the experimental result. But it will give us an inside view about the complexity of real combustor. These support the idea that multiple sensors are required for combustor. The calculations were done for 2D geometry of the swirl combustor and acoustic analysis was performed. The geometry modeling and geometry clean up was done in pre-processor Gambit 2.4.6. The processing and post-processing of the results were done in Fluent 6.3.26. For this appendix several sentences and consideration are used from the Fluent help and descriptions.

B.1. Structured meshing

Structured grid with quadrilateral elements for the combustor geometry was made in Gambit. Structured meshing was adopted as opposed unstructured meshing to avoid numerical diffusion in the results. Refinements were done at critical regions of the flow field to capture the recirculation zones by adapting the mesh to the flow field. The total grid size included 6750 quadrilateral elements. Figure B.1 shows the structured grid for the 2D model of the swirl combustor along with the boundary conditions used for the acoustic analysis of the same. The 2D geometry of the premixed swirl combustor was made exactly of the same dimensions as the combustor that was used for the experimental analysis.

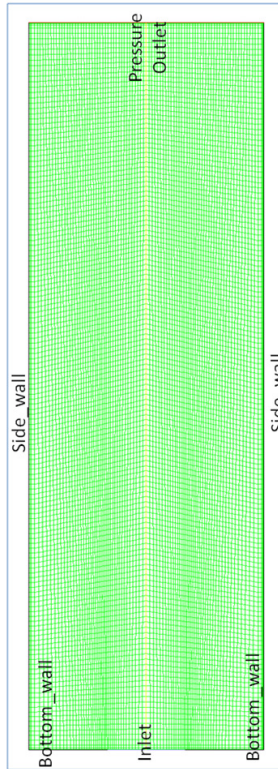


Figure B.1. Numerical meshing of the 2D premixed swirl combustor and its boundary conditions.

B.2. Boundary conditions and solvers used

The boundary conditions used for the given acoustic analysis are shown in figure B.1. The air-fuel inlet boundary condition was given at the inlet of the combustor where the premixed air/fuel mixture enters the combustion chamber. The air/fuel inlet velocity profiles were read from the experimental PIV data of the premixed swirl combustor. Figures B.2 and B.3 represent the inlet velocity profiles for the given combustor for swirl vane angles of 30 and 60 degree. Methane gas was used as the fuel in the CFD numerical computations.

The bottom wall of the combustor was taken as no heat transfer. No slip walls with constant temperature have been used. Heat transfer coefficients and emissivity were defined. The side walls were considered as a mixed thermal boundary condition. The walls of the combustor were assumed to lose radiation through. The DO model covers the entire range of optical thicknesses. This allows having an answer of radiation at wall. The outlet of the given premixed combustor was considered atmospheric pressure.

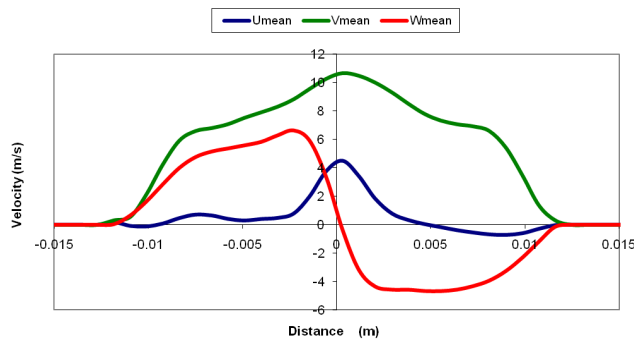


Figure B.2. Experimental velocity profiles for 30 degree swirl geometry.

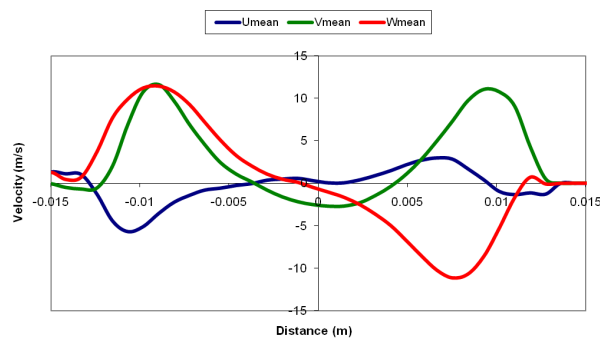


Figure B.3. Experimental velocity profiles for 60 degree swirl geometry.

High resolution techniques for the description of turbulent flows, offer the possibility to determine the unsteady flow structure. The Reynolds stress model (RSM) is used. RSM considered for streamline curvature, swirl, rotation, and changes in strain rate. The modeling for the dissipation rate and pressure strain was not easy and other methods should be used.

In Fluent the Reynolds stress transport equations is obtained. In this regard as it is mentioned in the software, “several of the terms in the exact equation are unknown and modeling assumptions are required in order to close the equations”. The pressure solver was used for the given acoustic analysis. Acoustic analysis of the premixed swirl combustor was done for both the steady and unsteady case. Green-gauss node based gradient option was chosen for both the steady and unsteady case. For the unsteady case, 2nd order formulation was chosen. The species transport model was used in Fluent.

The pressure discretization has been done in Fluent. PRESTO scheme was used. The pressure velocity coupling method option was chosen for calculations. A time step for the calculation set $10\mu\text{s}$. To consider the unsteady acoustic analysis case, the segregated sound propagation method (SSPM) selected. For considering the steady state, stochastic noise generation and radiation method option was chosen for the acoustic analysis of the premixed swirl combustor. Broadband noise source model was used for considering the acoustic field.

B.3. Acoustic modeling of the combustor

Sound propagation has essential characteristics of the wave. It has a source which can be any kind of oscillatory disturbance. Sound propagates in a medium and transports energy without transporting matter. Fluid movement always produces pressure oscillations. This pressure oscillation inherently is a source of sound. It is considerable that sound waves carry only a tiny fraction of the energy contained in the mean flow. Figure B.4 shows the how the sound travels from a given acoustic source to the receiver at a given distance.

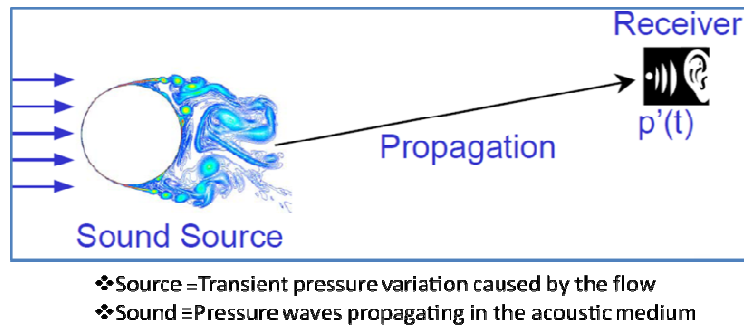


Figure B.4. Pressure waves propagating.

Fluent uses two main methods for the acoustic analysis. These are segregated source-propagation method (SSPM) and stochastic noise generation and radiation (SNGR) method. For steady case the SNGR method has been used. It is accurate for steady state. It is the only model available for the steady state acoustic analysis. For unsteady case the SSPM method along with Hawkings method have been used.

B.3.1. Stochastic noise generation and radiation method (SNGR)

The SNGR models in Fluent are time consuming program. Steady Reynolds averaged Navier Stokes (RANS) results contain information such as mean velocity, mean pressure, and rate of dissipation. This information can be used to get information on broadband noise.

B.3.2. Segregated source propagation methods (SSPM)

In SSPM program, problem domain divided into two layers. The first one is the flow field and the second layer can be regarded the acoustic field. SSPM follows following steps. First, it resolved of the flow in and around the sound source regions. Secondly, it saves required data (such as Lighthill's tensor) on source regions.

After the above steps, saved data is read into the sound propagation solver FLUENT's inbuilt FWH module. Sound computation is then done in FWH module. FWH method stores time-varying pressure at all points on the source surfaces during CFD simulation. Then, CFD simulation is completed, an automatic routine provides sound pressure signal at predefined receiver locations.

B.4. Numerical results and discussion

The numerical computations were done for the acoustics behavior inside the premixed swirl combustor. The cases have been done for both steady and unsteady reacting flow. Steady case for the non-reacting flow was also run to identify the differences in the acoustic signatures acquired for reacting and non-reacting flow.

Figure B.5 shows the contours of velocity magnitude for steady state reacting flow for different swirl intensities namely 30 degree and 60 degree swirl. It is seen that at higher degrees of swirl (60 degree swirl) strong radial and axial pressure gradients are set up near the inlet, resulting in axial recirculation in the form of a central recirculation zone, CTRZ, which is not observed at weaker degrees of swirl.

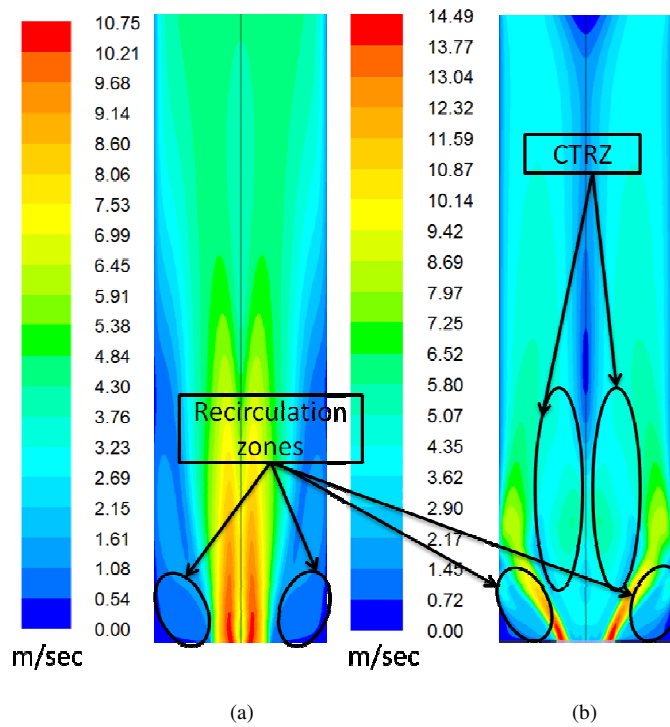


Figure B.5. Numerical velocity magnitudes. (a) For 30 degree swirl. (b) For 60 degree swirl.

The flow was found to be high of shear and values of turbulence intensity. Large fluctuations and stagnation pressures observed on the boundary of the combustor. Flame inside the combustor was stabilized are shortened significantly. It seems that recirculation zones worked as the main turbulent noise sources within the premixed swirl combustor.

Figure B.6 shows the different contours of acoustic power level for steady state reacting flow for different swirl intensities namely 30 degree and 60 degree swirl. The acoustic power level in 60 degree was higher than in the case of 30 degree swirl. For the higher degree swirl (60 degree), the recirculation zones were strong and the power associated with recirculation flame flow increased. The acoustic power level was maximum in the flame zone and it decreases substantially downstream of the combustor (the same as open flame) which was according to the experimental results (the results of experiments is not presented here).

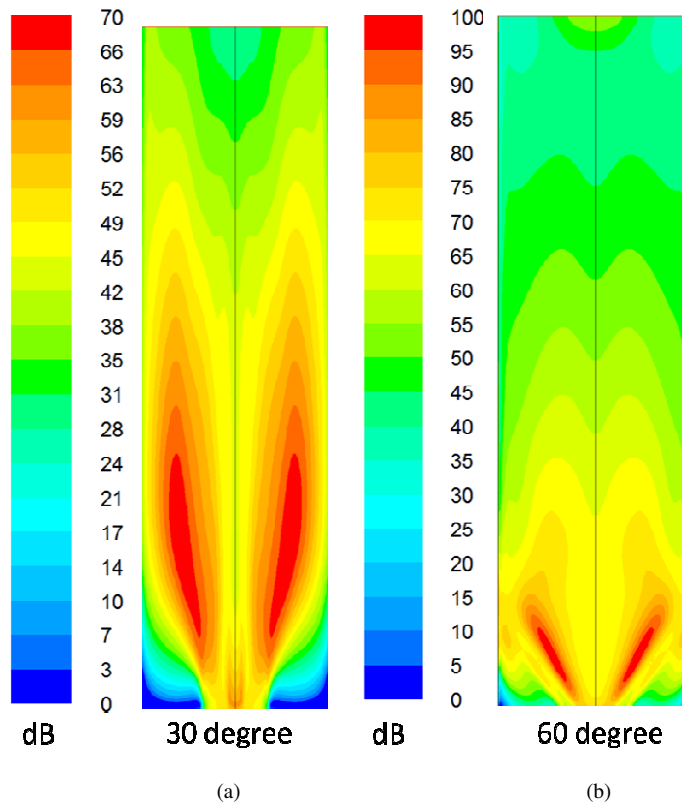


Figure B.6. Numerical acoustic power level. (a) For 30 degree swirl. (b) For 60 degree swirl.

Figure B.7 shows the figure of acoustic power with change in axial position. The maximum acoustic power was 70 dB at an axial position of $x= 0.0532$ m for 30 degree swirl and it was 100.43 dB at an axial position of $x= 0.015$ m for 60 degree swirl.

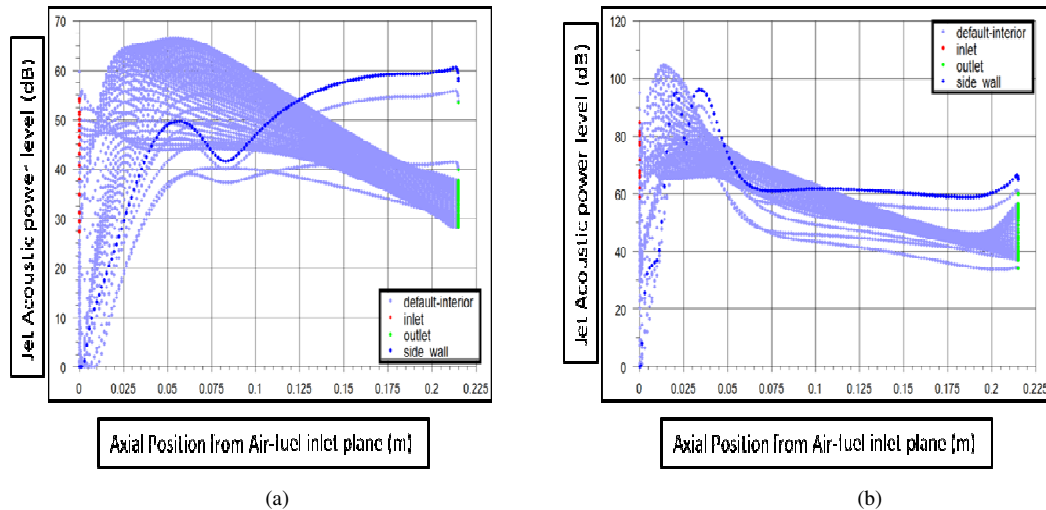


Figure B.7. Numerical power level. (a) For 30 degree swirl. (b) For 60 degree swirl.

Figure B.8 shows the figure for acoustic power level with change in axial position above the inlet plane for different swirl intensities and steady state reacting flow.

Figure B.9 shows the contours of velocity magnitude for reacting state non reacting flow for different swirl 30 degree and 60 degree. The velocity gradients were more severe and distributed in the case of reacting flow compared with the non reacting flow.

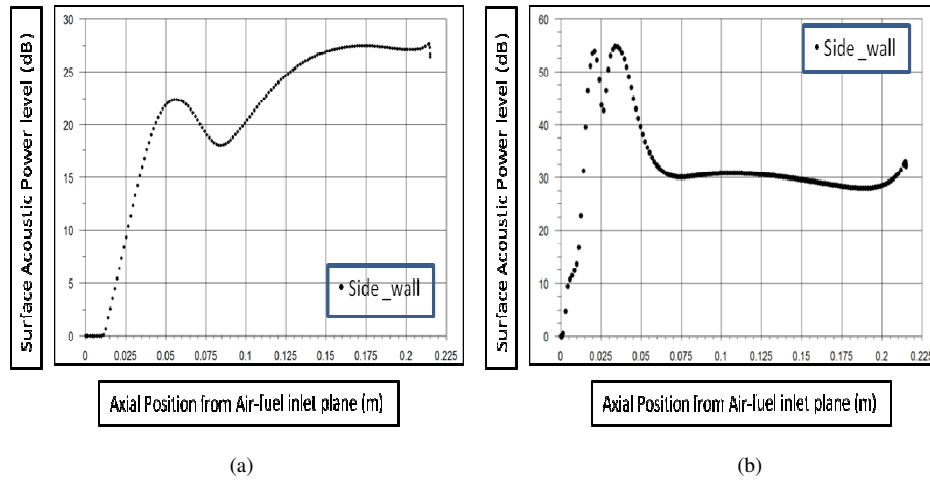


Figure B.8. Numerical surface acoustic power level. (a) For 30 degree swirl. (b) For 60 degree swirl.

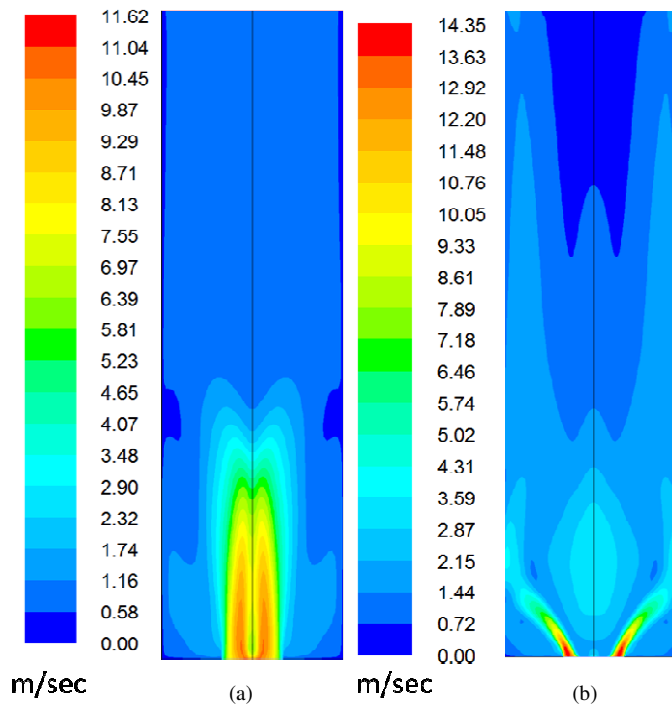


Figure B.9. Velocity magnitudes. (a) For 30 degree swirl. (b) For 60 degree swirl.

Figure B.10 shows the contours of power level for reacting flow for different swirl intensities namely 30 degree and 60 degree swirl. The acoustic power level for the

steady non-reacting case was found to be lower as compared to the non reacting case. In the non-reacting case the combustion noise shows a lower noise level as compared to the reacting case. When heat was added to a fluid (air and fuel) the density of the fluid was a function of two parameters, the pressure and the heat supplied to unit mass of fluid. The sound field was changed by the rate of change in the heat addition rate to the combustor. Steady heating method was less noisy when compared to unsteady heating method. Hence, though the acoustic power level for the non-reacting case was less it was almost similar to the steady reacting flow in the combustor.

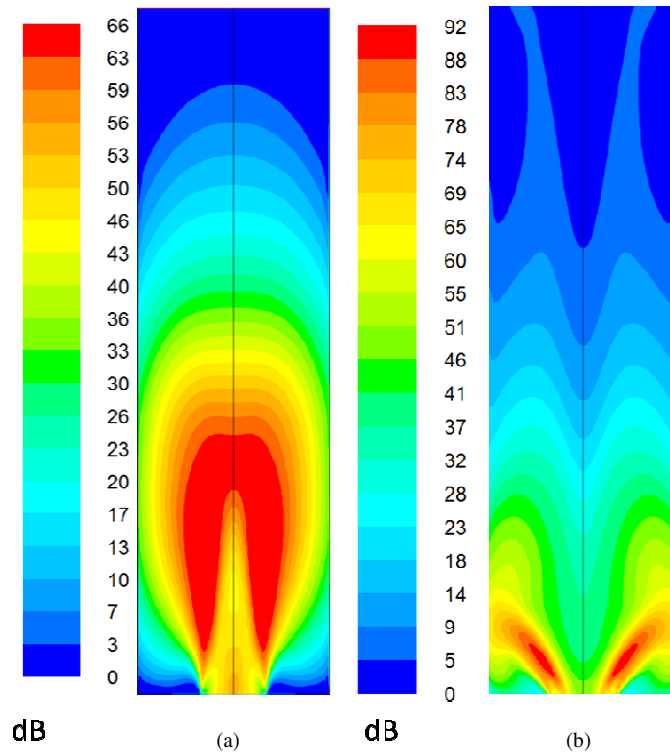


Figure B.10. Numerical Contours of acoustic power level. (a) For 30 degree swirl.
(b) For 45 degree swirl.

Figure B.11 shows the acoustic power level with change in axial position above the inlet plane for steady state non reacting flow for different swirl intensities 30 degree and 60 degree swirl. The concentrated acoustic power level for 30 degree swirl geometry was 66 dB at an axial position of $x=0.036653$. The concentrated acoustic power level for 60 degree swirl geometry was 92 dB at an axial position of $x=0.010558$.

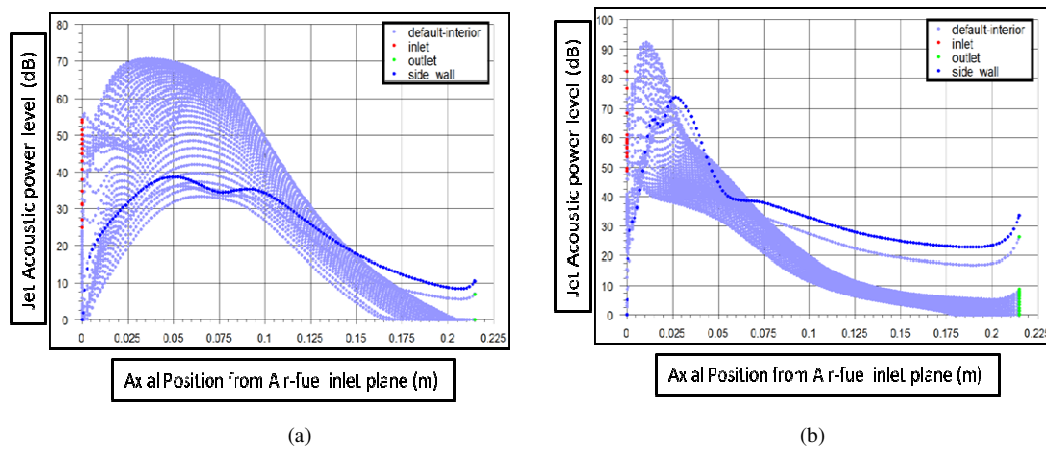
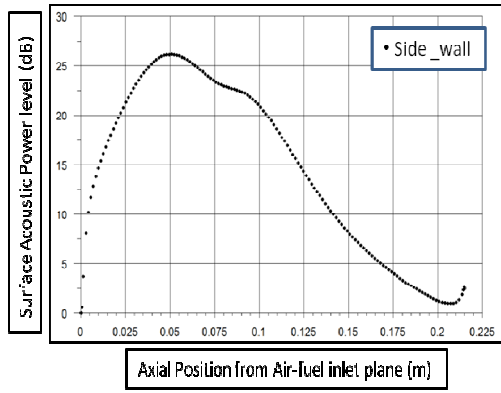
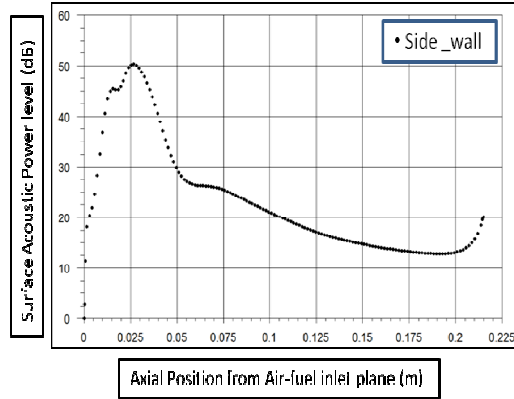


Figure B.11. Numerical plot of power level. (a) For 30 degree swirl (b) For 60 degree swirl combustor.

Figure B.12 shows acoustic power in axial position above the inlet plane for steady state reacting flow for different swirl intensities i.e. 30 degree and 60 degree swirl. The trend observed in the variation of surface acoustic power level was different in the 2 30 degree and 60 degree swirl and it was seen that as swirl intensity increases the surface acoustic power level for inside wall increases in level. The levels were found to be smaller as compared to reacting case.



(a)



(b)

Figure B.12. Numerical surface acoustic power level. (a) For 30 degree swirl. (b)

For 60 degree swirl.

Appendix C: List of publications

Journal

Eshaghi A., Singh, A. V., Yu, M., Gupta, A. K., and Bryden, K. M., “Heterogeneous Sensors on Thermal and Acoustic Behavior of a Premixed Swirl Flame,” 2012. (Will be submitted to Applied Energy Journal).

Conferences

Singh, A. V., Eshaghi A., Yu, M., Gupta, A. K., and Boyden , K. M., “Acoustic Source Localization using Microphone Arrays by TDOA Method,” 48th AIAA/ASME/SAE/ASEE Joint Propulsion Conference & Exhibit 10th Annual International Energy Conversion Engineering Conference, 2012.

Discussion on Advances in Sensors and Monitoring

Singh, A. V., Eshaghi A., Yu, M., Gupta, A. K., and Boyden, K. M., “Effect of Multisensors on Noise Source Estimation in 2D,” The 37th International Technical Conference on Clean Coal & Fuel Systems, June 3-7, Clearwater, U.S.A, 2012.

References

- [1]- Yu, M., K. Bryden, and A. K. Gupta, "Sensor Response and Sensor Network Development for Practical Combustor", IEEEES conference, Honolulu, Hawaii, 2007, pp. 1327-1332.
- [2]- Docquier, N., Candel, S, "Combustion control and sensors: a review", Progress in energy and combustion science, 2002, pp. 107-150.
- [3] A.K. Gupta, N. Syred, and J. M. Beer, "Fluctuating temperature and pressure effects on the noise output of swirl burners" Symposium (International) on Combustion, 1975, pp. 1367-1377.
- [4] A.K Gupta, N. Syred and Beer, "Noise Sources in swirl burners" Applied Acoustics, 1976, pp. 151-163.
- [5] M. Yukio, T. Nakayama and T. Yuminaka, "A study on the structure of premixed Turbulent Flame by the Microphone Technique" Combustion and flame 1975, pp. 5-14.
- [6] Wojcik W., "Application of fiber optic flame monitoring system to diagnostics of combustion process in power boiler," Technical Science Vol. 56, 177-195. W. 2008.
- [7] Chong H.S. Chong, Tan C. Wilcox S., Thai S., Ward J., and Andrews G., "Development of an intelligent flame monitoring system for gas-fired steel reheating furnaces", European Thermal-Sciences Conference, The Netherlands, 2008
- [8]- M. Lackner, "Tuneable diode laser absorption spectroscopy (TDLAS) in the process industries: a review". Reviews in Chemical Engineering 2007

- [9]- R. Hanson, J. Jeffries, X., H. Li, “Mattison D et al. Smart sensors for advanced combustion systems” 2005
- [10]- R. Hanson, J. Jeffries, “Diode laser sensors for ground testing”, *mol spect, chemistry, ohio-state.edu* 2006
- [11]- S. Candel, “Combustion dynamics and control: Progress and challenges,” *Proceedings of the Combustion Institute* 2002; pp. 1–28.
- [12]- GI Sivashinsky, “Instabilities, pattern formation, and turbulence in flames”, *Annual Review of Fluid Mechanics*, 1983
- [13]- A. Sanz, J. Ballester, R. Herna, “Cerecedo LM. Advanced monitoring of industrial burners based on fluctuating flame signals”. 2008, pp. 1063–75.
- [14] Ballester J., Hernandez R., Sanz , A., Smolarz A., “Chemiluminescence monitoring in premixed flames of natural gas and its blends with hydrogen” *Elsevier* 2009, pp. 2983-2991.
- [15]- R. Rajaram, T. Lieuwen, “Effect of approach flow turbulence characteristics on sound generation from premixed flame” , *AIAA Aerospace Sciences Meeting and Exhibit* 2004, Paper 2004-0461.
- [16] Gupta, A. K.; Lilley, D. G.; and Syred, N., “Swirl Flows,” *Abacus Press, Tunbridge Wells, England*, 1984.
- [17] Lieuwen, T.C. and Vigor Yang, 2005, “Combustion Instabilities in Gas Turbine Engines: Operational Experience, Fundamental Mechanisms and Modeling”, *Volume 210, Progress in Astronautics and Aeronautics, AIAA*, 2005.
- [18] Habisreuther, P.; Bender, C.; Petsch, O.; Büchner, H. and Bockhorn, H., “Prediction of Pressure Oscillations in a Premixed Swirl Combustor Flow and

Comparison to Measurements”, Flow, Turbulence and Combustion, 2006, Volume 77, pp.147-160.

[19] Reese, J. L., “State of the art of NO_x Emission control technology,” ASME, 1994, Paper No. 94-JPGC-EC-15.

[20] Qi, S.; Gupta, A. K.; and Lewis, M. J., “Effect of Swirl on Temperature Distribution in Premixed Flames,” 35th AIAA Aerospace Sciences Meeting, 1997, Paper No. 97-0373.

[21] Marshall, A. W. and Gupta, A. K., “Effects of Jet Momentum Distribution of Thermal Characteristics of Co-Swirling Flames,” AIAA 34th Aerospace Sciences Conference, Reno, NV, AIAA, Jan. 15–18, 1996, Paper No. 96-0404.

[22] Hinze, J.O., Turbulence, Mc Graw-Hill Book Co., New York, 1959.

[23] Lockwood, F. C.; Moneib, H., “Fluctuating temperature measurements in a heated round free jet”, Comb.Sci. 1980, Tech. 22, 63-81.

[24] Yule, A. J.; Taylor, D.S.; Chigier, N.A., “On-line compensation and processing of thermocouple signals for temperature measurement in turbulent flames”, AIAA, 1978, paper 78-30.

[25] Lockwood, F.; and Odidi. A. O. O., “Measurement of Mean and Fluctuating Temperature and of Ion Concentration in Round Free-Jet Turbulent Diffusion Flames,” Proc. 15th Symposium (intl.) on Combustion, The Combustion Institute, Pittsburgh, PA, 1975, 561–571.

[26] Daurer, M.; Gupta, A. K., and Lewis, M. J., “Swirl Effects on Combustion Characteristics of Premixed Flames,” Proc. Intl. Joint Power Generation Conference, Baltimore, MD, Aug., ASME FACT-Vol. 22, ASME, New York, 1998, pp. 573–578.

- [27] Miles, P. C. and Gouldin, F.C, “Determination of the time constant of fine wire Thermocouples for compensated temperature measurements in Premixed turbulent flames”, *Combustion Science and Technology*, 1993, pp. 181-199.
- [28] Archer, S.S., “Morphology of unconfined and confined swirling flows under non- reacting and combustion conditions”, 2005, Ph.D. thesis, University of Maryland, College Park, MD.
- [29] Ballantyne, A. and Moss J. B., “Fine Wire Thermocouple Measurements of Fluctuation Temperatures”, *Combustion Science and Technology*, 1977, Vol. 17, pp. 63-72.
- [30] Marshall A.W., “Effects of Jet Momentum Distribution Combustion Characteristics in Co-Swirling Flames”, 1996, Ph.D.-thesis, University of Maryland, College Park, MD.
- [31] Yukio, M., Nakayama, T. and Yuminaka, T. “A study on the structure of premixed Turbulent Flame by the Microphone Technique” *Combustion and flame* 1975, pp. 5-14.
- [32]- Ebrahimi I., “A method for the measurement of the local distribution of turbulent intensity in jet flame” *Combust. Flame*, 1967, pp. 255-259.
- [33] Brandstein, A. J. E., and Silverman, H. F., “A closed form location estimator for use with room environment microphone arrays,” *IEEE Transactions on Speech and Audio Processing*, vol. 5, no. 1, pp. 45–50, 1997.
- [34] Knapp, C. H. and Carter, C. G., “The Generalized Correlation Method for Estimation of Time Delay”, *IEEE Trans, Acoust, Speech, Signal Processing*, vol. ASSP-21, 1976, pp. 320-327.

- [35] Carter, G. C., "Coherence and time delay estimation: an applied tutorial for research, development, test, and evaluation engineers", Piscataway, NJ: IEEE Press, 1993
- [36] Bédard, S., Champagne, B. and Stéphenne, A., "Effects of Room Reverberation on Time-Delay Estimation Performance", IEEE, Acoustics, Speech, and Signal Processing, vol.2, April 1994, pp.261-264.
- [37] Jacovitti, G. and Scarano, G.,: "Discrete Time Techniques for Time Delay Estimation", IEEE Transactions on Signal Processing, Vol.41, No.2, pp.525-533 February, 1993
- [38] Khaddour, H, "A Comparison of Algorithms of Sound Source Localization Based on Time Delay Estimation", Elektrevue, volume 2, no.1, 2011.
- [39] Jian, M., Kot. K. C. and Er, M. H., "Performance Study of Time Delay Estimation in a Room Environment", IEEE, Circuits and Systems, vol.5, June 1998 , pp.554-557.
- [40]- Englund D., "The infinite line pressure probe" Proposed for presentation at the 30th Intern. Instrumentation symp, 1984.
- [43] Bendat, J. S. and Piersol, A. G., Random data: Analysis and Measurement procedure, 2nd edition, New York, 1986.
- [44] Qi, S.; Gupta, A. K.; and Lewis, M. J., 1997, "Effect of Swirl on Temperature Distribution in Premixed Flames," 35th AIAA Aerospace Sciences Meeting, Paper No. 97-0373.

- [45] Heitor, M.V., Taylor, A.M.K.P. and Whitelaw, J.H., 1985, " Simultaneous velocity and temperature measurements in a premixed flame", Experiments in Fluids 3, 323-339.
- [46] - Dowling, A. P. and Williams, E. F, "Sound and Sources of Sound", Ellis Horwood Limited (1893).
- [47] Bai T, Cheng, XC, Daniel BR, Jagoda JI, Zinn BT (1993) Vortex shredding and periodic combustion processes in a Rijke type pulse combustor, Combustion Science Technology, 94, 245-258.
- [48] K`uhlsheimer C, B`uchner H (2002) Combustion Dynamics of Turbulent Swirling Flows, Combustion and Flame, 131 (1-2), 70-84.
- [49] Baukal, C, Schwartz, R, Company, J, "The John Zink combustion handbook," Boca Raton, FL, CRC Press, 2001.
- [50] Carter, G. C., "Tutorial Overview of Coherence and Time Delay Estimation," in Coherence and Time Delay Estimation an Applied Tutorial for Research, Development, Test, and Evaluation Engineers, vol. 1, 1993, pp. 1-27.
- [51] Saarnisaari, H., "ML Time Delay Estimation in a Multipath Channel," in International Symposium on Spread Spectrum Techniques and Applications, Mainz, GERMANY, Sept. 1996, pp. 1007-1011M.

[52] Jacovitti, G. and Scarano, G., “Discrete Time Techniques for Time Delay Estimation”, IEEE Transactions on Signal Processing, 1993, Vol.41, No.2, pp.525-533.

[53] http://en.wikipedia.org/wiki/Colors_of_noise